Dissertation ETH No. 25882

Precipitation and drought persistence in global climate models and observations

A thesis submitted to attain the degree of
Doctor of Sciences of ETH Zurich
Dr. sc. ETH Zurich

presented by
Heewon Moon
Master of Science in Engineering
Sungkyunkwan University
born on 22.11.1990
citizen of Republic of Korea

accepted on the recommendation of
Prof. Dr. Sonia I. Seneviratne
Dr. Lukas Gudmundsson
Dr. Benoit P. Guillod
Prof. Dr. Hayley J. Fowler

2019

Acknowledgements

This thesis and my Ph.D. could only be completed with help from so, so, so many people. First of all, I would like to thank Sonia for giving me the opportunity to start the whole journey. Your enthusiasm for research has always inspired me and will keep doing so. Lukas, I feel truly lucky to have had you as my supervisor, I cannot imagine how it would have been without you. Also, you actually managed to make me like statistics. Benoit, thank you for the co-supervision and sparing so many hours to discuss with me (coming all the way from the opposite side of the building). I sincerely thank Hayley Fowler for her constant encouragement and advice while serving as an examination committee member.

I would like to thank all the current and past Landclim members! Especially, I want to thank my current office mates, Martha, Clemens, and Mathias for giving me one more reason to come to the office every day. I really enjoyed sharing air with you even when it was 35°C. Also, many thanks for helping me when I encountered "German" problems, including the abstract of this thesis. To my previous office mates, Vincent, Richard, and Peter, thank you for helping out a confused newcomer! I wish to thank Barbara again for all her support.

To my dear friends in Zurich, Korea and US, I loved all the little moments we spent together. Also, thank you for putting up with the ugliest version of myself, which appeared more frequently during the last four years. To Catkat, my special friend, you are one of the reasons I could overcome the final hurdle in this journey. Thank you and I will miss you.

Carlos, my coração doce, thank you for always staying by my side through all the ups and downs (sometimes, very deep downs) during the last three years, I'm afraid you will have to do so for many many years ahead.

My parents, Kyeungmin Moon and Jeonghwa Lee, even though I don't tell you, I think of you every day. By just doing that, I know things will be alright. My brother, Heekyun, sister-in-law, Yunjeong, and my auntie Seunghee, thank you for being there for me and I wish to spend more and more time together from now on. Because of all of you, I could appreciate life more and despair less. I love you all.

Finally, I dedicate this thesis to my grandma, Yuja Park, the strongest and most giving woman I knew.

Contents

Abstract

Prolonged spells with too much or too little precipitation can lead to extreme events with severe socioeconomic and ecological impacts. Aside from the magnitude of precipitation anomalies, the persistence of such anomalies also strongly contributes to the extent of their impacts as persistence of precipitation can drive persistence in other variables on land such as soil moisture, water storage, and temperature. Observational evidence supports that there have been changes in the distribution of dry and wet spells at daily to interannual time scales during the 20th century in several regions around the globe, some indicating an increase in the frequency of extremely prolonged droughts or increase in the frequency of heavy rainfall. Thus, it is of high importance to evaluate the capability of current general circulation models (GCMs) to simulate precipitation persistence in the past and present climate as it contributes to the uncertainty of future projections of the climate extremes.

In Chapter 2 of this thesis, the persistence of droughts and wet spells at monthly and annual scales are assessed using parameters of the statistical Markov model in multiple global observations and GCMs. Drought is in this study defined as negative precipitation anomaly and the persistence is calculated as a probability of a dry month (year) to be followed by another dry month (year), and persistence of wet spells, indicated by a positive precipitation anomaly, is assessed in the same manner. The transition probabilities were used to statistically simulate dry and wet spell lengths distributions are shown to be a good approximation of the observed distributions. Results show that GCMs systematically underestimate the observed dry and wet persistence at both monthly and annual scales, which is consistent with models' underestimating the risk of extremely prolonged droughts identified in the previous studies. Furthermore, the analysis of variance of the model errors suggests that some regions would require more extended time series or consistent observational reference to validate such an underestimation.

In the second study presented in this thesis, the approach used for the first study is applied to precipitation persistence at the daily time scale. The transition probabilities (dry-to-dry and wet-to-wet probabilities) were found to be less representative of the daily dry and wet spell length distributions. The analysis focuses on the long-term mean and interannual variability of

the two indices. Models overestimate the wet persistence with a relatively homogeneous spatial bias pattern. In particular, models tend to overestimate dry persistence in the Amazon and Central Africa but also underestimate dry persistence in several regions such as southern Argentina, western North America, and the Tibetan Plateau. The model errors are statistically robust despite the considerable spread across different precipitation data products. Compared to the results in the previous chapter, model errors of precipitation persistence at the daily scale have the opposite sign as those at monthly and annual scales. However, the contradicting signs of the error can at least be partially explained by a general underestimation of the interannual variability of both daily dry and wet persistence in GCM.

Chapter 4 assesses soil moisture-precipitation feedbacks in a large ensemble of GCM simulations under temporal and spatial perspectives and in terms of heterogeneity at the sub-daily time scale. Three different metrics were used to assess the feedback in each perspective. Positive (negative) spatial feedback indicates that afternoon rainfall occurs more frequently over the wetter (drier) land surface than its surroundings. A positive (negative) temporal feedback indicates preference over temporally wetter (drier) conditions and positive (negative) heterogeneity feedback indicates preference over more spatially heterogeneous (homogeneous) soil moisture conditions. Results highlight a dominantly positive spatial feedback in the models as opposed to observations. The temporal and heterogeneity feedbacks are better simulated on average, although inter-model variability is largest for these metrics. Soil moisture-precipitation feedback is one of the main processes in the field of land-climate interactions that could affect precipitation persistence. In the discussion, the possible collective influence of the model error of the three soil moisture-precipitation feedbacks is analyzed. The chapter concludes that such influence may lead to more localized precipitation persistence, both dry and wet, in models than in observations, which corresponds to results from previous studies.

The results of this thesis highlight systematic errors of current GCMs in simulating precipitation persistence across different time scales. The opposite signs of the model error at longer (monthly and yearly) scales and shorter (daily) scale indicate that the persistence of precipitation may not propagate linearly across the time scales and different processes underlie those. The results also show how the uncertainty in soil moisture-precipitation feedback contributes to the error especially at a daily scale. Additionally, in the three studies, observational uncertainty of precipitation persistence was commonly found to be comparable to model uncertainty in several regions indicating its importance for robust model evaluation.

Zusammenfassung

Fällt über lange Zeit zu viel oder zu wenig Niederschlag, kann dies zu Extremereignissen mit drastischen sozioökonomischen und ökologischen Auswirkungen führen. Neben der Grösse der Niederschlagsanomalien trägt auch deren Persistenz zum Ausmass ihrer Auswirkungen bei, da die Niederschlagspersistenz die Persistenz anderer Landvariablen wie Bodenfeuchte, Bodenwasserspeicherung und Temperatur beeinflussen kann. Beobachtungen legen nahe, dass es während des 20. Jahrhunderts Veränderungen in der Verteilung von Trocken- und Niederschlagsperioden auf täglicher und interannueller Zeitskala in verschiedenen Regionen der Erde gab. Tendenziell gab es einen Anstieg in der Frequenz von sehr langen Trockenperioden aber auch von Starkniederschlägen. Deshalb ist die Evaluation gängiger globaler Klimamodelle (GCMs) hinsichtlich ihrer Fähigkeit zur Simulation von Niederschlagspersistenz in der Vergangenheit und im aktuellen Klima sehr wichtig, da diese zu Unsicherheiten in zukünftigen Projektionen von Klimaextremen beiträgt.

In Kapitel 2 dieser Doktorarbeit wird die Persistenz von Trocken- und Niederschlagsperioden auf monatlichen und jährlichen Skalen in verschiedenen globalen Beobachtungsdatensätzen und GCMs betrachtet und als statistische Markov-Kette modelliert. Dabei wird Trockenheit als negative Niederschlagsanomalie definiert und Persistenz als Wahrscheinlichkeit berechnet, dass ein trockener Monat (ein trockenes Jahr) auf einen trockenen Monat (trockenes Jahr) folgt. Die Persistenz von Niederschlagsperioden, die durch eine positive Niederschlagsanomalie definiert wird, wird auf dieselbe Art berechnet. Übergangswahrscheinlichkeiten werden verwendet, um die Länge der Trocken- und Niederschlagsperioden statistisch zu simulieren. Die resultierenden Verteilungen erweisen sich als gute Näherung der beobachteten Verteilungen. Die Resultate zeigen, dass GCMs die Persistenz von beobachteten Trocken- und Niederschlagsperioden sowohl auf monatlicher als auch auf jährlicher Zeitskala systematisch unterschätzen, konsistent mit der aus früheren Studien bekannten Unterschätzung des Risikos von extrem langer Trockenheit durch GCMs. Die Varianzanalyse der Modellfehler legt nahe, dass für einige Regionen längere Zeitserien beziehungsweise konsistente Beobachtungsreferenzen nötig wären, um solche Unterschätzungen zu validieren.

In Kapitel 3 wird die Niederschlagspersistenz in verschiedenen globalen

Beobachtungsdatensätzen und Klimamodellen auf täglicher Skala unter Verwendung desselben Markov-Modells wie im vorherigen Kapitel untersucht. Die Übergangswahrscheinlichkeiten (trocken zu trocken und nass zu nass) erweisen sich als weniger repräsentativ für die Verteilung der Trocken- und Niederschlagsperioden. Die Analyse beschäftigt sich mit dem langzeitlichen Mittelwert und der interannuellen Variabilität dieser beiden Indizes. Die Klimamodelle überschätzen die Persistenz von Niederschlagsperioden mit einem ziemlich homogenen geographischen Muster. Die Persistenz von Trockenperioden hingegen, wird im Amazonasgebiet und Zentralafrika überschätzt und im Süden von Argentinien, dem westlichen Nordamerika und dem Hochland von Tibet unterschätzt. Die Modellfehler sind statistisch robust, sogar in Anbetracht der beträchtlichen Streuung der verschiedenen Niederschlagsdatenprodukte. Verglichen mit den Ergebnissen des vorhergehenden Kapitels zeigen die Modellfehler der Niederschlagspersistenz auf täglicher Skala ein entgegengesetztes Vorzeichen zu den monatlichen und jährlichen Skalen. Allerdings kann das sich widersprechende Vorzeichen der Fehler zumindest teilweise darauf zurückgeführt werden, dass GCMs die interannuelle Variabilität und Persistenz generell unterschätzen.

Kapitel 4 untersucht die Wechselwirkung zwischen Bodenfeuchte und Niederschlag im Tagesverlauf in einem grossen Ensemble von GCM-Simulationen. Dabei werden die räumliche und zeitliche Perspektive sowie die räumliche Heterogenität betrachtet. Drei Metriken quantifizieren je eine dieser drei Wechselwirkungen. Eine positive (negative) räumliche Wechselwirkung bedeutet, dass Nachmittagsniederschlag öfter über Landoberflächen auftritt, die feuchter (trockener) sind als deren Umgebung. Eine positive (negative) zeitliche Wechselwirkung ist gegeben, wenn Regen eher zu Zeiten feuchter (trockener) Böden auftritt und eine positive (negative) Heterogenitätsmetrik quantifiziert die Präferenz von Niederschlag bei räumlich heterogener (homogener) Verteilung von Bodenfeuchte. Im Gegensatz zu den Beobachtungsdaten zeigen die Modelle eine mehrheitlich positive räumliche Wechselwirkung. Die Resultate für die zeitliche Wechselwirkung sowie die Heterogenitätsmetrik stimmen besser überein, allerdings ist die Streuung zwischen den Modellen bei diesen Metriken besonders gross. Die Wechselwirkung zwischen Bodenfeuchte und Niederschlag ist einer der Prozesse im Bereich der Land-Klima-Interaktionen, welche die Niederschlagspersistenz beeinflussen können. Deshalb wird der mögliche gemeinsame Einfluss der drei Wechselwirkungen zwischen Bodenfeuchte und Niederschlag in Modellen und Beobachtungen besprochen. Das Kapitel kommt zum Schluss, dass sie sowohl für Trocken- als auch für Niederschlagsperioden zu mehr Niederschlagspersistenz führen können, was den Ergebnissen früherer Studien entspricht.

Die Resultate dieser Doktorarbeit zeigen den systematischen Fehler aktueller GCMs bei der Simulation von Niederschlagspersistenz auf verschiedenen Zeitskalen auf. Die unterschiedlichen Vorzeichen des Modellfehlers auf langen (monatlichen und jährlichen) und kürzeren (täglichen) Zeitska-

len weisen darauf hin, dass die Niederschlagspersistenz sich nicht linear über die Zeitskalen fortpflanzt und, dass ihnen verschiedene Prozesse zugrunde liegen. Die Resultate zeigen auch, wie die Unsicherheit von Bodenfeuchte-Niederschlagswechselwirkungen zum Fehler beitragen, besonders auf täglicher Zeitskala. Darüber hinaus zeigen die drei Studien, dass die Unsicherheit der Niederschlagspersistenz der Beobachtungen in verschiedenen Regionen mit der Modellunsicherheit vergleichbar ist, was deren Wichtigkeit für robuste Niederschlagsevaluierungen in Modellen zeigt.

1 Introduction

1.1 Persistence in the climate system

Many variables in the climate system feature persistence ("memory"), i.e. a tendency for high values to remain high or low values to remain low for several weeks to years depending on the processes they are associated with. For example, sea surface temperature (SST) shows long-term persistence due to the large thermal inertia of the ocean, and exerts such persistence to the overlying atmosphere as well. Soil moisture, which is the main storage of water on land, shows persistence dominantly at subseasonal to seasonal scales, regulated by precipitation, evapotranspiration and runoff. Persistence of precipitation, which is the main topic of this thesis, is regulated by SST in the long-term, while serving as a main forcing for soil moisture persistence and also locally affected by the coupling in the short-term. High precipitation persistence increases the likelihood for prolonged dry and wet spells. Prolonged spells with no rain or anomalously low rain result in droughts with high economic and societal costs and harder recovery of plants (Trifiló et al., 2017), even with non-extreme magnitude of drought. On the other hand, intense rainfall events continuing for several days can cause floods or create a hazardous environment for some tree species (Rozas and García-González, 2012). Furthermore, dry spells can lead to hot spells due to increased sensible heat and vice versa during wet spells together with the effect of increased cloud cover can lead to negative temperature anomalies.

Several statistical approaches have been used in the literature to quantify persistence in climate variables. The lag autocorrelation function of order p is one of the most commonly used measures of persistence, defined as

$$\rho = \frac{cov(x_n, x_{n+p})}{\sigma_{x_n}\sigma_{x_{n+p}}} \tag{1.1}$$

where x_n refers to the variable of interest on a time step n (for instance day or month). For its application in quantifying persistence of soil moisture, this lag-correlation function was used to analyse the impact of other variables on

soil moisture persistence. In previous studies (), based on the soil water balance equation of a single soil column, soil moisture persistence was expressed as $c_s w_{n+lag} = c_s w_n + P_n - E_n - Q_n$, where c_s is the column's water-holding capacity, w_n is the soil water content, P is precipitation, E is evapotranspiration and Q is runoff. The latter three variables (P, E, and Q) are determined to be the main influential factors on soil moisture persistence. Results of the studies show different soil moisture persistence, estimated as 1-month lag autocorrelation function, when treatments to disentangle the influence of other variables on the soil moisture memory was handled differently (Koster and Suarez, 2001; Orth and Seneviratne, 2012; Seneviratne et al., 2006).

Another commonly used approach to quantify persistence is to statistically characterize spell length distributions of certain events or states, e.g. rainy days with threshold of 1 mm/day, and the binary state first-order Markov model was found to be a good approximation for the distribution (Moon et al., 2018). As in lag-1 autoregressive models, a first-order Markov model predicts the status of the current time step based on the previous time step. Under the framework, the probability that the length of a certain status, L, is larger than d is written as:

$$P(L > d) = p^d \tag{1.2}$$

following a geometric distribution, where p is the probability that a current status will continue to the next time step (e.g. probability that a rainy day will be followed by another rainy day in a given period). For large samples, P(X>d) can be approximated as $e^{-\lambda d}$, where $\lambda\tau = p^{(\tau)}$ when τ, the length of time step, tends to zero. The continuation probability p (or λ) has been used as a proxy for persistence, more frequently for droughts and dry spells (Jackson, 1975; Moon et al., 2018; Sharma and Panu, 2014; Wilby et al., 2015), and temperature (Pfleiderer and Coumou, 2018).

1.2 Large-scale climate variability affecting precipitation

Various modes of large-scale variability influence long-term persistence of precipitation in different regions around the globe. Such low-frequency variability is associated with variation in ocean, which is rather a slower component of the climate system, and its interaction with the atmosphere. In this section, some selected large-scale modes of ocean-atmosphere variability in the tropics and extra-tropics, and the atmospheric blocking as a synoptic-scale atmospheric phenomenon and their impact on precipitation are mainly described.

The El Niño-Southern oscillation (ENSO) is the most dominant mode of interannual variability in the tropics, that is characterized by positive SST anomaly in Central/Eastern equatorial Pacific with an irregular cycle ranging 3 - 8 years. During ENSO, the suface pressure gradient between east and west gets weak resulting in shift of the convection zone towards East pacific.

Bjerknes (1969) described such chain of processes occurring in the ocean and atmosphere as a positive feedback loop in which initial positive SST anomaly in Central/Eastern equatorial Pacific leads to decreased East-West SST gradient then weakens the Walker circulation and thus weaker trade wind that brings less equatorial upwelling of cold water and consequently reinforces the positive SST anomaly. Besides the tropics, precipitation in many regions around the globe are largely influenced by different phases of ENSO, that are warm (El Niño) and cold phases (La Niña), usually featuring the switched signs of changes (see Figure 2.1 for the influence of warm phase ENSO in different regions of the world). Meanwhile, the response of regional precipitation can vary during different ENSO events due to interdecadal modulation in the ENSO-rainfall teleconnection (Gershunov and Barnett, 1998).

The Madden-Julian oscillation (MJO), which is another major component of tropical atmospheric variability, refers to the large-scale intraseasonal atmospheric variability that is characterized by eastward propagation of convective systems along the Indian and Pacific oceans. In the Kelvin-Rossby paradigm, which is a widely accepted model for the MJO, its vertical structure is determined by the first baroclinic mode and its horizontal structure is determined by the planetary-scale response to a moving heat source (Houze et al., 2000). The equatorial plane of the MJO can be detected with the negative anomaly in outgoing long-wave radiation (OLR), which works as a proxy for deep tropical convection, or by using the zonal wind at the upper and lower troposphere, over Indian Ocean and Indonesia (Wheeler and Hendon, 2004).

The impact of the MJO is most prominent on monsoon systems around the globe, e.g. Australia, South Asia, West Africa, pan-American monsoons, and it also affects precipitation outside the monsoon regions and monsoon rainy seasons. The eastward propagation of the MJO has a major impact on Australian monsoon as the center of convection locates over the northern part of Australia and initiates the monsoon onset, accounting for more than 80 % of onset dates (Wheeler et al., 2009; Zhang, 2013). The onset of the South Asian monsoon tends to occur during the early phase of MJO when the convection starts over the Indian Ocean and is more affected by the northward propagation of the MJO which only appears during boreal summer (Zhang, 2013). The MJO is known to be closely related to the development of ENSO. The warm phase of ENSO indicated by warming in the eastern Pacific was found to be enhanced by MJO activities and their associated westerly winds by 6-12 months (Zhang and Gottschalck, 2002). Observations also suggest that the recent major ENSO warm phase events were preceded by anomalously strong MJO episodes (McPhaden et al., 2006).

The North Atlantic Oscillation (NAO) is the dominant mode of interannual variability in the Euro-Atlantic region during winter. It is characterized by the sea level pressure (SLP) difference between the Icelandic Low and the Azores

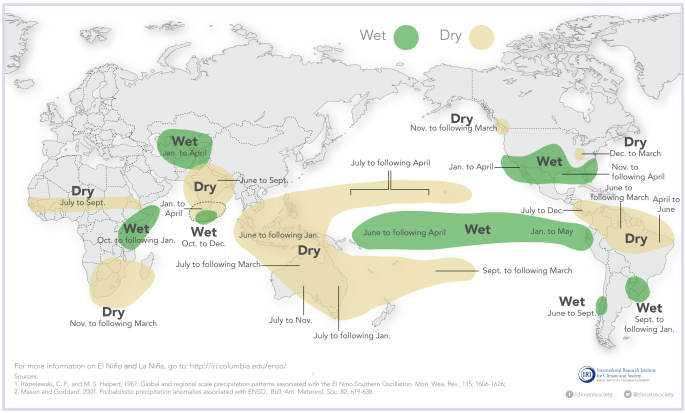

Figure 1.1: *Probabilistic precipitation anomalies associated with the warm phase of ENSO. From International Research Institute for Climate and Society, Earth Institute, Columbia University (http://iridl.ldeo.columbia.edu/maproom/)*

High. The positive (negative) NAO is defined with larger (smaller) SLP difference from the stronger (weaker) Icelandic Low and Azores High which causes stronger (weaker) westerlies. A positive NAO index corresponds to positive precipitation anomalies in northern Europe (western Scandinavia, Denmark, and northern parts of Ireland and Great Britain) and negative anomalies in southern Europe (the Iberian peninsula, and western Balkans) (HURRELL and VAN LOON, 1997; Wibig, 1999), and a negative NAO index generally corresponds to the switched signs of anomalies.

The Pacific North American pattern (PNA) is one of the most prominent modes of interannual variability in the mid-latitude Pacific which is most pronounced during winter, and it emerges as the second principal component of extra-tropical SLP in the northern hemisphere. The positive phase of the PNA is associated with positive precipitation anomalies in the Gulf of Alaska and Pacific Northwestern United States, negative precipitation anomalies over the upper Midwestern United States and an enhanced East Asian jet (Harding and Snyder, 2015).

Atmospheric blocking, a persistent high pressure system that can last days to weeks, occurs in mid-latitudes though the year but more frequently during spring and winter when the jet stream is stronger. It can occur when the dominant westerly flows are interrupted by meridional flows, and such interruption can be considered as a planetary wave breaking. A relationship between the blocking pattern and precipitation has been generally identified with a

decrease in precipitation at the centre of the blocked region where the high pressure is located and a slight decrease in the flanks of the blocks (Lenggenhager et al., 2018). Such a relationship was observed in different regions, e.g. in Europe (Sousa et al., 2017; Trigo et al., 2004; Yao and Luo, 2015) and South America (Rodrigues and Woollings, 2016). The impacts are featured as persistent wet or dry spells, which could lead to droughts and floods. A negative phase of both the NAO and PNA is strongly related to an increased frequency of atmospheric blocking in the Euro-Atlantic and mid-latitude Pacific regions (Croci-Maspoli et al., 2007; Scherrer et al., 2006).

Large scale variability in general circulation models (GCMs) is closely related to prediction of precipitation. Coupled simulations of GCMs generally show shorter cycles of ENSO ranging 1-3 years than observations (3-8 years) (Bellenger et al., 2014; Jha et al., 2014), with realistic amplitude of SST anomaly in Nino3 or Nino4 regions. For the MJO, most CMIP5 models were found to underestimate its amplitude detected with OLR and also its eastward propagation (Ahn et al., 2017). The two major modes in the northern extratropics, NAO and PNA, are generally well represented in CMIP5 models (Ning and Bradley, 2016). Several model experiments were conducted to quantify the sensitivity of precipitation to prescribed SST in different ocean parts. The Atmospheric Model Intercomparison Project (AMIP) was designed to systematically evaluate atmospheric GCMs and participating models were prescribed with observed monthly averaged SST and sea-ice distributions during the decade 1979-88 (Gates et al., 1999). Overall, in AMIP simulations, the global rainfall distribution and rain-rate frequency was found to resemble the observed but with less skill in the extratropcis (Lau et al., 1996).

1.3 Land-atmosphere interactions and precipitation

This section introduces land-atmosphere interactions that contribute to precipitation variability at smaller spatial scales and shorter time scales than the previous section has covered.

Soil moisture-precipitation feedback refers to the two-way coupling between soil moisture and precipitation. The main mechanisms behind this coupling can be explained with evaporative fraction (EF), and Figure 1.2 shows a conceptual framework of the feedback. Relationship A represents soil moisture-EF coupling in which the increase in soil moisture leads to an increase EF (also evapotranspiration) and subsequently causes a decrease in initial soil moisture anomaly. This coupling features more strongly in regions with a transitional soil moisture regime. [explain transitional regime] Relationship B, the EF-precipitation coupling, is the most uncertain part of the whole feedback loop as it involves a large number of processes. Due to different effects of EF on precipitation at varying spatial scales, the observational and modelling studies

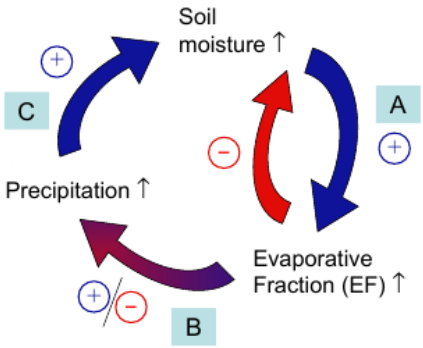

Figure 1.2: *Schematic description of soil moisture-precipitation coupling and feedback loop. Positive arrows (blue) indicate processes leading to a positive soil moisture-precipitation feedback (wetting for positive soil moisture anomaly, drying for negative soil moisture anomaly), the negative arrow (red) indicates a potential negative feedback damping the original soil moisture anomaly, and the red-blue arrow indicates the existence of both positive and negative feedbacks between evaporative fraction (EF) and precipitation anomalies. (A), (B), and (C) refer to the different steps of the feedback loop (see text). Modified from Seneviratne et al. (2010), adapted from Guillod et al. (2014).*

have reported both negative and positive signs of the coupling. Relationship C depicting higher precipitation leading to higher soil moisture, is considered as direct except for a few extreme cases where a large portion of precipitation input is partitioned into runoff due too oversaturated or extremely dry soils. In the following section, a more detailed description of soil moisture-precipitation coupling focusing on the processes involved in relationship B is presented.

As previously mentioned, soil moisture influences precipitation through EF via various processes. Soil moisture-precipitation coupling was first investigated with the concept of moisture recycling, quantified as the ratio of precipitation directly contributed by regional evapotranspiration (Dirmeyer et al., 2006; Eltahir and Bras, 1996; Trenberth, 1999; van der Ent et al., 2010), which is referred to as direct soil moisture-precipitation feedback. Indirect soil moisture-precipitation feedback was mainly investigated with two types of approaches which respectively focus on local coupling and induced mesoscale circulation, respectively. Local coupling refers to the influence of soil moisture conditions on boundary layer characteristics and convective initiation, and thereby, precipitation formation (Alfieri et al., 2008; Duerinck et al., 2016; Findell and Eltahir, 2003; Gentine et al., 2013; Guillod et al., 2014), and a positive feedback can appear when the increase of moisture is more critical for the cloud formation and precipitation, often under low stability in the free troposphere. A negative feedback corresponding to the local coupling usually appears when a strong stability barrier locates at the top of the planetary boundary layer, which requires larger sensible heat to allow sufficient turbulent mixing (Hohenegger et al., 2009). A radiative impact of albedo via an increase of net radiation on a wetter soil due to its darker color, and thus lower albedo, was also suggested as a main process in the local coupling but the impact was found to be limited (Seneviratne et al., 2010). Induced mesoscale circulation considers spatial soil moisture gradients (Taylor and Lebel, 1998) whereby heterogenous soil dryness induces a mesoscale atmospheric circulation leading to increased convergence over the drier region leads to convection (Taylor et al., 2012a, 2011), indicating a negative feedback (Figure 1.3). Finally, when strong gradients of soil moisture impact the atmospheric pressure and circulation, the coupling can also appear via large-scale circulation.

Vegetation affects precipitation through its regulation on surface energy and the water budget, which can be understood with the concept of moisture recycling mentioned in the previous section (Bonan, 2008; Spracklen et al., 2012). While the coupling between soil moisture and precipitation was mainly mediated through evapotranspiration, plant transpiration accounts for 45 % - 90 % of the continental evapotranspiration (Trenberth et al., 2007). The maintained atmospheric moisture through evapotranspiration returns to land as rainfall in the highly vegetated region, specifically in forests. On a regional and local scale, vegetation patterns can affect precipitation by affecting the

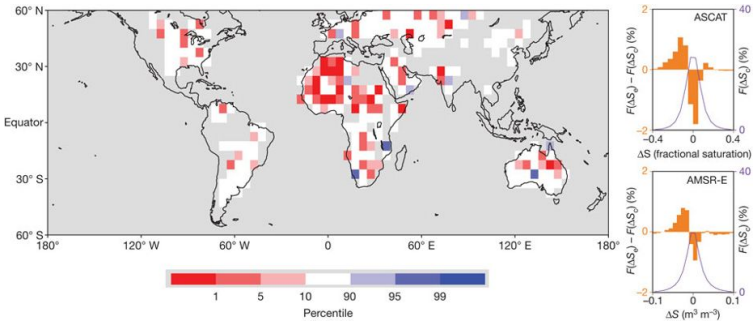

Figure 1.3: *Preference for afternoon precipitation over soil moisture anomalies. Low (high) percentiles indicate where rainfall maxima occur over locally dry (wet) soil more frequently than expected. Insets: frequency histograms of soil moisture difference in the global control sample (purple), and the difference between the histograms of the global event and global control samples (orange shading). Adapted from Taylor et al. (2012a).*

thermodyamic profile and development of the induced mesoscale circulation (Garcia-Carreras and Parker, 2011). These couplings could partially affect the soil moisture-precipitation feedback as soil moisture and vegetation are in general positively correlated.

The Global Land-Atmosphere Coupling Experiment (GLACE) is a modelling framework to investigate the strength of land-atmosphere coupling in GCMs and a series of modelling experiments were conducted under this framework, designed to assess the influence of soil moisture at different time scales on climate. In the GLACE-1 (Koster et al., 2004), 16-member ensembles of fully coupled, partially coupled, and uncoupled simulations were generated. The results of this first experiment highlighted the regions of strong land-atmosphere coupling (Figure 1.4) but with considerable spread across different models. In GLACE-2 (Koster et al., 2010), two sets of forecasts were compared, one with realistic initial land conditions from offline land model simulations and the other with randomly chosen initial land conditions. The GLACE-CMIP5 (Seneviratne et al., 2013) was designed to estimate long-term effects of soil moisture on climate compared to the two former experiments. Two sets of simulations were generated, additional to the fully coupled control simulation in one of which the seasonal cycle of soil moisture is prescribed as the 1971-2000 climatology and the other of which the seasonal cycle of soil moisture is prescribed as a transient climatology. In the former simulation, a main signal in precipitation appears as enhanced wet extremes in the tropics and in the latter, as decreased wet extremes in the tropics and enhanced dry extremes in Mediterranean and Australia (Lorenz et al., 2016).

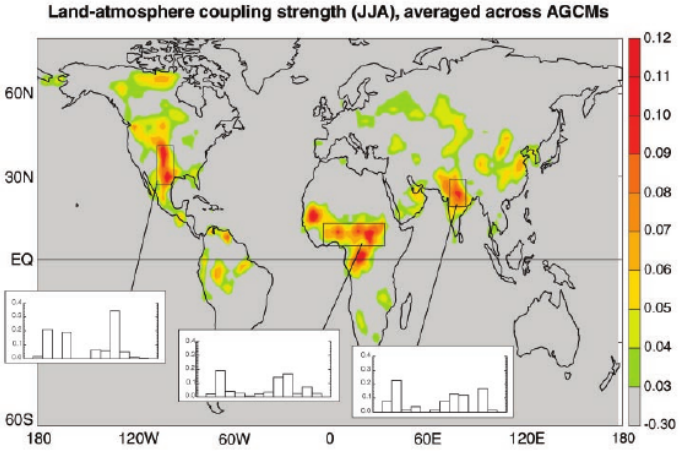

Figure 1.4: *The land-atmosphere coupling strength diagnostic for boreal summer (dimensionless, describing the impact of soil moisture on precipitation), averaged across the 12 models participating in the Global Land-Atmosphere Coupling Experiment (GLACE). (Insets) Areally averaged coupling strengths for the 12 individual models over the outlined, representative hotspot regions. No signal appears in southern South America or at the southern tip of Africa. Adapted from Koster et al. (2004).*

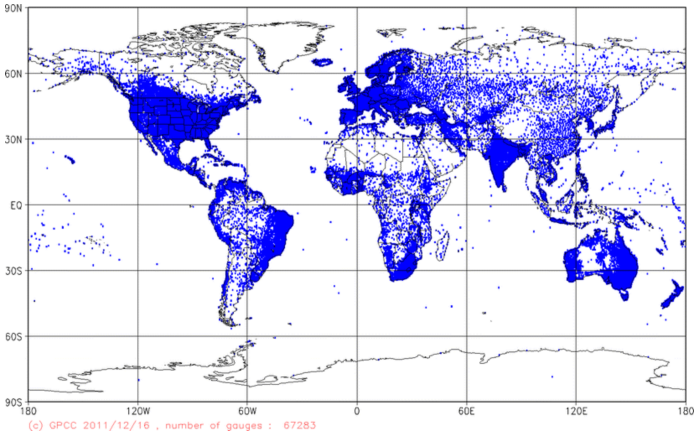

Figure 1.5: *Spatial distribution of 67,283 stations with precipitation climatology in the Global Precipitation Climatology Centre (GPCC) data set. Each dot indicates a single rain gauge. Adapted from Schneider et al. (2014)*

1.4 Observational uncertainty

Precipitation is one of few climate variables that has been monitored with extensive spatial and temporal coverage throughout the past century. Nevertheless, different types of observation-based precipitation products possess uncertainties inherited from each measurement device and data processing. Such uncertainties can be critical when using a certain precipitation product as a reference to evaluate models. In this section, different types of precipitation data are introduced and their uncertainties are discussed.

Interpolated stations Uncertainty in gridded precipitation data based on interpolated stations mainly originate from three sources, systematic errors from rain gauge measurements, stochastic sampling error, and residual error related to data homogeneity (Becker et al., 2013). The first type of error includes under-catch of precipitation due to wind, and can be particularly large for snowfall. The stochastic sampling error is largely due to sparse density of rain gauges, in regions such as desert areas, tropical forests, and in high latitudes. In these regions, the results are highly sensitive to interpolation methods. The residual error occurs when there is temporal discontinuation in the record. Different precipitation products apply quality control procedures to exclude stations with various criteria, including those mentioned. Figure 1.5 shows the spatial distribution of stations with long enough precipitation records (30 years or more), featuring ca. 67,200 stations overall.

Satellite observations Satellite-based precipitation measurements have contributed tremendously to the improved understanding of global precipitation climatology with their broad spatial coverage and regular scanning frequency. Spatial coverage and scanning frequency are determined by the type of satellite orbits. Satellite platforms are equipped with instruments measuring the properties of the atmosphere at a broad range of frequency bands. Visible and infrared sensors were on-board some of the earliest meteorological satellite missions and are used to mainly measure cloud-top temperatures. Precipitation can be retrieved based on an empirical relationship between surface precipitation and cloud coverage with cold tops over given time and/or space domains. This method is most suitable when convective precipitation systems are dominant as the amount of cold cloud is related to the amount of vertical uplift. Passive microwave sensors detect signals in the range between 10-85 GHz, where the lower range (< 20 GHz) dominantly detects the thermal emission of raindrops or rain-size particles and the higher range (> 60 GHz) detects the scattering of upwelling of radiation due to ice particles above the rain layer. Both empirical (Ferraro et al., 1996) and physically based (Kummerow and Giglio, 1994) retrieval algorithms can be applied to passive microwave measurements, and the latter is based on a radiative transfer model in which cloud and precipitation profiles are optimized to match with measurements from the passive microwave sensors. Different merging techniques have been developed, where measurements from different types of sensors complement each other. Satellite measurements are often calibrated with observations to provide better precipitation measurements (Kidd and Levizzani, 2011).

Reanalysis Reanalyses produce data sets of climate variables required for monitoring analysis of climate variability by assimilating irregularly distributed observations of various sources and model forecasts onto a common grid. Surface pressure, wind speed, and surface radiative fluxes are commonly assimilated variables. Uncertainties in precipitation reanalyses can be derived from errors in observations and models used in individual reanalyses. Precipitation uncertainty is specifically sensitive to changes in the input observation system, e.g. newly added observations have introduced series of jumps or shifts in precipitation trend in some reanalysis products like MERRA and ERA-Interim (Cui et al., 2017; Rienecker et al., 2011). Precipitation as an output of a reanalysis is known to be less constrained by observations than other variables and thus, might be similar to model outputs (Kalnay et al., 1996).

1.5 Sources of uncertainty in general circulation models

GCMs are used to simulate natural processes on the land, ocean, and atmosphere based on governing equations on the energy and mass conservation on a discretized grid system. Due to the complexity or lack of understanding of some processes and large computational cost, processes relevant for precipita-

tion are parameterized rather than explicitly resolved. In this section, sources of uncertainty in GCMs mainly regarding simulations of precipitation are introduced. Subsequently, commonly used ensemble approaches to cope with different sources of uncertainty in climate model predictions are introduced.

GCMs produce two types of precipitation, i.e. precipitation from stratiform (large-scale) and convective clouds, based on their respective parameterization schemes. In current GCMs, prognostic condensate schemes with bulk representation of microphysics, which assumes a functional form for the cloud particle size distribution and predicts one or more moments of the distribution, are commonly used (Morrison and Gettelman, 2008). Due to the coarse spatial resolution of GCMs, convection is represented with rather simplified parameterization of the actual process. The most commonly used approach for convection parameterization is the mass flux approach (Gregory and Rowntree, 1990; Tiedtke, 1989), some GCMs use the convective adjustment scheme (Betts, 1986) and the sub-grid plume and buoyancy-based scheme (Rio and Hourdin, 2008).

Errors in convection parameterization schemes have various impacts on aspects of simulated precipitation in GCMs. The intertropical convergence zone (ITCZ) pattern is highly dependent on the convection schemes as they determine the response of the convection to a given large-scale environment. Additionally, initial errors in the convection scheme such as too early rainfall compared to the observed diurnal cycle of precipitation could also lead to a larger fraction of rainfall evaporated into the atmosphere, and eventually reduce soil moisture (Lauer et al., 2018). A wrong representation of the soil moisture-precipitation feedback in GCMs can be attributed to convection parameterizations Hohenegger et al. (2009).

As mentioned earlier, different choice of the model configuration, such as physical assumptions and model resolutions, contributes to modeling uncertainty and error that limit their deterministic predictability. Several ensemble approaches are widely used to compensate such a limitation by exploring the uncertainties from different sources. A multi-model ensemble (MME) approach (weighted or non-weighted) is found to provide better prediction of climate than individual model performances (Stensrud et al., 2000; Weigel et al., 2008). However, individual models in the ensemble might share common systematic error and the sampling cannot span the full range of model configurations (Lambert and Allen, 2009). Another approach is to use ensemble of simulations with varying initial conditions from a single model (Kharin and Zwiers, 2002). As climate is a highly nonlinear system it has high sensitivity in responding to different initial conditions, which can be revealed by studying the initial-condition ensembles. Another approach to generate ensembles using different model physical parameterizations based on a single model. Aside from the shared core between ensembles, results from physical

perturbation ensemble (PPE) can be treated similarly with MMEs (Knutti et al., 2009).

1.6 Objectives and outline

Precipitation persistence at different time scales is affected by large-scale atmospheric variability and land-atmospheric interactions. Due to different responses of other climate variables to highly persistent dry or wet conditions, persistence characteristics should be investigated separately to frequency of precipitation, though highly related. This thesis therefore aims at a systematic evaluation of precipitation persistence in current GCMs, with the following leading research questions.

1. How is precipitation persistence at different time scales (e.g. daily, monthly, yearly) characterized in observations and climate models?
2. Which types of uncertainty are associated with GCM evaluations regarding precipitation persistence?
3. Do models show systematic errors in precipitation persistence? Are the errors consistent across different time scales? Which processes contribute to such errors?

This thesis consists of an introduction, followed by three chapters from two scientific research articles that are published (Chapters 2 and 4) and one to be submitted (Chapter 3), and conclusions and outlook are drawn in the last chapter. Three appendices refer to the three chapters, respectively.

Chapter 2 Drought Persistence Errors in Global Climate Models This chapter characterizes precipitation persistence at monthly and annual scales in multiple global observations and climate models using the Markov framework. While a general underestimation of GCMs in both dry and wet persistences at both time scales is found, an analysis of variance of the model errors suggests that some regions would require longer time series or a consistent observational reference to validate such underestimations.

Chapter 3 Intercomparison of daily precipitation persistences in multiple global observations and climate models This chapter characterizes precipitation persistence at the daily time scale in multiple global observations and climate models using the same Markov framework as in the previous chapter. As opposed to the results in Chapter 2, a general overestimation of both dry and wet persistence is found in GCMs, while a underestimation of interannual variability may provide a link for reasons behind the contrasting signs of the model errors.

Chapter 4 Soil moisture effects on afternoon precipitation occurrence in current climate models In this chapter, the sensitivity of afternoon rainfall occurrence on morning soil moisture condition is assessed with the aim to quantify soil moisture-precipitation coupling at the subdaily scale. Three different metrics adopted from previous studies are used to individually quantify the soil moisture-precipitation feedback regarding temporal, spatial and spatial heterogeneity perspective. While a large model spread is found for temporal and heterogeneity feedbacks, all models reveal a consistently positive spatial feedback.

2 Drought persistence errors in global climate models

published in *Journal of Geophysical Research: Atmospheres*,
doi:10.1002/10.1002/2017JD027577
Heewon Moon[1], Lukas Gudmundsson [1], Sonia I. Seneviratne[1]

Abstract *The persistence of drought events largely determines the severity of socioeconomic and ecological impacts, but the capability of current global climate models (GCMs) to simulate such events is subject to large uncertainties. In this study, the representation of drought persistence in GCMs is assessed by comparing state-of-the-art GCM model simulations to observation-based data sets. For doing so, we consider dry-to-dry transition probabilities at monthly and annual scales as estimates for drought persistence, where a dry status is defined as negative precipitation anomaly. Though there is a substantial spread in the drought persistence bias, most of the simulations show systematic underestimation of drought persistence at global scale. Subsequently, we analyzed to which degree (i) inaccurate observations, (ii) differences among models, (iii) internal climate variability, and (iv) uncertainty of the employed statistical methods contribute to the spread in drought persistence errors using an analysis of variance approach. The results show that at monthly scale, model uncertainty and observational uncertainty dominate, while the contribution from internal variability is small in most cases. At annual scale, the spread of the drought persistence error is dominated by the statistical estimation error of drought persistence, indicating that the partitioning of the error is impaired by the limited number of considered time steps. These findings reveal systematic errors in the representation of drought persistence in current GCMs and suggest directions for further model improvement.*

2.1 Introduction

The persistence of droughts is one of the main attributes that determines the level of their socioeconomic and ecological impacts (Bêche et al., 2009; Harou et al., 2010; Kelley et al., 2015). Lately, several studies have highlighted that

[1]Institute for Atmospheric and Climate Science, ETH Zürich, Zurich, Switzerland

climate models tend to underestimate drought persistence compared to the observational record (Ault et al., 2014; Wetter et al., 2014), which contributes to the uncertainty of future projections of drought risk. Furthermore, the characteristics of extremely prolonged droughts have been found to be similar over different time frames, including the twentieth century and longer paleoclimatic records (Ault et al., 2014). However, the driving mechanism of such droughts remains controversial and likely differs between individual events (Ault et al., 2014; Cook et al., 2015; Dai, 2011; Griffin and Anchukaitis, 2014; Shanahan et al., 2009; Stine, 1994). Thus, an in-depth assessment of the underestimation of drought persistence in current climate models in the recent past century may help to better understand similar issues found for longer time scales.

Measures of persistence (or memory) of drought events and related climate phenomena have been used to analyze drought variability in both models and observations. Commonly used measures include power spectra of the time series (Ault et al., 2014; Pelletier and Turcotte, 1997) or the Hurst exponent (Mandelbrot and Wallis, 1969) which have been used, for example, to measure long-term persistence in time series of drought indices (Tatli, 2015) or precipitation (Bunde et al., 2013; Kumar et al., 2013). By transforming continuous time series of drought indicators into categorical time series of dry and wet spells, the persistence of drought can be effectively estimated through the parameters of a binary first-order Markov chain model (Sericola, 2013). In this case the dry-to-dry transition probability (P_{dd}) is used as a measure of drought persistence (Jackson, 1975; Sharma and Panu, 2014; Wilby et al., 2015). The primary assumption for this measure is that the probability of drought and nondrought events is conditional only upon the previous time step. Interestingly, the dry spell length distribution can also be approximated by the geometric distribution given the assumption that the dry spell lengths that are estimated are binary sequences of independent trial results (in this case, drought and nondrought), and the probability of success (in this case, probability of drought) is equal for all the trials (Lee et al., 1986; Mathier et al., 1992).

Quantifications of drought persistence errors in a model ensemble are themselves subject to several sources of uncertainty, which include (i) uncertainty of the considered observations, (ii) uncertainty of the individual models, (iii) internal variability, and (iv) errors related to the statistical estimation of drought persistence (i.e., finite sample effects). Assessing the relative contribution of each of these sources to the total uncertainty will aid interpretation in a model validation exercise. Uncertainty in the observation-based data sets generally refers to the combination of observational errors and the uncertainty related to data processing methods which depend on the interpolation scheme, station density, and quality control tools (Xie et al., 1996) as well as the subset of selected stations. Previous studies that have assessed global climate models (GCMs) globally usually relied on a single observational data set as a reference and sometimes accounted for observational uncertainty in the analysis by

excluding the regions where observations were deemed unreliable. An alternative approach to account for observational uncertainty is to use independent observation-based data sets for the analysis and to investigate the associated spread. Model uncertainty can be characterized as the spread across different models, mainly generated from the discrepancy in their structure. Internal climate variability (or natural climate variability) corresponds to fluctuations generated in the climate system without changes in external forcing and can thus be approximated from the spread across initial condition ensembles of individual GCMs. Lastly, the fact that model evaluation is based on finite data sources leads to uncertainty in the statistical characterization of model performance. This statistical estimation error is often omitted in model validation studies, although it could affect the robustness of the analysis and hence also the conclusions.

In this study, we aim to investigate the ability of GCMs to simulate drought persistence, measured through the dry-to-dry transition probability (P_{dd}) in a Markov chain framework. Currently, a number of drought indicators are used in the scientific literature. Typically, these indices are tailored to specific types of analysis and are often categorized into meteorological (Keyantash and Dracup, 2002) hydrological (Tallaksen and van Lanen, 2004), or agricultural drought (Quiring and Papakryiakou, 2003). In addition, indicators like the Standardized Precipitation Index (McKee et al., 1993) or the Standardized Precipitation and Evapotranspiration Index (Vicente-Serrano et al., 2009) depend on the choice of a model distribution which in turn needs to be calibrated and is subject to uncertainty (Stagge et al., 2015). Finally, the choice of threshold to discriminate droughts from nondrought events is highly contextual and sometimes even subjective (Steinemann, 2014). Consequently, there is no single unifying drought definition, and the choice of drought indicator is usually dependent on the scope of individual assessments. Here we use precipitation anomalies as a drought indicator to separate dry (negative anomalies) from wet spells, which form the basis for estimating P_{dd}. The rationale underlying this decision is that precipitation is one of the climate variables that has been monitored with the best spatial and temporal coverage throughout the past century, and few additional assumptions are required (see section 3). In order to robustly assess the representation of P_{dd} in the models and to fully characterize the spread of the model error, we compare multiple observation-based data sets with a large ensemble of GCMs runs. Finally, we assess to which degree the spread in drought persistence error can be attributed to differences among models, observation uncertainty, internal variability, and the statistical estimation error of P_{dd} using an analysis of variance (ANOVA)-based approach. We close with a discussion on the link between the drought persistence error identified in this study to the issues found in precipitation variability and suggest potential implication of using the error partitioning method introduced in this study for the interpretation of climate model projections.

Table 2.1: *GCMs Used in This Study*

GCM	Institution (country)	Ensemble members
CanESM2	Canadian Centre for Climate Modeling and Analysis (Canada)	5
CCSM4	National Center for Atmospheric Research (United States)	6
CESM1-CAM5	National Science Foundation, Department of Energy, National Center for Atmospheric Research (United States)	3
CNRM-CM5	Centre National de Recherches Météorologiques / Centre Européen de Recherche et Formation Avancées en Calcul Scientifique (France)	5
CSIRO-Mk3-6-0	Commonwealth Scientific and Industrial Research Organisation in Collaboration with the Queensland Climate Change Centre of Excellence (Australia)	10
EC-EARTH	EC-EARTH Consortium	6
FIO-ESM	The First Institute of Oceanography, SOA (China)	3
GISS-E2-H	NASA Goddard Institute for Space Studies (United States)	5
GISS-E2-R		5
HadGEM2-ES	Met Office Hadley Centre (UK)	4
IPSL-CM5A-LR	Institut Pierre Simon Laplace (France)	4
MIROC5	Atmosphere and Ocean Research Institute, The University of Tokyo (Japan)	3
MPI-ESM-LR	Max Planck Institute for Meteorology (Germany)	3

2.2 Data

2.2.1 Precipitation From the Fifth Phase of Coupled Model Intercomparison Projects Model Simulations

With the international consensus on establishing global Coupled Model Intercomparison Projects (CMIP), there have been continued phases of CMIPs since the early 2000s. The GCM simulations of the fifth phase of CMIP (CMIP5; Taylor et al. (2012c)) include historical simulations for the period 1850-2005 and Representative Concentration Pathways experiments built according to different greenhouse gas concentration scenarios from 2006 onward. Here we consider historical simulations (1901-2005) and Representative Concentration Pathway 8.5 simulations (2006-2010) to cover the 1901-2010 period. Only models with at least three initial condition ensemble members were included in the analysis to account for internal variability (Table 2.1).

Table 2.2: *Observation-Based Data Set Used in This Study*

Observation-based data set	Data features	Provided resolution
CRU TS3.1	3,500-9,000 weather station records from CLIMAT	Monthly, $0.5^\circ \times 0.5^\circ$
UDEL	4,100-18,000 weather station records mainly from GHCN v2	Monthly, $0.5^\circ \times 0.5^\circ$
GPCC	11,000-49,450 gauge stations	Monthly,$0.5^\circ \times 0.5^\circ$, $1.0^\circ \times 1.0^\circ$, and $2.5^\circ \times 2.5^\circ$
20CR	Assimilating variable: surface pressure	Subdaily, daily, and monthly, $2^\circ \times 2^\circ$
ERA-20C	Assimilating variable: surface pressure, surface winds	Subdaily, daily, and monthly, approximately 128 km $\times$ 128 km

2.2.2 Interpolated Precipitation Observations and Reanalysis Products

To quantitatively assess the performance of the considered GCM simulations, five observation-based global precipitation data sets were selected, all covering at least the 1901-2010 time period (Table 2.2). The Climatic Research Unit Timeseries version 3.1 (Harris et al., 2014), University of Delaware version 3.0.1 (Matsuura and Willmott, 2012), and Global Precipitation Climatology Centre (Schneider et al., 2014) data are generated from interpolated station data, and each data product uses a different subset of available stations as well as different interpolation and quality control methods. In addition, we use the 20CR (20th Century Reanalysis; Compo et al. (2006)) and the European Centre for Medium-Range Weather Forecasts twentieth century reanalysis (Poli et al., 2016), which assimilate different variables and differ both with respect to the underlying models and assimilation schemes.

2.3 Methods

2.3.1 Quantifying Drought Persistence

To quantify drought persistence, we convert observed and modeled precipitation values into binary time series indicating dry (negative) and wet (positive) anomalies. For annual time series anomalies are computed by subtracting the linear trend (least squares estimate). For the monthly resolution, the series were first detrended using linear least squares regression. Subsequently, the long-term mean of each month was removed from the detrended time series. Drought persistence is then measured through the dry-to-dry transition probability P_{dd}, which is defined as the proportion of dry-to-dry transition out of all transitions from a dry status. The theoretical minimum of P_{dd} is 0.5 by construction as this value indicates a white noise system without memory (unless there is a tendency to systematically have wetter conditions after dry conditions). In a few cases P_{dd} values estimated from observed or simulated climate variables are slightly below the theoretical minimum, which can be explained by the sampling uncertainty. In the analyses, we consider both month-to-month and year-to-year transitions. In addition to the dry-to-dry

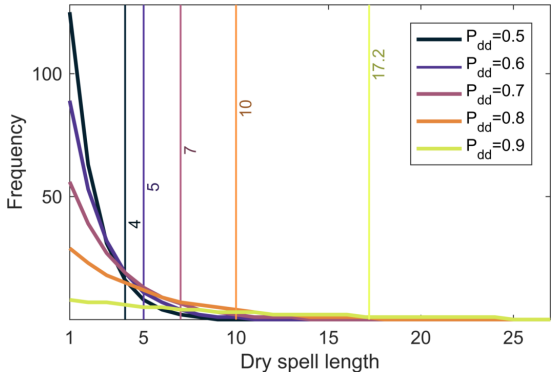

Figure 2.1: *Dependence of the dry spell length frequency distribution on different P_{dd} values with constant P_{ww} (0.5). Vertical lines indicate the 90th percentile of the distributions for different P_{dd} values. The unit of x axis (dry spell lengths) is omitted as it varies depending on the temporal scale, for example, months for monthly time series and years for annual time series.*

transition probability P_{dd}, also dry-to-wet (P_{dw}), wet-to-wet (P_{ww}), and wet-to-dry (P_{wd}) transition probabilities can be estimated from the time series. The transition probabilities are related to each other such that P_{dd} = 1 - P_{dw} and P_{ww} = 1 - P_{wd}, implying that the dynamics of the binary series can be captured by two parameters only. Under a first-order Markov chain assumption, these transition probabilities can then be used to simulate stochastic ensembles resembling the original binary time series, which in turn can be used to generate estimates of the dry spell length distribution. The statistical simulation of a Markov chain is conducted by first taking a random initial status (either dry or wet) of which subsequent statuses are determined based on the prior status and the corresponding transition probabilities derived from the original time series. The process is repeated until the length of constructed binary time series equals the length of the original time series. To facilitate the interpretation of the persistence metric (P_{dd}), Figure 2.1 shows how the drought length distribution depends on the value of P_{dd}. For constructing this figure, 1,000 time steps were considered for the statistical simulation of binary time series with a constant P_{ww} value of 0.5. For each P_{dd} value, the statistical simulation was repeated 1,000 times and median of the simulated samples was taken as the best estimates of dry spell length distributions. Dry spell lengths at 90th of each distribution are also presented, which increase with increasing P_{dd}.

Figure 2.2 shows an example of an annual precipitation anomaly time series at a grid cell in Eastern Europe from the Climatic Research Unit Timeseries version 3.1 data together with the dry spell length distribution derived from

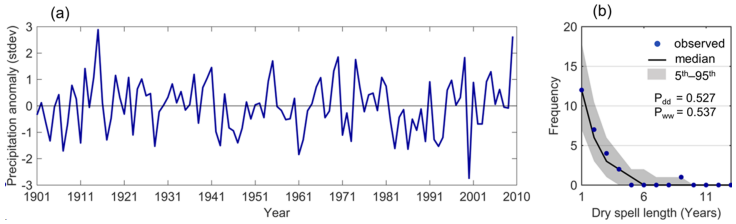

Figure 2.2: *(a) Precipitation anomaly for 1901-2010 at a randomly chosen grid cell in Eastern Europe. The time series is taken from the Climatic Research Unit Timeseries version 3.1 data set. (b) Dry spell length distribution derived from the observed time series and median and 5th to 95th uncertainty range of 300 dry spell length distributions from statistical simulation of Markov chain.*

the time series with the uncertainty range obtained by statistical simulation. P_{dd} and P_{ww} estimated in this grid cell are also provided for better understanding of the conversion between Markov chain parameters and dry spell length distribution. More examples in different regions are presented in Figure A.1.

To assess whether the Markov chain model and thus also the dry-to-dry transition probability (P_{dd}) later used for model validation are reasonable approximations for observed and modeled dry spell length distributions, a two sample Kolmogorov-Smirnov (KS) test was conducted to compare dry spell length distributions derived from the original time series to those derived from statistical simulation. For doing so, the previously described statistical simulation was repeated 1,000 times and the median of the bootstrapped distribution (black line in Figure 2.2b; gray shading corresponds to the range spanned by the individual simulations) compared with the observed or modeled dry spell length distributions using the KS test with a 0.05 significance level. Failure to reject the null hypothesis of equal distributions indicates that the Markov chain (and thus P_{dd}) is a reasonable approximation of the observed and modeled dry spell length distributions. Figure 2.3 shows the total number of cases at which the KS test rejects the null hypothesis that observed and modeled dry spell length distributions can be approximated with a Markov chain model at the monthly time scale. For observation-based data sets, there are no cases of rejection in most of the regions while a few grid cells located in Sahara, Northeast Brazil, and Southeast Asia have one to five cases of rejection out of five observation-based data sets indicating that the dry spell length distribution is not well presented with Markov chain model in the respective regions. For model simulations, the spatial distribution of rejections is similar to the observation-based estimates, with one to six cases out of 63 model simulations in the same region, which in this case confirms the reliability of the Markov

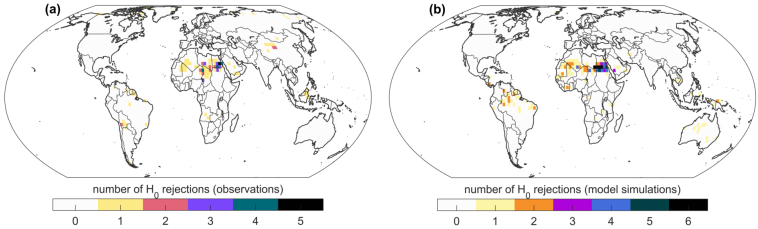

Figure 2.3: *Assessment of the suitability of the Markov-chain assumption for approximating observed (a) and modeled (b) dry spell length distributions. Shown are the number of cases at which a two-sample Kolmogorov-Smirnov test rejects the null hypothesis that the observed (a) or modeled (b) dry spell length distribution can be approximated by a first-order Markov chain.*

chain assumption. At the annual time scale, there were no cases of rejection for model simulations and less than 10 grid cells had one to two rejections for observations (thus not shown in the figures).

Uncertainty in P_{dd} estimation is related to the finite number of samples in the observed and modeled time series at both time scales, and it is critical to assess whether this uncertainty substantially affects the model validation results. To quantitatively assess the uncertainty due to finite sample size, which also can be referred to as statistical estimation error, we generate the uncertainty distribution of P_{dd} using parametric bootstrapping (Basawa et al., 1990; Efron and Tibshirani, 1994). In each grid cell, 1,000 samples of binary time series are generated through statistical simulation under Markov chain assumption (described in the previous paragraph of this chapter) based on the P_{dd} and Pwd parameters estimated from the original time series. P_{dd} is then calculated for each statistical ensemble member, resulting in the uncertainty distribution for each P_{dd} estimate from the observational data and the ensemble runs of the GCMs. The bth bootstrapped sample of P_{dd} from observation o can be denoted as $P_{dd\ \ ob}$ and from ensemble r in model m as $P_{dd\ \ mrb}$. We compute the drought persistence error of ensemble r in model m against observation o as

$$E_{omrb} = P_{dd\ \ mrb} - P_{dd\ \ ob} \tag{2.1}$$

so that the uncertainty range of the estimated error can be spanned by the differences between bootstrapped samples from the observations and the models.

2.3.2 Partitioning the Spread of the P_{dd} Error

To investigate the respective roles of the sources of uncertainty on the drought persistence error, we aim at partitioning the spread of E_{omrb}. For doing so, we adapt a methodology that has been previously used to partition the spread in climate model projections (Hawkins and Sutton, 2009; Orlowsky and Seneviratne, 2013), with modifications that allow to account for observation uncertainty and the statistical estimation error of P_{dd}. Using an ANOVA-based approach, we aim to quantify the relative contribution of (i) differences among observational products, (ii) differences among climate models, (iii) internal climate variability, and (iv) statistical estimation uncertainty of P_{dd} to the total spread of E_{omrb}. As ensemble members are subordinate to the models and bootstrapped samples are subordinate to the ensemble members and observations (Figure 2.4), we apply a crossed and nested ANOVA (Krzywinski et al., 2014). A schematic of the partitioning is shown in Figure 2.5. This approach partitions the total sum of squares of E_{omrb} (SS_t) into model uncertainty (SS_m), observation uncertainty (SS_o), internal variability (SS_i), and sampling error (SS_s) as

$$SS_t = SS_o + SS_m + SS_i + SS_s = \sum_{o=1}^{N_o}\sum_{m=1}^{N_m}\sum_{r=1}^{R_m}\sum_{b=1}^{N_b}(E_{omrb}^2) - cf \qquad (2.2)$$

where N_o is the number of observation data sets, 5, N_m is the number of models, 13, R_m is the number of ensemble members available for each model m, minimum 3 to maximum 10 (Table 2.1), and N_b is the number of bootstrapped samples per observation or model, 1000. We introduce the correction factor (cf) defined as

$$cf = (\sum_{o=1}^{N_o}\sum_{m=1}^{N_m}\sum_{r=1}^{R_m}\sum_{b=1}^{N_b}E_{omrb})^2/N_t \qquad (2.3)$$

to correct the sum of squares of nonnested factors (Crawley, 2005) by subtracting it from the raw sum of squares of average error of each observation ($\overline{E_{o...}^2}$) and model ($\overline{E_{.m..}^2}$) to adjust them as deviations from the total mean as

$$SS_o = N_s N_b \sum_{o=1}^{N_o}\overline{E_{o...}^2} - cf \qquad (2.4)$$

and

$$SS_m = N_o N_b \sum_{m=1}^{N_m} R_m \overline{E_{.m..}^2} - cf \qquad (2.5)$$

where N_s is total number of model simulations, $\sum R_m$, and N_t is the total number of E_{omrb} calculated as $N_o N_b N_s$. Note that for SS_i, additional terms

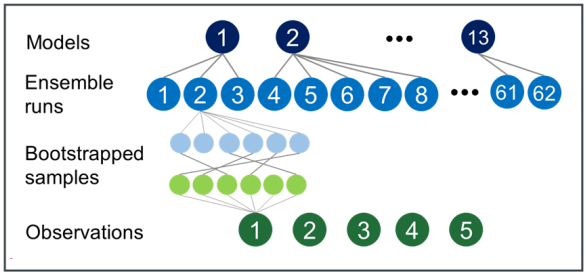

Figure 2.4: *Hierarchical structure of drought persistence (P_{dd}) error.*

are subtracted from the raw sum of squares of average error of each ensemble simulation to account for the hierarchical structure of the problem.

$$\begin{aligned} SS_i &= N_o N_b \sum_{m=1}^{N_m} \sum_{r=1}^{R_m} \overline{E^2_{.mr.}} - (SS_m + cf) \\ &= N_o N_b \sum_{m=1}^{N_m} \sum_{r=1}^{R_m} \overline{E^2_{.mr.}} - N_o N_b \sum_{m=1}^{13} \overline{E^2_{.m..}} \end{aligned} \tag{2.6}$$

SS_s is calculated as the sum of squared deviations of bootstrapped samples from average error of each ensemble simulation against each observation or as a residual sum of squares

$$SS_s = SS_t - N_b \sum_{o=1}^{N_o} \sum_{m=1}^{N_m} \sum_{r=1}^{R_m} \overline{E^2_{omr.}} = SS_t - SS_m - SS_o - SS_i \tag{2.7}$$

2.4 Results

2.4.1 Observed Global P_{dd} Patterns

Figure 2.6 shows the mean dry-to-dry transition probability (P_{dd}) over all observational data sets at each grid cell around the world for both monthly and annual time scales. At the monthly scale, global mean P_{dd} is 0.62 (with [0.58, 0.65] interquartile range) and at annual scale global mean P_{dd} is 0.57 (with [0.54, 0.60] interquartile range). The global means of observed maximum dry spell lengths are 19.1 months and 8.9 years for each time scale.

Monthly and annual P_{dd} values display clear different spatial patterns (Figure 2.6), indicating that monthly persistence does not necessarily propagate

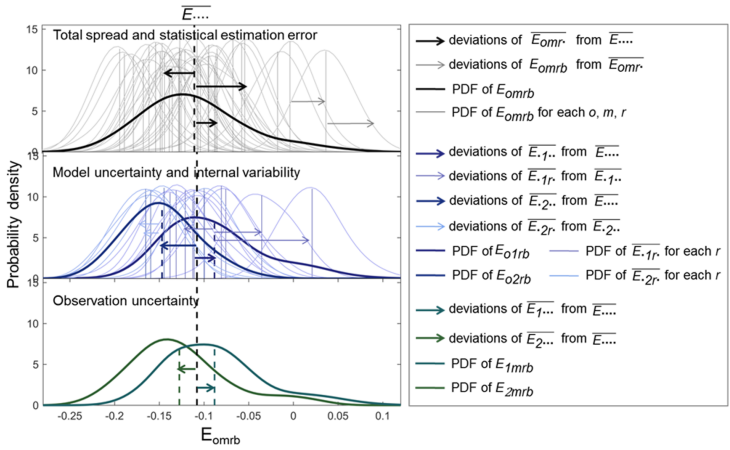

Figure 2.5: *Schematic of partitioning the spread in the error, for the case N_m = 2, N_o = 2, R1 = 5, R2 = 6, and N_b = 30. See text for details and definitions.*

linearly to the yearly persistence. Some of the desert areas, for example, Sahara, Gobi, and Atacama, are commonly recognizable in both temporal scale with larger P_{dd} values. The results of KS test (Figure 2.3) also suggest higher uncertainty in P_{dd} estimation in Sahara.

2.4.2 Drought Persistence Error of CMIP5 Model Simulations

Figures 2.7a and 2.7c show the drought persistence error (E_{omrb}) averaged over all observational data sets and all model simulations. Overall, the models tend to underestimate P_{dd} at both monthly and annual scales, a feature that is particularly pronounced in western North America, western South America, Africa, and Northeast Asia. In around 40% of the land grid cells (38.9% at monthly scale and 37.9% at annual scale) at least 80% of the model simulations agree on the negative sign of E_{omrb}. For the positive sign, the same percentage of agreement was only found in 2.7% of the land grid cells at monthly scale and 1.5% at annual scale. Figures 2.6b and 2.6d show the global distribution of E_{omrb} and for each observational data set. For all considered observational data sets the tendency of the models to underestimate drought persistence is visible, but it should be noted that 20CR has stronger drought persistence at annual scale and suggests even larger negative drought persistence biases in the climate models than when using other reference data sets. It should be noted for this result that 20CR relies on less direct observations than the other considered products (see Table 2.2). The "drizzle problem", where GCMs overestimate the number of days with light rainfall (Dai, 2006), might contribute to

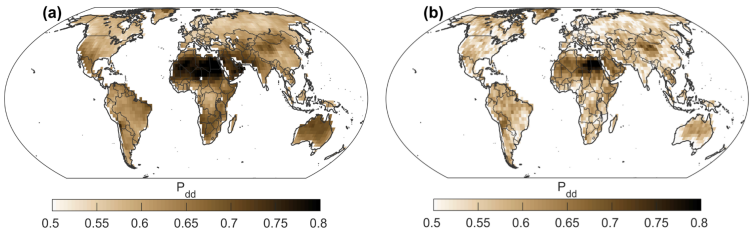

Figure 2.6: *Mean drought persistence (Pdd) estimated from five observation-based data sets for 1901-2010 at (a) monthly and (b) annual scales.*

the larger biases found in desert regions.

Although the mean drought persistence bias indicates that the considered climate models tend to underestimate drought persistence, there are a few regions in which overestimation of P_{dd} is found. This is most pronounced at the monthly scale in the Arabian Peninsula and India, and there is a tendency for overestimation in the Mediterranean, southeastern South America, South Australia, and Southeast Asia. South Australia and India also show overestimation in annual P_{dd}.

Additionally, most of these regions also show underestimation of wet persistence (P_{ww}) (Figure A.2), which indicates that models are generally underestimating persistence of both dry and wet anomalies, at monthly and annual time scales.

Figure 2.8 shows the mean drought length bias at the 95th percentile of the dry spell length distribution, estimated on the multisimulation and observation mean P_{dd}. For doing so the observed and modeled dry spell length distributions were estimated on the basis of the multi-observation and multi-simulation mean P_{dd} and P_{ww} values (using statistical simulation; see section 2.3). Subsequently, the difference between the observed and the modeled dry spell length distribution at the 95th percentile was calculated. The spatial distribution of drought length bias generally follows the pattern of the drought persistence bias in Figure 2.7. At monthly scale, the strongest underestimation in drought length (up to 5 months) is found in Sahara. Substantial overestimation of drought length in Arabian Peninsula and India is also noticeable. The spatial pattern at annual scale is rather homogenous over all regions. Considering the scale difference, drought length bias at annual scale is considerably smaller than monthly, unlike the larger persistence bias (Figure 2.7) which is related to the generally smaller values of P_{dd} at annual scale. Drought length

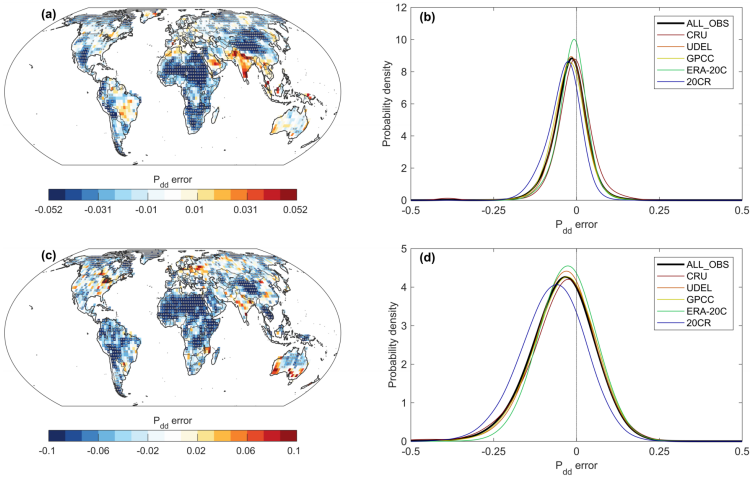

Figure 2.7: *Spatial distribution of multi-simulation mean drought persistence error (E_{omrb}) for (a) monthly and (c) annual scales. Stippling indicates agreement in the sign of drought persistence error among more than 80% of the model simulations. Global distribution of drought persistence error for (b) monthly and (d) annual scales. CRU = Climatic Research Unit Timeseries version 3.1; UDEL = University of Delaware; GPCC = Global Precipitation Climatology Centre; ERA-20C = ECMWF twentieth century reanalysis; 20CR = twentieth century reanalysis.*

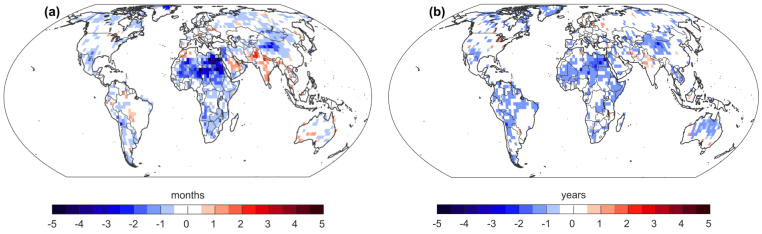

Figure 2.8: *Spatial distribution of multi-simulation mean drought length bias against observed mean drought length at 95th percentile for (a) at monthly scale and (b) at annual scale.*

biases at other percentiles are presented in Figure A.3.

Figures 2.9a and 2.9c show the standard deviation of model error at monthly and annual scales. While the spread of E_{omrb} at monthly scale is only large in a few regions (e.g., Amazon, central Andes, Tibetan Plateau, and Sahara), most of the regions show substantial spread in E_{omrb} at annual scale. To compare the relative magnitude of spread against the magnitude of multi-simulation mean bias, the coefficient of variation is calculated (Figures 2.9b and 2.9d). In many regions, the absolute value of the coefficient exceeds 1, which indicates that the standard deviation is larger than the mean of E_{omrb}. Nevertheless, pronounced underestimation can be confirmed at monthly scale, in western North America, central, and South Africa, and at annual scale, in Greenland, western South America, Tibetan Plateau, and mainland Southeast Asia, while there are only few grid cells with mean overestimation larger than the spread.

2.4.3 ANOVA of Drought Persistence Error

As a substantial spread in the drought persistence error is found, we apply the ANOVA-based partitioning to quantitatively assess the relative contribution from the four possible sources of uncertainty to the total spread (see section 2.5.2). Figure 2.10 shows the spatial patterns determined by the relative contribution from, which are observation uncertainty, model uncertainty, and internal variability, where contribution from the statistical estimation error is only used for indicating reliability of the partitioning. Interestingly, the overall spatial patterns clearly differ depending on the considered time scale. The spread in monthly drought persistence error is mostly related to differences among the considered observational products and model uncertainty, except

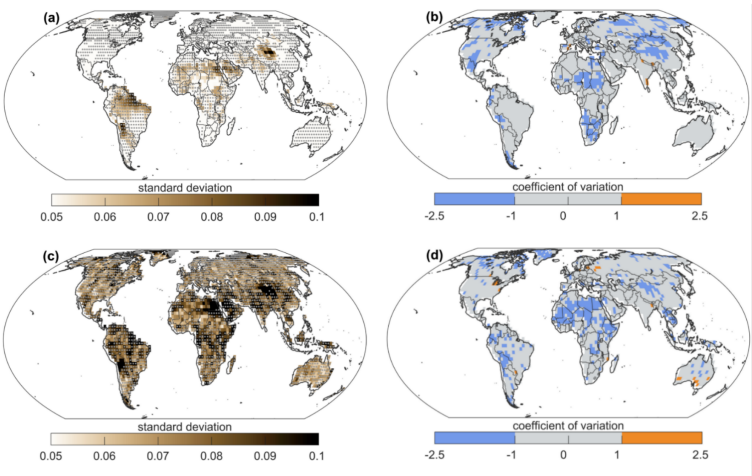

Figure 2.9: *Standard deviation of drought persistence error at (a) monthly and (c) annual scales and grid cells at which the coefficient of variation E_{omrb} is larger or smaller than one for the (b) monthly and (d) annual scales. Stippling in (a) and (c) indicates regions with absolute value of coefficient of variation less than 1.*

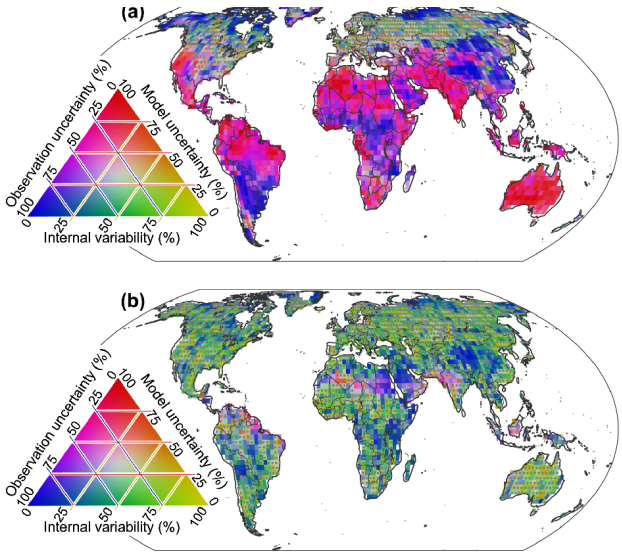

Figure 2.10: *Partitioning the spread of the drought persistence error (E_{omrb}) into model uncertainty, observation uncertainty, and internal variability for (a) monthly and (b) annual scales. Stippled areas indicate that the summated contribution from the other sources is smaller than contribution from statistical estimation error.*

for high-latitude regions. Dominant contributions from model uncertainty are especially pronounced in western North America, Amazon, Northeast Brazil, Algeria, India, and Australia. Even some regions with scarce ground measurements, for example, Sahara, Amazon, and Australia, show similar or even higher contributions from model uncertainty to the spread in E_{omrb} at the monthly time scale, although a higher contribution of observation uncertainty might have been expected. In southern South America, central Africa, Arabian Peninsula, and East Asia, observation uncertainty is dominating to the total spread. Interestingly, a large spread among observation-based data sets for monthly precipitation in North Africa and Arabian Peninsula and other low-precipitation regions was reported in a previous study (Tanarhte et al., 2012). In contrast, the spread in annual drought persistence error is dominated by a combination from observation uncertainty and internal climate variability. In the Arabian Peninsula, Eastern Africa, and the Tibetan Plateau, observation uncertainty is more pronounced. Note, however, that for the annual scale, the statistical estimation error is larger than the sum of the relative contribution of all other sources of uncertainty at most locations, indicating that most of the spread (Figure 2.9c) is caused by finite sample effects.

Figure 2.11 shows the global distribution of the contributions from each

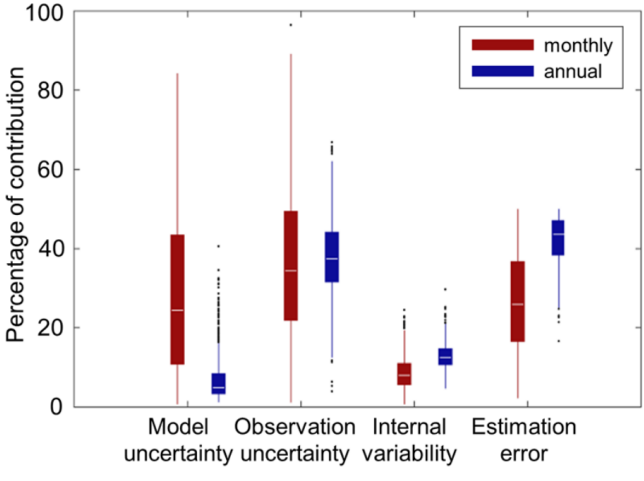

Figure 2.11: *Box plots showing global distribution of contribution from each source of uncertainty to the total spread of drought persistence error for monthly (red) and annual (blue) scales. Each box represents the interquartile range, and the median is shown as white line. The whiskers show the range (25th quantile - 1.5·IQR, 75th quantile +1.5·IQR), and values outside this range are indicated as dots.*

source to the total spread in drought persistence error. At the monthly scale, overall contribution from observational and model uncertainty is clearly larger than that from internal variability. At the annual scale, the median of the contribution from statistical estimation error is larger than any other source, implying that the partitioning is unreliable in most of the regions (Figure 2.10b). In addition, a substantially lower contribution from model uncertainty is also noticeable at the annual scale.

2.5 Discussion

2.5.1 Drought Persistence Error

While previous studies have highlighted the underestimation of interannual to multidecadal precipitation variability in current climate models (Ault et al., 2012; Dai, 2006; Kumar et al., 2013), we investigated here whether state-of-the-art climate models capture meteorological drought persistence at shorter time scales. We find a systematic underestimation of the persistence of drought at both the monthly and annual scales in the considered CMIP5 models, when compared to five observational reference products over the 1901 to 2010 time

frame. This underestimation is clear, despite the large spread in drought persistence error, which is in many regions attributable to observational uncertainty. Consequently, this study complements previous research (Ault et al., 2014; Wetter et al., 2014) by showing that the underestimation of drought persistence already occurs if year-to-year or month-to month variability is considered.

Overall, the climate models' ability to simulate precipitation variability at long time scales is likely related to the representation of tropical sea surface temperature and El Niño-Southern Oscillation variability in the GCMs, as previously suggested (Meinke et al., 2005; Schubert et al., 2016). Consequently, it is not unlikely that drought persistence in current climate models also depends on how well large-scale ocean-atmosphere variability is represented. On shorter time scales, the general underestimation of drought persistence shown in this study could possibly be attributed to issues in the representation of land-atmosphere couplings, such as the soil moisture-precipitation coupling at the regional scale (Guillod et al., 2015; Koster et al., 2006; Orlowsky and Seneviratne, 2010; Taylor et al., 2012a). Consequently, the differences in the spatial distribution of the drought persistence error at monthly and annual time scales identified in this study might be related to differences in the governing processes. However, to which degree this is the case and how errors on short time scales (e.g., day to day) translate to errors on long time scales (e.g., year to year) remains to be investigated.

2.5.2 Partitioning the Spread in the Drought Persistence Error

While the considered GCMs display a systematic underestimation of drought persistence, the range of underestimation spanned by these models and by the observational data sets is substantial. To further investigate this issue, we developed an ANOVA-based approach that allows to partition the contribution of unprecise observations, differences among climate models, internal climate variability, and statistical uncertainty to the total spread in the drought persistence error. The partitioning method applied in this study is motivated by an approach that is used to partition the uncertainty in future climate projections into model uncertainty, scenario uncertainty, and internal variability (Addor et al., 2014; Hawkins and Sutton, 2009; Orlowsky and Seneviratne, 2013; Taylor et al., 2012b). In this study, we expand this framework for the model validation task. To this end, we incorporated observation uncertainty together with the statistical estimation error of E_{omrb} into the existing framework. The analysis showed that both observational uncertainty and the statistical estimation uncertainty can play a significant role in climate model validation.

The results of the partitioning of the spread in the drought persistence error have interesting implications both for future model validation studies and for model development. On the one hand, the analysis highlights that differences among the considered climate models are in many cases larger than the uncertainty of observations, highlighting the potential of future model development. On the other hand, the analysis also shows that issues with the

considered observational data products (especially in data scarce regions) as well as finite sample effects (annual time scale) can impair the model validation exercise. Consequently, the results highlight the importance of considering the latter uncertainties in future model validation studies. Furthermore, the partitioned spread in this study might be used to assess the efficiency of model selection based on observational constraint for reducing the model spread in future projections (Cox et al., 2013; Hall and Qu, 2006). The efficiency is expected to be higher in the regions where the range of observation uncertainty is substantially narrower than the model uncertainty.

2.6 Conclusions

Persistent meteorological drought triggers subsequent drying of other hydrological variables on land (Van Loon, 2015) such as soil moisture or water storage, which can, for example, have strong impacts on vegetation (Nicolai-Shaw et al., 2017) and regional temperature (Seneviratne et al., 2010). In this study, we investigated how well current generation GCMs represent drought persistence over the twentieth century and the recent past. For doing so we focused on meteorological drought and compared dry-to-dry transition probabilities (P_{dd}) at yearly and monthly time scales of an ensemble of simulations from the CMIP5 archive with observational data sets (interpolated observations and reanalyses). Overall, the results highlight that the considered models tend to underestimate drought persistence at monthly and annual time scales. This is an interesting addition to previous results (Ault et al., 2014; Kumar et al., 2013), which indicate that CMIP5 models underestimate the risk of prolonged droughts on multidecadal time scales.

To investigate the substantial spread in the drought persistence error, we develop a new methodology to effectively partition the spread into its main components, which include (i) observation uncertainty, (ii) model uncertainty, (iii) internal variability, and (iv) statistical estimation error of the considered validation metric. At the monthly time scale, observation uncertainty (which is often neglected in model validation studies) and model uncertainty are the main contributors to the total spread. At annual time scales, the statistical estimation error is dominant in most regions, followed by combined contributions from internal variability and observational uncertainty. This analysis reveals regions where improvements of GCMs or model selection can substantially reduce the spread of model uncertainty. Reducing uncertainty of drought simulations is important for improving drought projections in a changing climate.

Acknowledgements This research was funded by the ERC DROUGHT-HEAT project (contract 617518). We acknowledge the World Climate Research Programme's Working Group on Coupled Modeling, which is responsible for CMIP, and we thank the climate modeling groups (listed in Table 2.1 of this paper) for producing and making available their model output. For CMIP the U.S.

Department of Energy's Program for Climate Model Diagnosis and Intercomparison provides coordinating support and led development of software infrastructure in partnership with the Global Organization for Earth System Science Portals. We thank Jan Sedlacek and Urs Beyerle for the retrieval and preparation of CMIP5 model data. We also acknowledge the providers of precipitation data of the following products: GPCC (http://gpcc.dwd.de), CRU TS (https://crudata.uea.ac.uk/cru/data/hrg/), UDEL (http://climate.geog.udel.edu/ climate/), 20CR (https://www.esrl.noaa.gov/psd/data/20thC_Rean/), and ERA-20C (http://apps.ecmwf.int/datasets/).

3 Intercomparison of daily precipitation persistence in multiple global observations and climate models

in review in *Environmental Research Letters*
Heewon Moon[1], Lukas Gudmundsson [1], Benoit P. Guillod [2], Venugopal V.[3], Sonia I. Seneviratne[1]

Abstract *Daily precipitation persistence is affected by various atmospheric and land processes and provides complementary information to precipitation amount statistics for understanding the precipitation dynamics. In this study, daily precipitation persistence is assessed in an exhaustive ensemble of observation-based daily precipitation datasets and evaluated in global climate model (GCM) simulations for the period of 2001 - 2013. Daily precipitation time series are first transformed into categorical time series of dry and wet spells with a 1 mm/day precipitation threshold. Subsequently, P_{dd} (P_{ww}), defined as the probability of a dry (wet) day to be followed by another dry (wet) day is calculated to represent daily precipitation persistence. The analysis focuses on the long-term mean and interannual variability of the two indices. Both multi-observation and multi-model means show higher values of P_{dd} than P_{ww}. GCMs overestimate P_{ww} with a relatively homogeneous spatial bias pattern. They overestimate P_{dd} in the Amazon and Central Africa but underestimate P_{dd} in several regions such as southern Argentina, western North America and the Tibetan Plateau. The interannual variability of both P_{dd} and P_{ww} is generally underestimated in climate models, but more strongly for P_{ww}. Overall, our results highlight systematic model errors in daily precipitation persistence that are substantially larger than the already considerable spread across observational products. These findings also provide insights on how precipitation persistence biases on daily time scale relate to well-documented*

[1]Institute for Atmospheric and Climate Science, ETH Zürich, Zurich, Switzerland
[2]Institute for Environmental Decisions, ETH Zürich, Zurich, Switzerland
[3]Centre for Atmospheric and Oceanic Sciences & Divecha Centre for Climate Change, Indian Institute of Science, Bangalore

persistence biases at longer time scales in state-of-the art global climate models.

3.1 Introduction

Daily precipitation persistence on land is regulated by various regional weather features, such as atmospheric blocking (Sousa et al., 2017), mesoscale convective systems (Tuttle and Davis, 2006), and monsoon (Trenberth et al., 2000), that are often under the influence of large-scale modes of climate variability which is governed by sea surface temperature (SST) variability (Chang et al., 2000; Hoy et al., 2014; Krishnan and Sugi, 2003; Kushnir et al., 2010; Power et al., 1999) or, in some regions to the similar degree by land processes (Koster et al., 2004; Langford et al., 2014; Matsui et al., 2003; Small, 2001; Tuttle and Salvucci, 2016). Prolonged dry or wet spells spanning from several days to weeks, as a result of all such processes that affect daily precipitation dynamics can have considerable impacts on agricultural productivity (Dash et al., 2009; Groisman and Knight, 2008; Laux et al., 2010; Seleshi and Zanke, 2004) and thus, on human society. Hence daily precipitation persistence is an important criteria for evaluating precipitation data sets and models regarding their ability to capture or simulate precipitation dynamics. Still, there is the lack of evidence on how observations characterize daily precipitation persistence globally and how global climate models (GCMs) simulate it.

Only a few studies have focused on analyzing daily precipitation persistence in observations, and they are often very regional and mainly investigate changes in the daily precipitation persistence. Changes in precipitation persistence associated with change in the intensity of extreme rainfall were identified in the northeastern US (Guilbert et al., 2015) and Europe (Valdes-Abellan et al., 2017; Zolina et al., 2010) during the 20th century. In Switzerland, little change in spell-length statistics associated with significant trends in precipitation intensity during the 20th century was reported (Schmidli and Frei, 2005). Conversely, (Alexander et al., 2006) documented a significant decreasing trend of annual maximum consecutive dry days (CDD) in Australia. Significant trends with different signs and magnitude regarding the characteristics of dry and wet spell lengths during the 20th century was identified in India (Dash et al., 2009; Singh et al., 2014; Vinnarasi and Dhanya, 2016). While these studies show that some regions of the world have experienced significant changes in daily precipitation persistence, a lack of consensus on the metrics used to characterize precipitation persistence makes it difficult to compare the results from different studies.

Studies evaluating precipitation persistence in GCMs have typically focused on indices such as CDD, maximum consecutive wet days (CWD), heavy precipitation days (number of days with rainfall more than 10 mm, R10mm) and very heavy precipitation days (R20mm), recommended by the WMO/WCRP/JCOMM Expert Team on Climate Change Detection and Indices (ETCCDI) (Zhang et al., 2011), and commonly used to measure daily precipitation persistence in pre-

vious studies (Alexander and Arblaster, 2017; Alexander et al., 2006; Sillmann et al., 2013). While these indices measure extreme dry or wet persistence, they are all based on yearly maxima of a given variable and do not account for mean persistence characteristics. Furthermore they might artificially introduce a large interannual variability (IAV) on a grid-scale analysis depending on how the maximum values located at the beginning or end of a year are treated (Sillmann et al., 2013).

In the following, we analyse global daily precipitation persistence using indices that represent its mean characteristic in an exhaustive set of observational data sets and use these results to evaluate a comprehensive ensemble of GCM simulations. Section 3.2 describes the observational data and models used in the analysis. Section 3.3 describes the two indices representing dry and wet precipitation persistence. In Section 3.4, comparisons of long-term daily precipitation indices and their IAV in observational products and GCMs are presented with discussions on the results. The major conclusions of our analyses are presented in Section 3.5.

3.2 Data

3.2.1 Observation-based precipitation products

23 observation-based precipitation products at daily temporal and $1^\circ \times 1^\circ$ spatial resolution in the Frequent Rainfall Observations on GridS (FROGS) (Roca et al., 2019) data collection were used (Table 3.1). All considered products belong to one of the following categories: interpolated station measurements, satellite-only products, satellite products calibrated with station measurements, and atmospheric reanalysis and the common time period 2001-2013 is used in our analysis. More information regarding the observation datasets are available in Table 2 of (Roca et al., 2019). All observational precipitation products were aggregated to a common $2.5^\circ \times 2.5^\circ$ resolution before calculating the indices to facilitate comparison with GCMs.

3.2.2 Model simulations

Daily precipitation outputs in the historical and the representative concentration pathway 8.5 (RCP8.5) simulations, covering the period 1950-2013, from 33 global climate models (GCM) belonging to the Coupled Model Intercomparison Project Phase 5 (CMIP5) (Taylor et al., 2012c) have been used (Table B.1). For the analysis in this study, the longest common observational period 2001-2013 was used. All model outputs were regridded to a to a common $2.5^\circ \times 2.5^\circ$ resolution before calculating the indices.

Table 3.1: *Observational precipitation products used in this study*

Product name (main reference)	Temporal coverage	Product category
GPCC-FDD-v1.0 (Schamm et al., 2015)	1988-2013	Interpolated stations
GPCC-FDD-v2018 (Schamm et al., 2015)	1982-2016	
REGEN-ALL (Contractor et al., 2019)	1950-2013	
REGEN-LONG (Contractor et al., 2019)	1950-2013	
TRMM 3B42-IR (Huffman et al., 2007)	1998-2016	Satellite-only
TRMM 3B42-MW (Huffman et al., 2007)	1998-2016	
CHIRPv2.0 (Funk et al., 2015)	1981-2016	
CMORPH-RAW (Joyce et al., 2004)	1998-2017	
GSMAP-nogauges-NRT (Kubota et al., 2007)	2001-2017	
GSMAP-nogauges-RNL (Kubota et al., 2007)	2001-2013	
TRMM 3B42-v7 (Huffman et al., 2007)	1998-2016	Satellite calibrated with stations
CHIRPSv2.0 (Funk et al., 2015)	1981-2016	
CMORPH-v1-CRT (Joyce et al., 2004)	1998-2017	
GPCP-CDR-v1.3 (Huffman et al., 2001)	1997-2017	
GSMAP-gauges-NRT (Kubota et al., 2007)	2001-2017	
GSMAP-gauges-RNL (Kubota et al., 2007)	2001-2013	
PERSIANN-v1 (Ashouri et al., 2014)	1983-2017	
CFSR (Saha et al., 2010)	1979-2017	Reanalysis
ERAi (Dee et al., 2011)	1979-2017	
JRA-55 (Kobayashi et al., 2015)	1958-2017	
MERRA1 (Rienecker et al., 2011)	1979-2015	
MERRA2 (Rienecker et al., 2011)	1980-2017	

3.3 Methods

In order to estimate day-to-day wet (i.e., rainy) and dry (i.e., nonrainy) persistence, daily precipitation time series are transformed into binary time series using a 1 mm/day precipitation threshold. Subsequently, the two precipitation persistence indices, P_{dd} and P_{ww} are calculated as the fraction of dry (wet) day that are followed by another dry (wet) day. For the analyses conducted in this study, the indices are calculated in two ways: annual values and long-term values. For the calculation of long-term values, daily precipitation during 2001-2013 is considered. Annual values are estimated using data for each year and allow us to investigate the IAV. IAV is quantified as the standard deviation of the yearly values and it partially also reflects the statistical uncertainty of the indices.

To estimate the robustness of the multi-observation and multi-model mean error of P_{dd}, P_{ww} and their IAV, we use the coefficient of variation (CV), defined as the ratio of the standard deviation to the mean. In this case, the standard deviation is calculated for all combinations of observations or models, respectively. When the absolute value of CV is smaller than 1, the estimate is considered robust.

Besides using P_{dd} and P_{ww} as indicators for precipitation persistence, previous studies also used P_{dd} and P_{ww} to simulate the original daily categorical time series under a first-order Markov chain assumption, whereby the goodness-of-fit between the original and simulated dry and wet spell length distributions was assessed using a two-sample Kolmogorov-Smirnov test (Lee et al., 1986; Mathier et al., 1992; Moon et al., 2018). At monthly and annual time scales, the test suggested for both observations and models that P_{dd} and P_{ww} can be used to represent the dry and wet spell length distributions. We conducted the same statistical test at daily time scale to check whether such approximation is valid at a shorter time scale (Figure B.1, supporting information). For dry spell lengths, in a few regions such as eastern North America and South Australia, its approximation using Markov model was statistically confirmed across different observational products and models but not for other regions. For wet spell lengths, the hypothesis does not hold mainly in the tropics, while they are reproducible with P_{dd} and P_{ww} in the other regions of the world. The fact that P_{dd} and P_{ww} do not allow good simulation of the spell length distributions at daily scale might be due to strong seasonality or long-term variability in the time series, which violates the first-order Markov chain assumption. Hence, P_{dd} and P_{ww} alone do not allow to represent dry and wet spell length distribution at daily time scales. Nonetheless they remain useful indicators of precipitation persistence and are used for that purpose in this paper.

3.4 Results and Discussion

3.4.1 Long-term mean persistence characteristics of daily precipitation

Figure 3.1 shows the multi-observation and the multi-model mean of daily P_{dd} and P_{ww} over the period 2001-2013. The observations and models show similar spatial patterns of P_{dd} and P_{ww}. While P_{dd} is lowest in the regions around the equator and increases towards the poles, P_{ww} shows the opposite pattern, with highest values observed over the whole tropics consistently with precipitation climatologies. Also, the global mean of P_{dd} is generally higher than the global mean of P_{ww}. Equivalent results for different seasons are presented in supporting information (Figures B.2 - B.5). Compared to monthly and annual P_{dd} and P_{ww} presented in (Moon et al., 2018), both indices expectedly show wider range of values towards both extremes at daily scale.

Multi-model mean errors in both dry and wet persistence are shown in Figure 3.2. The P_{dd} error shows a more heterogeneous spatial structure, while the P_{ww} error is consistently positive in most regions of the world. This is consistent with the broad notion that models tend to rain more frequently than that observed, although spread across the observational products in the frequency of light precipitation events are larger than more intense categories

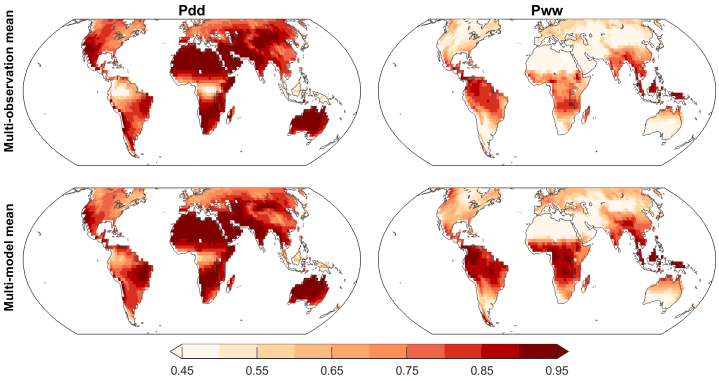

Figure 3.1: *Multi-observation (top) and multi-model mean (bottom) of daily dry (P_{dd}, left) and wet persistence (P_{ww}, right).*

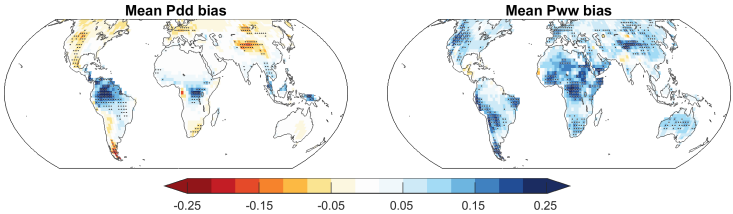

Figure 3.2: *Multi-model mean error of daily dry (P_{dd}, left) and wet persistence (P_{ww}, right). The stippling indicates grid cells where the absolute value of coefficient of variation of the model error is smaller than 1. Highlighted are regions that correspond to Western North America (WNA), the Amazon (AMZ), and Southern Africa (SAF) as defined in SREX (Seneviratne and Nicholls, 2012) and are considered for detailed analysis.*

of precipitation events (Sun et al., 2018). These errors are not sensitive to the choice of threshold within the range of light intensity rainfall (5 mm/day) (not shown here). In addition, in both observations and models, Pdd and Pww are significantly correlated with total amount and frequency of precipitation in most regions (Figure B.8). The different spatial structure between the error of the two indices contrasts with what was identified at monthly and annual time scale where both indices were dominantly underestimated by GCMs (Moon et al., 2018). The positive P_{dd} error is largest in the Amazon and Central Africa. Other regions including southern Argentina, western North America, central Europe and Tibetan Plateau show a small but robust negative bias. While there is a clear seasonality in both indices, spatial patterns of the errors are similar across different seasons (Figures B.2-B.5).

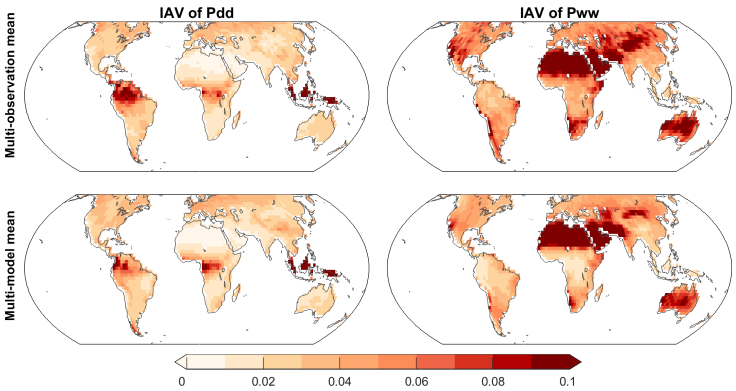

Figure 3.3: *Multi-observation (top) and multi-model mean (bottom) of interannual variability (IAV) of daily dry (P_{dd}, left) and wet persistence (P_{ww}, right).*

3.4.2 Interannual variability in daily precipitation persistence

Figure 3.3 shows the multi-observation and multi-model mean of the standard deviation of the yearly values of daily P_{dd} and P_{ww}, here also referred to as IAV of the respective index. The spatial structure of the IAV has some commonalities with that of the mean P_{dd} and P_{ww} values (Fig. 3.1). The IAV is large in regions with low P_{dd} and P_{ww} values that are the Amazon, central Africa, the Sahara, Australia, and South Africa. In other parts of the world, the magnitude of IAV is relatively constant.

Figure 3.4 shows the multi-model mean error of IAV of P_{dd} and P_{ww}. For IAV of P_{dd}, the Amazon stands out with the largest mean error but with large spread either across the observations or the models indicated by CV larger than 1. Overall, there is a robust underestimation of IAV of P_{ww} in most regions, except for the Sahara and Middle East, where it is overestimated. The strong underestimation in the IAV of P_{ww} in models suggests that they are oversimplifying some aspects of daily precipitation dynamics. This might also explain how consistent overestimation of daily P_{dd} and P_{ww} can be concurrent with previously identified underestimation of the two indices at monthly and annual time scales (Moon et al., 2018).

3.4.3 Observational Product Intercomparison

Based on the previously presented results, we identify four regions (Western North America, Amazon, West Africa, and South Africa) where the errors of daily precipitation persistence or errors of their IAV is relatively large. The regions were defined according to the Risks of Extreme Events and Disasters to Advance Climate Change Adaptation (SREX; (Seneviratne and Nicholls, 2012), see Table B.2 and Figure B.7 for the definition of the regions) and are indicated

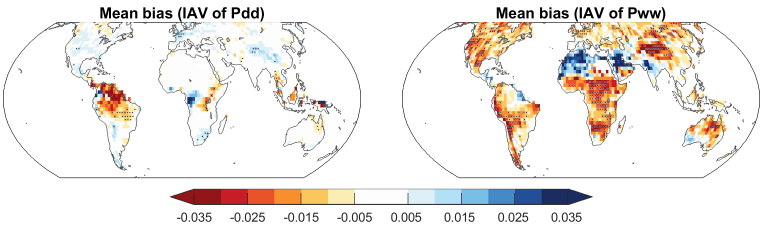

Figure 3.4: *Multi-model mean error of interannual variability (IAV) in daily dry (P_{dd}, left) and wet persistence (P_{ww}, right). The stippling indicates grid cells where the absolute value of coefficient of variation of the model error is smaller than 1.*

in Figure 3.2. In Figure 3.5, the time series of regionally averaged annual P_{dd} and P_{ww} over the period 1950-2013 are presented. The dark and light grey shades indicate the interquartile and the total range of model simulations whereas the black line indicates median. Colored lines indicate each category of observational products (see also Table 3.1). Results in the all other SREX regions are presented in the Supporting Information (Figures B.8-B.12).

For the simulations from GCMs used in this study, the year-to-year evolution is not expected to agree among themselves or with observations year-by-year, unlike the long-term mean magnitude of IAV in individual models quantified as standard deviation (Figure 3.3). Therefore, the models' yearly values in Figure 3.5 cannot be directly compared to observations. A larger (smaller) IAV in the regions with constantly very low (high) P_{dd} or P_{ww} values is partially due to statistical uncertainty of the yearly indices themselves, which is affected by number of transitions from dry or wet statuses.

In Western North America, both observations and models show relatively small spreads in both P_{dd} and P_{ww}. The IAV of the P_{dd} in observations are generally small compared to other regions and shows good agreement among observations on year-by-year variation. For P_{ww}, the IAV differs depending on the observation product, for instance, some of the satellite products show different temporal behavior than the rest. Also the full range of P_{ww} in observations is below the interquartile range of the models indicating consistent overestimation in the models. In the Amazon, both observations and models show large inter-product spread, evident from the magnitude of IAV in P_{dd}. In particular, the reanalysis products show larger IAV than the other products. West Africa is one of the regions with the largest spread in P_{ww} across observational products, even larger than that of models. The range of P_{ww} in the reanalysis products is well separated from the rest. In South Africa, there is a good agreement in P_{dd} between observations, with small spread across both. For P_{ww}, the median of the models is larger than any observational products, confirming consistent overestimation of the models. The very low or high values of indices in some satellite products at the beginning of their time series in

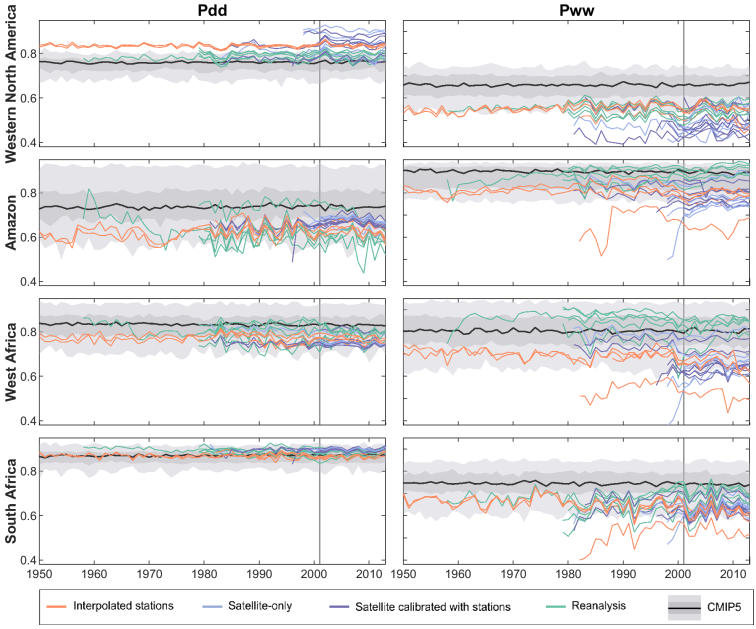

Figure 3.5: *Time series of dry (P_{dd}, left) and wet persistence (P_{ww}, right) in four different regions. Individual lines indicate different observation products that are grouped into four categories. Light grey and dark grey shades indicate the total range and the interquartile range of the CMIP5 models. The black line indicates the median.*

the Amazon and West Africa are due to temporarily smaller spatial coverage.

Figure 3.6 shows the globally averaged root-mean-square differences (RMSD) from the multi-observation mean of P_{dd} and P_{ww} as well as the IAV of both indices for observations and models. For P_{dd} and P_{ww}, the reanalysis products show largest RMSD values and while the remaining observational products show values smaller than 0.1. Models show a similar range of RMSD of P_{dd} as reanalysis products, and a higher RMSD for P_{ww} also with a larger intermodel spread. Similarity between the GCMs and reanalyses is likely due to the fact that the dynamical properties of reanalysis is highly dependent on the underlying atmospheric model and that precipitation is often not assimilated directly. Specifically they commonly simulate more frequent rainy days (Beck et al., 2017) which is significantly correlated with the persistent characteristics (Figure B.6). The RMSD of the IAV of P_{dd} is similar across observational products with slightly larger values in the reanalyses. The RMSD of the IAV of P_{ww} is consistent around 0.02 across all observational products. The RMSD of the IAV in both indices for models are larger than observations by around 0.01 with small intermodel spread. As observational estimates were analyzed in different categories based on data processing and measurement methods, similar a priori approach could be applied to GCMs considering the shared components between models (Annan and Hargreaves, 2017; Boé, 2018). Such an approach may help to identify the reasons underlying the model errors found in this study.

3.5 Conclusions

In this study, an exhaustive set of observational precipitation products was compared to GCMs with regards to their daily precipitation persistence. A consistent and statistically robust overestimation in P_{ww} in GCMs was identified, while the model errors in P_{dd} were spatially heterogeneous in both sign and magnitude. A statistically robust underestimation in the IAV of P_{ww} in GCMs was identified around the globe except for the Sahara, Arabian Peninsula, and India, where an overestimation was found. A majority of models show an underestimation in the IAV of P_{dd} in the tropics. In many regions, the spread of P_{dd} and P_{ww} across all observational products is similar or even larger than the intermodel spread, while the magnitude of year-to-year variations agree well between the observational products. At the global scale, the reanalysis products are found to exhibit a larger difference compared to the multi-product mean than other groups of observational products. The results of this study highlight the consistent model error in daily precipitation persistence, despite the considerable spread across observational products. Contrasting model errors of long-term mean of daily precipitation persistence and its interannual variability show how a consistent overestimation of daily persistence can relate to previously identified underestimation of dry and wet persistence at longer time scales (e.g. monthly and yearly).

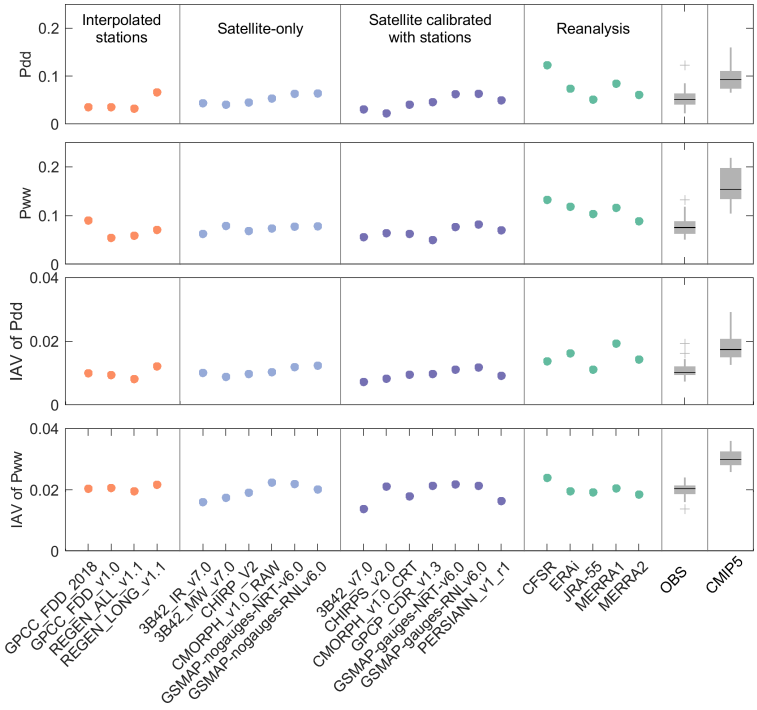

Figure 3.6: *Globally averaged root-mean-square differences (RMSD) from the multi-observation mean of P_{dd} (first row), P_{ww} (second row), and the interannual variability (IAV) of P_{dd} and P_{ww} (third and fourth rows), for observations and models. The boxplots indicate the median, interquartile range, and full range of all observational products (OBS) and models (CMIP5).*

3.6 Acknowledgements

Financial support on this work was provided by the European Union through the Copernicus Climate Change Service (C3S_511) implemented by ECMWF, and the European Research Council (ERC) "DROUGHT-HEAT" project funded through the European Commission's Seventh Framework Programme (grant agreement FP7-IDEAS-ERC-617518).

4 Soil moisture effects on afternoon precipitation occurrence in current climate models

published in *Geophysical Research Letters, doi:10.1002/10.1002/2017JD027577*
Heewon Moon[1], Benoit P. Guillod[1,2] Lukas Gudmundsson [1], Sonia I. Seneviratne[1]

Abstract *Soil moisture-precipitation feedbacks in a large ensemble of global climate model simulations are evaluated. A set of three metrics are used to assess the sensitivity of afternoon rainfall occurrence to morning soil moisture in terms of their spatial, temporal, and heterogeneity characteristics. Positive (negative) spatial feedback indicates that the afternoon rainfall occurs more frequently over wetter (drier) land surface than its surroundings. Positive (negative) temporal feedback indicates preference over temporally wetter (drier) conditions, and positive (negative) heterogeneity feedback indicates preference over more spatially heterogeneous (homogeneous) soil moisture conditions. We confirm previous results highlighting a dominantly positive spatial feedback in the models as opposed to observations. On average, models tend to agree better with observations for temporal and heterogeneity feedback characteristics, although intermodel variability is largest for these metrics. The collective influence of the three feedbacks suggests that they may lead to more localized precipitation persistence in models than in observations.*

4.1 Introduction

Despite substantial research over the past few decades, soil moisture-precipitation (hereafter SMP) feedbacks remain among the most uncertain processes in the field of land-atmospheric interactions (Santanello et al., 2017; Seneviratne et al.,

[1]Institute for Atmospheric and Climate Science, ETH Zürich, Zürich, Switzerland
[2]Institute for Environmental Decisions, ETH Zürich, Zürich, Switzerland

2010). Soil moisture influence on precipitation at seasonal to interannual scales has been investigated with the concept of moisture recycling (Dirmeyer et al., 2006; Eltahir and Bras, 1996; van der Ent et al., 2010), here referred to as direct SMP feedback. There has also been an increasing attention towards understanding indirect SMP feedback at subdaily to daily scales, which is also the focus of our study. Indirect SMP feedback can be narrowed down to the influence of soil moisture condition on boundary layer characteristics and convective initiation. Several studies have investigated such local effects of soil moisture using two main types of approaches. Some focused on the temporal effect of soil moisture on rainfall based on 1-dimensional frameworks which can yield both positive and negative effects (Alfieri et al., 2008; Duerinck et al., 2016; Findell and Eltahir, 2003; Gentine et al., 2013; Guillod et al., 2014). A positive temporal feedback appears when the increase of moisture is more critical for the cloud formation and precipitation, often under low stability in the free troposphere. A negative temporal feedback usually appears under a strong stability barrier at the top of planetary boundary layer, which requires larger sensible heat to allow sufficient turbulent mixing (Hohenegger et al., 2009). Another line of research considers spatial soil moisture gradients (Taylor and Lebel, 1998) whereby locally drier soils induce a mesoscale atmospheric circulation such that increased convergence over the drier region which leads to convection (Taylor et al., 2011). Conceptually, temporal and spatial feedbacks may interact: rainfall may produce spatial heterogeneities in soil moisture that subsequently lead to further rainfall events over the drier regions, thereby increasing precipitation occurrence over a wider area (Guillod et al., 2015; Hsu et al., 2017).

Taylor et al. (2012a) have demonstrated that observations display a negative spatial SMP feedback, contrary to global climate models (GCMs) which display a positive feedback. This misrepresentation of SMP feedback in GCMs suggests issues in the dynamics of rainfall and soil moisture, and could introduce systematic errors in the climate simulated by these models. Many studies have assessed the feedback in GCMs using different approaches, including modeling experiments. Koster et al. (2006) investigated the relative strength of the SMP feedback across GCMs in terms of precipitation variability explained by soil moisture and highlighted regions with stronger coupling such as the Sahel and central North America. Several regional studies analyzed the development of convective rainfall in model simulations with different soil moisture perturbations, in e.g. South Africa (Cook et al., 2006), the Indian and African monsoon region (Douville et al., 2001; Meehl, 1994), the Alpine region (Hohenegger et al., 2009), and the Sahel (Taylor et al., 2013). These studies commonly concluded that simulations with parameterized convection, as applied in most of the GCMs, are not able to simulate negative feedbacks. In addition, although the previous studies have proven the substantial contribution of parameterized convection to SMP feedback in models, the role of the land surface schemes should not be overlooked as surface variability induced from

land surface processes is likely to influence the development of convection and thus, the SMP feedback itself.

Previous studies mainly point to the spatial resolution of models and thereby parameterization of convection as the main issue that may prevent GCMs from correctly simulating SMP feedbacks. Nonetheless, there is a lack of understanding in how such feedbacks are represented in current GCMs, especially with respect to their spatial and temporal components. In this study, for the first time we evaluate both spatial and temporal SMP feedbacks in a large ensemble of fully coupled climate models using the diagnostics introduced by Taylor et al. (2012a) and Guillod et al. (2015). Section 4.2 describes the observational data and models used in the analysis. Section 4.3 describes the coupling diagnostics and their application to both observations and models. The analysis of SMP feedbacks in observations and models is presented in section 4.4.1. In section 4.4.2, the possible collective effects of spatial and temporal SMP feedbacks in observations and models are discussed. Conclusions are drawn in Section 4.5.

4.2 Data

4.2.1 Observational data

In this study, three precipitation data sets and four soil moisture data sets are used which resulted in 12 combinations of observational estimates of the SMP feedback metrics. Using multiple observational data sets allows to consider observational uncertainty in identifying the SMP feedback (Ford et al., 2018; Guillod et al., 2015). All observational data are sets commonly available over the period 2002-2011 at $0.25^\circ \times 0.25^\circ$ resolutions.

Precipitation

We use three different 3-hourly precipitation data sets that are commonly based on multiple satellite measurements: version 1.0 of the CMORPH (Climate Prediction Center morphing method, Joyce et al. (2004)) precipitation product, PERSIANN (Precipitation Estimation from Remotely Sensed Information using Artificial Neural Networks, Hsu et al. (1997)), and version 7 of TRMM3B42 (from the Tropical Rainfall Measuring Mission, Huffman et al. (2007), hereafter referred as TRMM). CMORPH precipitation is derived by propagating infrared data from geostationary satellites to precipitation estimates obtained from passive microwave sensor aboard polar-orbiting satellites, which complement each other with their different advantages on detection accuracy and spatio-temporal coverage. The PERSIANN algorithm also uses combined infrared and passive microwave information from multiple geostationary and low earth orbit satellites with an artificial neural network model of which parameters are updated with ground-based data. TRMM precipitation is a

combined precipitation estimates from multiple satellite systems which is adjusted with rain gauge observations. We adjusted the 3-hourly precipitation data sets to local time based on longitude before the analysis.

Soil moisture data

We use Land Parameter Retrieval Model (LPRM, Owe et al. (2008)) version of AMSR-E (The Advanced Microwave Scanning Radiometer for Earth Observing System) soil moisture (hereafter referred as AMSR), and three different soil moisture estimates from GLEAM (Global Land Evaporation Amsterdam Model, Miralles et al. (2011)), the latter resulting from the use of three precipitation data sets described in the former section as an input to GLEAM.

The LPRM is mainly based on the relationship between polarization ratios, vegetation optical depth, and the soil dielectric constant and the derived surface soil moisture represents the uppermost 1 - 1.5 cm, as the AMSR-E detects microwave brightness temperatures at X (8-12 GHz) and C band (4-8 GHz). We use the AMSR estimated at 1:30 am local time, which is the descending overpass time of AMSR-E. The soil moisture from GLEAM is derived as evaporative stress representing the whole root zone depth using remotely sensed radiation, precipitation, air temperature, soil moisture, vegetation optical depth and snow water equivalent as input. The GLEAM data used in this study (see also Guillod et al. (2015)) assimilates AMSR soil moisture available for 2002-2011 period and was driven by the three different precipitation data sets used in this study. Since a soil moisture estimate at a specific timing of day (9 am) is required for calculating the SMP feedback metrics, the original GLEAM formulation which provides estimates of daily averages (0-24 UTC) was modified such that the input variables are aggregated at a local daily cycle which starts and ends at 9 am local time and the estimated soil moisture hence corresponds to instantaneous values at 9 am. Further details of this specific version of GLEAM can be found in Guillod et al. (2015).

4.2.2 CMIP5 models

Global Climate Model (GCM) output data from historical simulations, for the period 1976-2005, from the CMIP5 (Taylor et al., 2012c) ensemble have been used. A longer time period (compared to observations) was necessary to ensure that enough afternoon rainfall events are captured in models, as their spatial resolutions are much coarser (see also Section 3). Hence, we assume that SMP feedback characteristics have remained constant over the considered time period (1976-2011). Models with 3-hourly precipitation and surface soil moisture output available at a spatial resolution finer than $2.5^\circ \times 2.5^\circ$ were chosen, leading to the nine GCMs listed in Table 4.1 together with a few relevant properties. A longitude-based time adjustment was also conducted to ensure that model outputs are arranged along local time. The surface soil moisture output of the models used in this study represents the uppermost 10 cm,

except for CNRM-CM5 of which represents the top 1 cm.

4.3 Coupling diagnostic

Diagnostics to assess SMP coupling are mainly adopted from Taylor et al. (2012a) and Guillod et al. (2015). A set of three metrics, which assess the sensitivity of afternoon rainfall occurrence to morning soil moisture spatially, temporally and in terms of heterogeneity, are calculated for each afternoon precipitation event. In this section, we first provide a description of the methodology as applied to the observational data, and we then describe the differences introduced for the analysis of models at the end of this section.

For each day, accumulated afternoon precipitation (12 pm - 12 am) is analyzed. Locations of precipitation maxima (Lmax, more than 4 mm) are first identified. An event domain (Levt) is subsequently defined as 5×5 grid cells centered at the Lmax locations, and locations of minimum rainfall on that day within Levt are called Lmin. Grid cells with highly varying topography, water bodies or morning (6am - 12pm) accumulated precipitation larger than 1 mm were masked out. The three metrics are then identified based on these locations as follows: The spatial metric Ys is defined as $\mathrm{S'_{Lmax}} - \mathrm{S'_{Lmin}}$, where S' is the morning (pre-event) soil moisture anomaly obtained by subtracting the seasonal cycle .The subscript refers to the location where S' is taken. The seasonal cycle of soil moisture was calculated by applying 31-day moving average filter to a multi-year daily climatology. In the case of multiple Lmins due to zero precipitation, S'_{Lmin} was calculated as the average soil moisture anomaly at all corresponding grid cells. The temporal metric Yt is defined as S'_{Lmax}. The heterogeneity metric Yh is defined as standard deviation of the 25 values, S'_{Levt}. Only the convective seasons determined by latitude are considered for the analysis, which are May-September for the North of $23°N$, November-March for the South of $23°S$, and all months in the tropics.

In addition to event samples which are metrics calculated for each event at the respective locations, we define a control sample as the same metrics at the same locations but from non-event days from the same month of all years.

All events within $5° \times 5°$ boxes are pooled together to assess the statistical strength of the mean metric value, which is determined by assessing whether the differences between the event and control samples are significantly larger (or smaller) than those generated by chance as follows: First, the climatology of the individual locations within the $5°$ boxes is removed by subtracting the long-term mean of the values within the control and the event samples (pooled together from both samples for each location). Second, the difference between the averages of the event sample and the corresponding control sample ($\delta(Y) = mean(Y_e) - mean(Y_c)$) is computed, and its strength is determined by the corresponding quantile of the distribution of the same difference in each of 1000 random samples. These samples consist of n values (where n is the size of the event sample) randomly selected from all values of the event and control

Table 4.1: *Model features related to atmospheric and land surface scheme*

Model name (main reference)	Resolution (° in latitude × ° in longitude)	Atmospheric model	Convection scheme	Land surface model (sub-grid variability, number of soil layers)
ACCESS1-0 (Dix et al., 2013)	1.2 × 1.9	Included (as in HadGEM2(r1.1))	Mass flux scheme (Gregory and Rowntree, 1990)	MOSES2 (tiled, 4)
ACCESS1-3 (Dix et al., 2013)	1.2 × 1.9	similar to GA1.0	Mass flux scheme (Gregory and Rowntree, 1990)	CABLE (tiled, 6)
CNRM-CM5 (Voldoire et al., 2013)	1.4 × 1.4	ARPEGE-climat	Mass flux scheme (Bougeault and Bougeault, 1985)	SURFEX (tiled, 14)
HadGEM-ES2 (Collins et al., 2011)	1.2 × 1.9	included	Mass flux scheme (Gregory and Rowntree, 1990)	MOSES2 (tiled, 4)
INMCM4 (Volodin et al., 2010)	1.5 × 2.0	included	Convective adjustment scheme (Betts, 1986)	included
IPSL-CM5A-MR (Hourdin et al., 2013)	1.3 × 2.5	LMDZ5	Mass flux scheme(Emanuel, 1991)	ORCHIDEE (mosaic, 2)
MIROC5 (Watanabe et al., 2010)	1.4 × 1.4	CCSR/NIES/FRCGC AGCM6	Entraining plume model (Chikira, 2010)	MATSIRO (single vegetation type per grid box, 13)
MRI-CGCM3 (Yukimoto et al., 2011)	1.1 × 1.1	MRI-AGCM3.3	Mass flux scheme (Yoshimura et al., 2015)	HAL (mosaic, 14)
MRI-ESM1 (Yukimoto et al., 2011)	1.1 × 1.1	MRI-AGCM3.3	Mass flux scheme (Yoshimura et al., 2015)	HAL (mosaic, 14)

samples pooled together (as a substitute for the event sample) and the remaining values within this pool (as a substitute for the control sample). Statistical significance of a positive (negative) feedback is claimed if the strength of δ(Y) is greater (smaller) than 0.9 (0.1). 5° boxes with less than 25 event samples were masked out as they cannot provide robust results.

The models and observations differ in terms of their spatial resolution. In addition, climate models consistently have an early initiation of afternoon rainfall compared to observations (Dai, 2006). To account for these mismatches, we follow previous assessments (Taylor et al., 2012a) and process observed and modelled data differently; Time steps were used with a 3-hour shift in models (9 am - 9 pm for afternoon, 3 am - 9 am for morning precipitation, and 6 am - 9 am for morning soil moisture), and Levt consists of 3×3 grid cells around Lmax instead of 5×5.

As mentioned earlier, the comparatively coarse spatial resolution of climate models requires parameterization of convection and this might itself affect the SMP feedback. We note that in previous studies (Taylor et al., 2012a), the metrics chosen to assess the SMP feedback were additionally calculated at coarser resolutions from observations, which resulted in weaker but consistent sign of the metrics. We find similar results in the Appendix C (Figure C.1), suggesting that the spatial resolution of the data on which the metrics are computed does not qualitatively affect the results. Nonetheless, the coarser spatial resolution of models compared to observations may cause the former to capture only the largest or most widespread events, while the observations capture many more smaller events. It should be noted that the metrics do not explicitly account for atmospheric pre-conditions (apart from the filter for morning rainfall, which ensures that rainfall was not already present in the morning), which might determine the preferred soil moisture condition or in some cases inhibit moist convection (Findell and Eltahir, 2003).

4.4 Results and Discussion

4.4.1 Average statistics of observations and models

Figure 4.1 shows the fractions of observational estimates and models belonging to each of the categories of significantly positive (> 0.9), significantly negative (< 0.1) or non-significant feedbacks. Spatial SMP feedback (Ys) in the models is dominantly positive as opposed to generally non-significant or negative Ys in observations. The highest fraction of models simulating positive Ys is found in South America, South Africa and northern Australia. Taylor et al. (2012a) also found dominantly positive Ys in model simulations of the Atmospheric Model Intercomparison Project (AMIP) which are forced with prescribed sea surface temperature. Some models still capture negative Ys in the western part of Sahel, which appears as one of the regions with the strongest negative Ys in the observations. In North America and North Asia, most of the models

simulate non-significant Ys.

The temporal feedback (Yt) in the models shows better agreement with observations than the other two feedback metrics. Positive Yt in Australia, South Africa, North Asia, and India and negative Yt in western South America and western Sahel are reasonably well captured by the models. Yet in North America the models show very different behaviour compared to observations, with strong negative Yt in the eastern part. Larger variability across the models is found in central North America, western and southern parts of Brazil, and Central Africa (indicated by light purple). Note also that large-scale factors such as the North Atlantic Oscillation, El Nino/Southern Oscillation or sea surface temperature variability could substantially affect precipitation persistence, which in turn may lead to a spurious correlation between soil moisture and subsequent precipitation (Guillod et al., 2014; Salvucci et al., 2002). For instance, precipitation persistence at the time scale of the order of weeks induced by oceanic or atmospheric processes could lead to a positive temporal metric even in the absence of SMP feedback mechanism (Orlowsky and Seneviratne, 2010; Tuttle and Salvucci, 2016). Although we cannot exclude such artifacts, the temporal feedback metric allows for a comparison between observations and models while providing an indication on the temporal feedback (Guillod et al., 2015). We note that the temporal metric also exhibits a negative sign in some regions, e.g. parts of the Sahel and Southern Great Plains, indicating that the metric does not systematically identify positive coupling mechanisms.

While the heterogeneity feedback (Yh) is dominantly positive or non-significant in observations, around 50 % of the models capture positive Yh correctly but show negative Yh in most of the regions where observations indicate non-significant Yh. In observations, Yt and Yh generally have a positive sign, if statistically significant. In the models, similarity between Yt and Yh is much stronger than in observations.

The feedback metrics for individual observations and models are shown in Figure C.3 and C.4, respectively. Inter-product variability is relatively large and clusters of model families can be identified (see also Appendix C). In addition, we note that observations and models also show substantially different spatial coverage of the feedback metrics, reflecting that a lower number of events are detected in several models (Figure C.4), since the same threshold for the minimum number of events is applied for both models and observation to ensure the statistical significance of estimated SMP feedback metrics. These differences in the number of analyzed precipitation events can be due to differences in spatial resolution (leading to more events in observations compared to models) and in the length of the time series (more events in models). In addition, a part of the difference may be due to the known drizzle issue, i.e. an overestimated frequency of light intensity precipitation, in GCMs (Dai, 2006; Rosa and Collins, 2013). Hence, masking out the days with morning precipitation could be more critical for SMP diagnostics in the models.

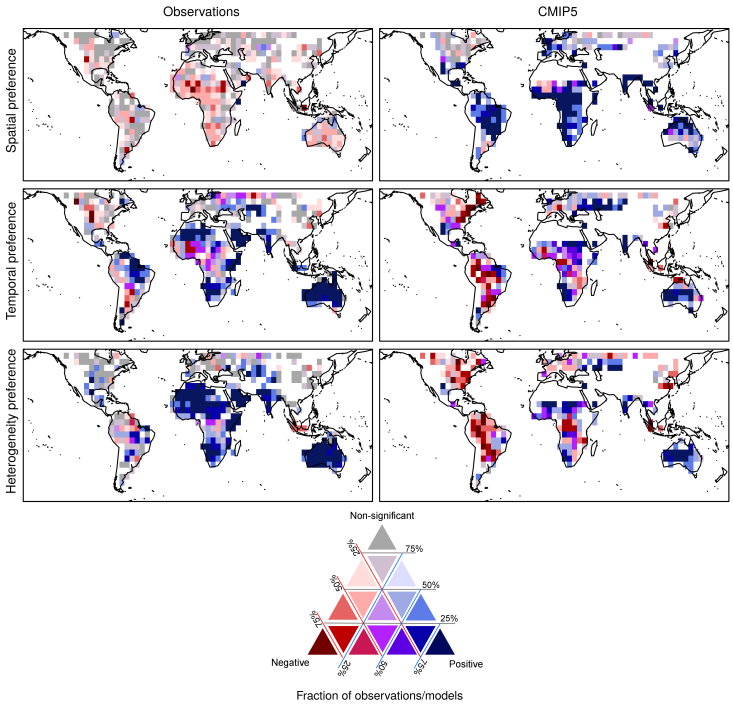

Figure 4.1: *The three soil moisture-precipitation feedback metrics (from top to bottom: spatial, temporal, and heterogeneity metrics) in observations (left) and CMIP5 models (right). Colors are determined by the fraction of observation data set combinations or models in the following three categories: negative, non-significant and positive with a 10 % significance level. 5° boxes with less than five valid observational or model SMP feedback estimates were excluded.*

4.4.2 Combined effects of SMP feedbacks

Figure 4.2 shows the fraction of land areas that feature combinations of the spatial and temporal SMP feedback metrics (top) and heterogeneity feedback metric (bottom) in observations and models. Results of the same analysis using different significant levels are presented in the Supplementary Information (Figure C.5 and C.6). Only $5^\circ \times 5^\circ$ boxes of which more than a third are land areas were classified as land are considered and the ratio of land area is calculated with area-weighted composition. Analyzing Ys and Yt in a combined way allows for a more comprehensive comparison of the pre-rainfall morning soil moisture conditions between observations and models. Additionally, with the consideration of Yh, we discuss possible mechanisms behind the

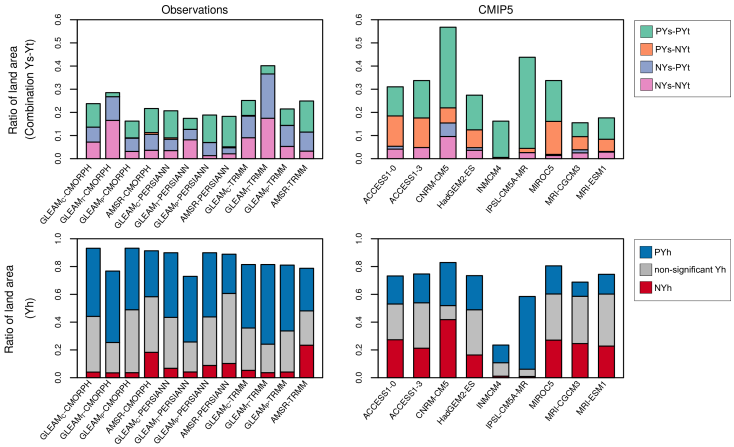

Figure 4.2: *Fractions of land area with different combinations of the spatial and temporal SMP feedback metrics (top) and the heterogeneity feedback metric (bottom) in observations and models. Ys, Yt and Yh indicate spatial, temporal and heterogeneity metric, respectively. P stands for positive sign of the feedback metrics and N for negative. Subscripts in $GLEAM_C$, $GLEAM_T$, and $GLEAM_P$ indicate the precipitation data set used to derive each of the soil moisture estimates.*

commonly found combinations of SMP feedback metrics in both observations and models and how they potentially contribute to the spatial and temporal structure of precipitation persistence. The combination of negative (hereafter, N) Ys and positive (hereafter, P) Yt occurs predominantly in the observations. While each observational estimate shows a similar fraction of land area, the regions where the combination appears vary across different observational data sets (Figure C.2). An important implication of this combination (NYs-PYt) is that the majority of the afternoon rainfall events occur when the whole event domain is anomalously wet, since the location of maximum afternoon precipitation occurs over a grid cell with positive soil moisture anomaly in the morning (PYt) while the surrounding grid cells have even higher soil moisture anomaly (NYs). Therefore, the dominant positive heterogeneity metric across all observed estimations (Figure 4.2, lower left) indicates high heterogeneity among positive soil moisture anomalies, which should be distinguished from high heterogeneity due to mixture of dry and wet soil moisture anomalies. The other dominant combination in observations is NYs-NYt. This combination still reflects significantly more frequent afternoon rainfall occurrence over regions drier than their surroundings, but also less precipitation persistence due to NYt. In addition, this combination does not reveal the large scale soil moisture condition in the entire event domain, unlike the former, and thus there

is larger uncertainty in how the positive Yh is driven. It should be noted that on Fig. 4.2, the combination of positive spatial and positive temporal metrics (PYs-PYt) also seems to appear relatively often. However, looking at the maps of the metrics (Figure C.2) reveals that this co-occurrence in fact stems from various, randomly distributed grid cells and does not cluster into consistent regions. Therefore, this signal appears not robust and should be interpreted with caution. In models, the combination of positive Ys and Yt (PYs-PYt) appears as the most common and is, unlike in observations, also confirmed by the maps in Figure C.4. This combination indicates localized (grid-scale) dry or wet persistence as it means that afternoon rainfall occurs more frequently over the temporally and spatially wetter regions. This is opposed to the observed estimate. PYs-NYt is the second most common combination in the models. PYs-NYt indicates that afternoon rainfall is more likely under dry soil condition and occurs over wetter regions in a given area. Thus, under this combination of feedbacks increase in precipitation likelihood might be only possible when there are sufficient drying down periods between the precipitation events, indicating a system with low precipitation persistence or high evaporative demands. The fraction of areas with different signs of Yh varies substantially across different models, but for each given model, the fractions of NYh and PYh are comparable. CNRM-CM5 appears as the only model where fraction of land areas with negative Ys and significant Yt is larger than 10 %. IPSL-CM5A-MR simulates dominantly positive signals in all three metrics.

4.5 Conclusions

We evaluated spatial and temporal SMP feedbacks in 9 GCMs stemming from the CMIP5 archive using three different metrics (Ys, Yt, and Yh) which quantify sensitivity of afternoon rainfall occurrence to morning soil moisture conditions compared to 12 observational estimates over the period of 1976-2011. We found dominantly positive spatial feedback metric (Ys) in all coupled climate models, contrasting to observations and consistent with the results of Taylor et al. (2012a), which were based on AMIP-type simulations. The temporal feedback metric (Yt) in the models shows better agreement with observations, but with a larger inter-model spread. When interpreting Yt, one should keep in mind that the sign of the feedback metric might be partially caused by atmospheric persistence, which may induce spurious positive relationship between soil moisture and precipitation. The heterogeneity feedback metric (Yh) and Yt have similar spatial patterns in models, unlike in observations where Yh is dominantly positive. The combinations of spatial and temporal SMP feedbacks in models, mainly PYs-PYt and PYs-NYt, indicate they might introduce more localized and stronger wet or dry persistence than the observations, where generally negative Ys is combined with positive Yh. The SMP feedback is an emergent property of climate models which is not parameterized, and certainly influences simulated climate or weather phenomena. In particular, it

reveals the spatio-temporal structure of precipitation persistence that could be favoured in a given climate model. Thus, the results in this study may help to understand how land-climate interaction in climate models contributes to errors in precipitation variability at different temporal scales that were identified in previous investigations (Langford et al., 2014; Moon et al., 2018), of which substantial parts are not explained by contributions from large-scale variability.

5 Conclusions and outlook

5.1 Conclusions

The thesis aimed to resolve research questions regarding the capability of current climate models to simulate precipitation persistence. Chapters 2 and 3 focused directly on evaluating precipitation persistence in the models, at different time scales with consideration of entailed uncertainties. In Chapter 4, representation of the spatial and temporal soil moisture-precipitation feedback in climate models was evaluated and its possible influence on the spatial and temporal structure of precipitation persistence was discussed. Here I provide three main conclusions of this thesis combinedly derived from the results of individual studies.

5.1.1 Markov framework for the representation of precipitation persistence

Both Chapters 2 and 3 investigated the dry and wet precipitation persistence at different time scales. The commonly used Markov framework for the representation of persistence was found to be sensitive to both the number of time steps considered and seasonality in the precipitation. Two types of statistical analysis were used to quantify the representation. First, statistical uncertainty of the dry-to-dry and wet-to-wet transition probabilities was compared to modelling uncertainty, observational uncertainty and internal variability in the model persistence error. Since the transition probabilities are estimated based on the number of dry or wet event, relatively short time series are the reason for uncertainty in transition probabilities estimates. In Chapter 2, the uncertainty was quantified as a spread of 1000 samples generated from parametric bootstrapping under the first-order Markov assumption. At the yearly scale, where 110 time steps could be considered during the period of 1901-2010, the contribution of the statistical uncertainty of both transition probabilities was found to be larger than other sources of uncertainty, modelling uncertainty, observational uncertainty and internal climate variability. This differs for the analysis at the monthly scale for the same period and for the daily scale analysis for the shorter period (2003-2013) where the statistical uncertainty was

much smaller than the contribution from the other sources, i.e. observational and modelling uncertainty. Secondly, the two-sample Kolmogorov-Smirnov test was applied to examine whether the transition probabilities provide a good enough approximation of the dry and wet spell length distributions, in other words, an approximation to the original daily categorical (dry or wet) time series. At monthly and annual time scales, the test showed that the simulated time series using transition probabilities under the Markov assumption are a good approximation, rejecting the hypothesis of same population only in a few grid cells. However for daily scale, the goodness-of-fit between the simulated and original categorical time series was found to be not as good as for the longer time scales based on the same test. This might be due to a strong seasonality or long-term variability in the daily time series, which violates the first-order Markov chain assumption. The results of the same test conducted for daily time series in each 3-month season only showed a small number of rejections, thereby indicating that effects of seasonality are indeed the reason for the reduced representativeness of the Markov frame for daily time series approximation. Despite the limitations listed here, the dry-to-dry and wet-to-wet transition probabilities as parameters for the Markov framework remain useful indicators of precipitation persistence.

5.1.2 Precipitation persistence error at different time scales

Results in Chapters 2 and 3 show systematic error of dry and wet persistence in current climate models at daily, monthly and annual scales. Such results are collectively presented in Fig. 5.1. The overall sign of the errors depends on the time scale, that is underestimation of the dry and wet persistence in monthly and annual scale and overestimation in daily scale (Fig. 5.2). While the reasons for the time-scale dependence of the signs of the model error remain an open question, the underestimation of interannual variability of the daily persistence in models might provide a link. A lack of yearly fluctuation in the daily precipitation persistence, which is closely related to the frequency, and thus to the amount of precipitation, might force the climate system to generate persistently high or low precipitation anomaly in a long-term. Also, precipitation variability in different time scales are governed by different processes. A long-term precipitation persistence is likely related to the large-scale modes of climate variability such as ENSO, MJO and NAO in different regions. Likewise, one can relate climate models' ability to represent the precipitation persistence at long time scales to the large-scale variability and its error in the models. On shorter time scales, precipitation persistence could be more dominantly affected by more regional processes, such as the soil moisture-precipitation coupling.

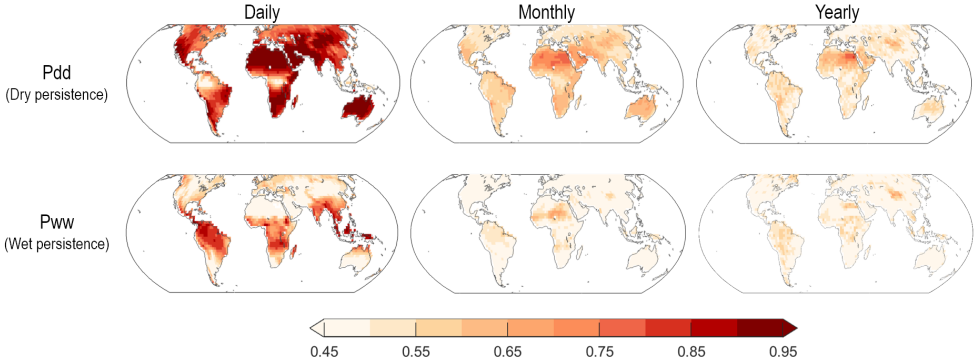

Figure 5.1: *Mean dry and wet persistence estimated from observation-based data sets at daily, monthly and yearly scales. See Figures 2.6 and 3.1 for details.*

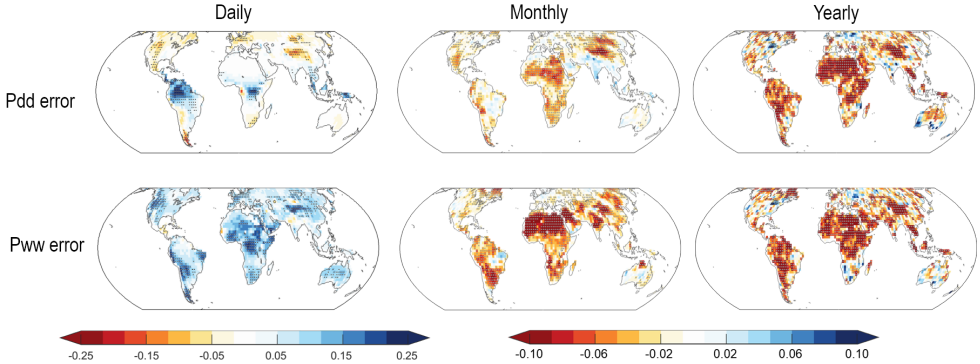

Figure 5.2: *Multi-model mean error of dry (top) and wet persistence (bottom). See Figures 2.7 and 3.2 for details.*

5.1.3 Potential contribution of soil moisture-precipitation feedback on precipitation persistence error

In Chapter 4, the spatial and temporal soil moisture-precipitation feedbacks were evaluated in nine GCMs. Positive (negative) spatial feedback indicates that the afternoon rainfall occurs more frequently over wetter (drier) land surface than its surroundings. Positive (negative) temporal feedback indicates preference over temporally wetter (drier) conditions, and positive (negative) heterogeneity feedback indicates preference over more spatially heterogeneous (homogeneous) soil moisture conditions. Results show dominantly positive spatial feedback in all models as found in AMIP simulations by Taylor et al. (2012a), and on average, a better agreement in temporal and heterogeneity feedbacks with a larger intermodel spread. To interpret their possible contribution on precipitation persistence, combined representation of the spatial and temporal feedbacks, with consideration of the heterogeneity metric, was analyzed. In the observations, combination of the negative spatial feedback and positive temporal feedback is most frequent. This combination indicates that the majority of the afternoon rainfall events occur when the whole event domain is anomalously wet, since the location of maximum afternoon precipitation occurs over a grid cell with positive soil moisture anomaly in the morning. In models, the combination of positive spatial and temporal feedback is the most common. This combination indicates localized (grid scale) dry or wet persistence as it means that afternoon rainfall occurs more frequently over the temporally and spatially wetter regions, which is opposed to the observational estimates. The positive spatial and negative temporal feedbacks are the second most common combination found in the models. It indicates that afternoon rainfall is more likely under dry soil condition and occurs over wetter regions in a given area. Thus, under this combination of feedbacks an increase in precipitation likelihood might be only possible when there are sufficient dry down periods between individual precipitation events, potentially indicating high dry persistence as well as low wet persistence. These interpretations correspond to the general overestimation of both dry and wet persistence in the GCMs at daily scale in Chapter 3, though only a subset of models were evaluated in Chapter 4. Though, care should be taken with this interpretation as the positive feedback identified in the models could be partially caused by atmospheric persistence, which may induce spurious positive relationship between soil moisture and precipitation.

5.2 Outlook

Soil moisture-precipitation feedback in convection permitting models One of the main conclusions of this thesis indicates that the misrepresentation of soil moisture-precipitation feedback in current GCMs contributes to the model error in precipitation persistence at daily scale (Chapter 4). This misrepresentation is known to be mainly related to errors in convection parameterization

schemes (Hohenegger et al., 2009). Therefore, it would be a rational thing to investigate soil moisture-precipitation feedback in convection permitting models and to check how it affects daily precipitation persistence. Several recent studies identified major improvements in simulation of precipitation at daily and shorter time scales in convection permitting regional climate models (RCM) (Fosser et al., 2015).

Future projections of precipitation persistence Observations in many regions show robust changes in the statistics related to persistence of precipitation (Alexander et al., 2006; Dash et al., 2009; Guilbert et al., 2015; Schmidli and Frei, 2005; Singh et al., 2014; Zolina et al., 2010). While general understanding of changes in the persistence characteristic of precipitation is less established, there have been consistent results from several studies generally supporting that there have been increase in the precipitation intensity with decrease in the precipitation frequency (Boberg et al., 2010; Semenov and Bengtsson, 2002). Although the analyses conducted in this thesis did not focus on the temporal variation of the precipitation persistence, and used relatively short time period to detect changes, some of the regions showed clear trends in observations that was distinguishable by inspection as opposed to the generally steady time series from models. Thus, investigating future projections of precipitation persistence in climate models with regards to their ability to simulate changes in the past would be an important contribution on enhancing the current understanding in future projections of precipitation in general.

Appendices

A Appendix for Chapter 2

A.1 Supplementary figures

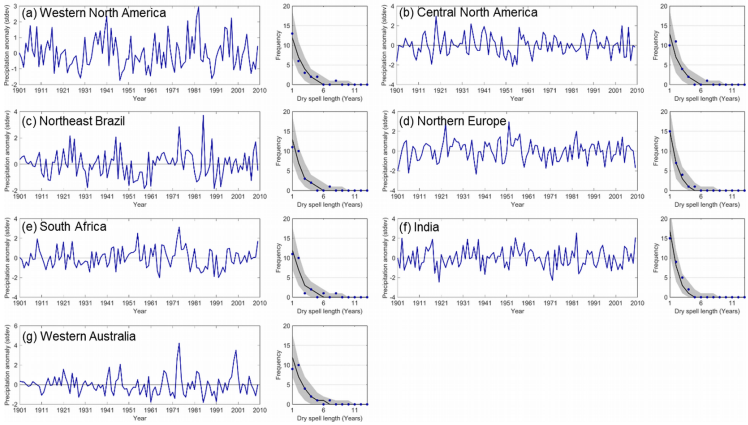

Figure A.1: *In each figure, left panel shows annual precipitation anomaly for 1901-2010 in a randomly chosen grid cell in each region. The time series is taken from the CRU TS3.1 dataset. Right panel shows dry spell length distribution derived from the observed time series and median and 5th to 95th uncertainty range of 1000 dry spell length distributions from statistical simulation of Markov chain. (Same as Figure 2.1 in the main article but for different regions.)*

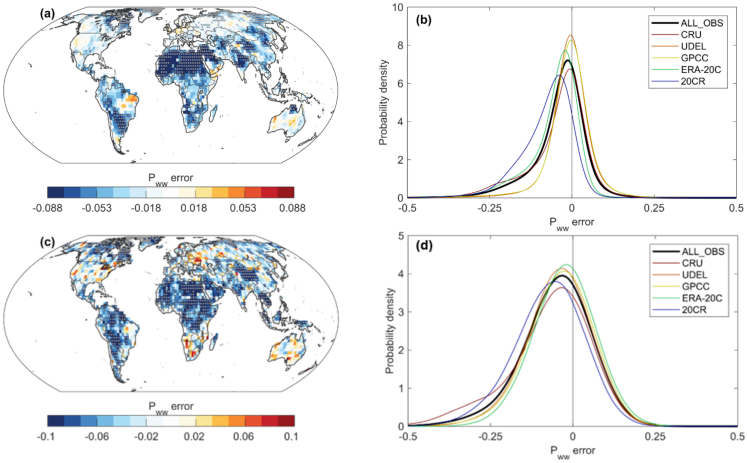

Figure A.2: *Spatial distribution of multi-simulation mean wet persistence (P_{ww}) error for (a) monthly and (c) annual scale. Stippling indicates agreement in the sign of wet persistence error among more than 80% of model simulations. Global histogram of wet persistence error for (b) monthly and (d) annual scale. (Same as Figure 2.6 in the main article but for P_{ww}.*

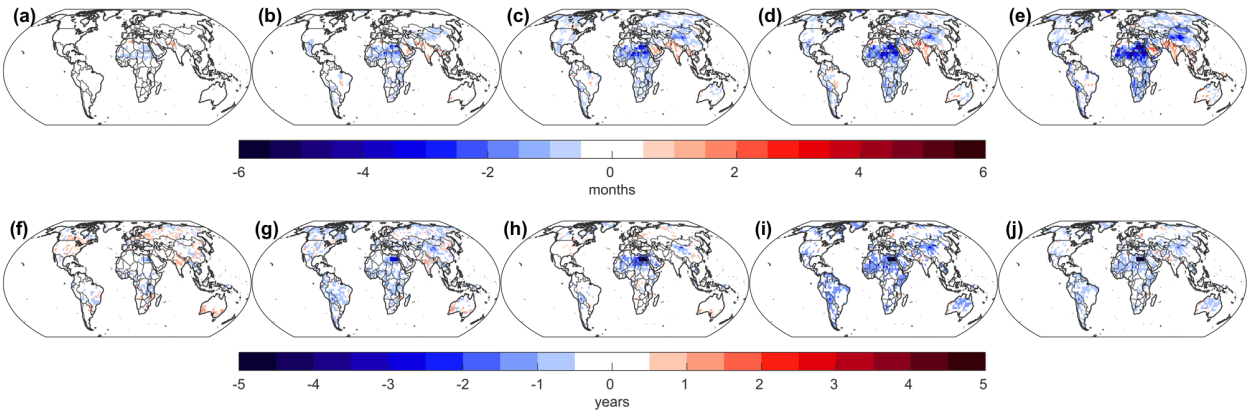

Figure A.3: *Spatial distribution of multi-simulation mean drought length bias against observed mean drought length at 50th, 75th, 90th, 95th, and 99th percentiles (in left-to-right order) in monthly (upper row) and annual scale (lower row).*

B Appendix for Chapter 3

B.1 Supplementary tables

Table B.1: *CMIP5 models used in this study*

Model name	Modelling institute	Original resolution (longitude × latitude)
ACCESS1-0	Commonwealth Scientific and Industrial Research Organization and Bureau of Meteorology, Australia	1.875 × 1.250
ACCESS1-3		1.875 × 1.250
BCC-CSM1-1-M	Beijing Climate Centre, China Meteorological Administration	2.81 × 2.77
BCC-CSM1-1		2.81 × 2.77
CanESM2	Canadian Centre for Climate Modelling and Analysis	2.81 × 2.79
CCSM4	University of Miami - RSMAS	1.25 × 0.94
CESM1-BGC	The National Science Foundation and the U.S. Department of Energy	1.25 × 0.94
CESM1-CAM5		1.25 × 0.94
CMCC-CESM	Centro Euro-Mediterraneo per I Cambiamenti Climatici	3.75 × 3.75
CMCC-CM		0.75 × 0.75
CMCC-CMS		1.875 × 1.875
CNRM-CM5	Centre National de Recherches Météorologiques /Centre Européen de Recherche et Formation Avancée en Calcul Scientifique	1.41 × 1.40
CSIRO-Mk3-6-0	Commonwealth Scientific and Industrial Research Organization in collaboration with Queensland Climate Change Centre of Excellence	1.875 × 1.86
EC-EARTH	EC-EARTH consortium	1.125 × 1.122
FGOALS-g2	LASG, Institute of Atmospheric Physics, Chinese Academy of Sciences	2.8125 × 2.8125
GFDL-CM3		2.5 × 2.0
GFDL-ESM2G	NOAA Geophysical Fluid Dynamics Laboratory	2.5 × 2.0
GFDL-ESM2M		2.5 × 2.0
HadGEM2-AO	Met Office Hadley Centre	1.875 × 1.25
HadGEM2-CC		1.875 × 1.25
HadGEM2-ES		1.875 × 1.25
INM-CM4	The Institute of Numerical Mathematics, Russian Academy of Sciences	2.0 × 1.5
IPSL-CM5A-LR	Institut Pierre-Simon Laplace	3.75 × 1.90
IPSL-CM5A-MR		2.5 × 1.25
IPSL-CM5B-LR		3.75 × 1.875
MIROC-ESM-CHEM	Japan Agency for Marine-Earth Science and Technology, Atmosphere and Ocean Research Institute (The University of Tokyo), and National Institute for Environmental Studies	2.81 × 1.77
MIROC-ESM		2.81 × 1.77
MIROC5		1.40625 × 1.40625
MPI-ESM-LR	Max-Planck-Institut für Meteorologie (Max Planck Institute for Meteorology)	1.875 × 1.85
MPI-ESM-MR		1.875 × 1.85
MRI-CGCM3	Meteorological Research Institute (JMA)	1.125 × 1.125
MRI-ESM1		1.125 × 1.125
NorESM1-M	Norwegian Climate Centre	2.5 × 1.9

Table B.2: *List of acronyms of the SREX regions used in the analyses*

Region	Acronym
Western North America	WNA
Central North America	CNA
Eastern North America	ENA
Central America/Mexico	CAM
Amazon	AMZ
Northeast Brazil	NEB
West coast of South America	WSA
Southeastern South America	SSA
Northern Europe	NEU
Central Europe	CEU
Southern Europe/the Mediterranean	MED
Sahara	SAH
Western Africa	WAF
Eastern Africa	EAF
Southern Africa	SAF
Northern Asia	NAS
Western Asia	WAS
Central Asia	CAS
Tibetan Plateau	TIB
Eastern Asia	EAS
Southern Asia	SAS
Southeast Asia	SEA
Northern Australia	NAU
Southern Australia/New Zealand	SAU

B.2 Supplementary figures

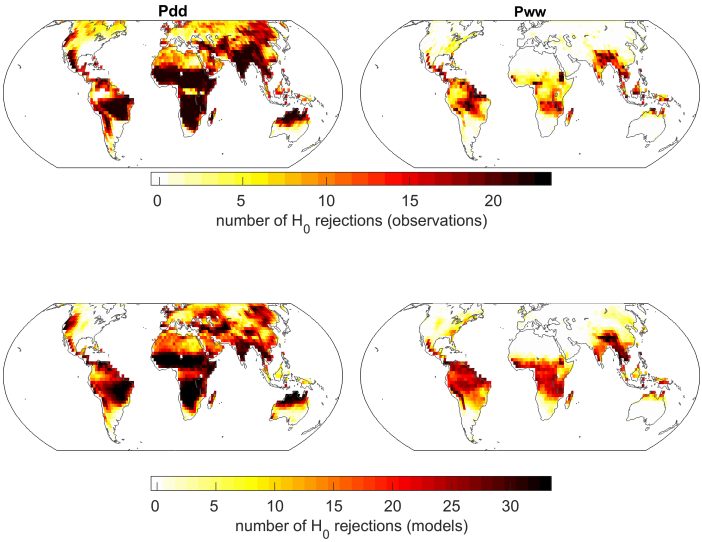

Figure B.1: *Number of observations and models rejecting null hypothesis of the same population.*

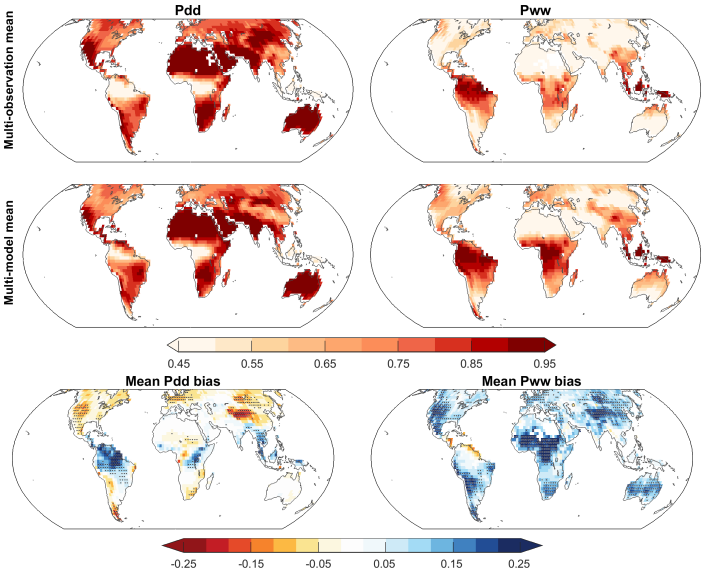

Figure B.2: *Multi-observation and multi-model mean Pdd and Pww and their model model error for March-May.*

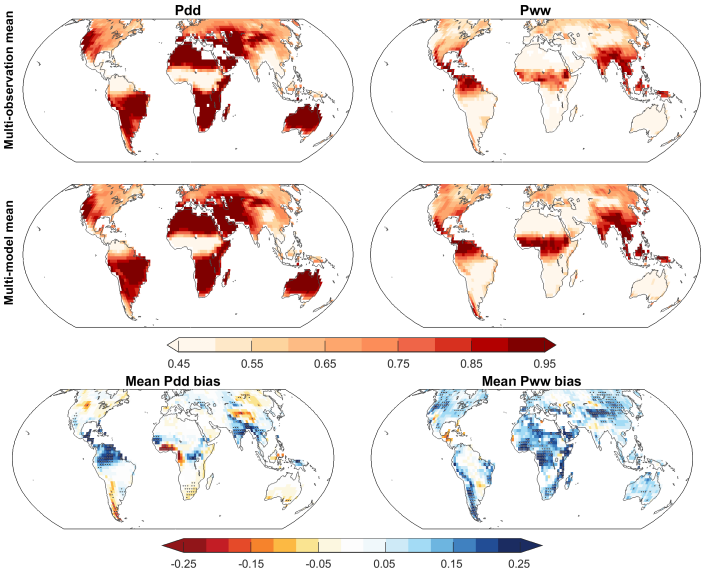

Figure B.3: *Multi-observation and multi-model mean Pdd and Pww and their model model error for June-August.*

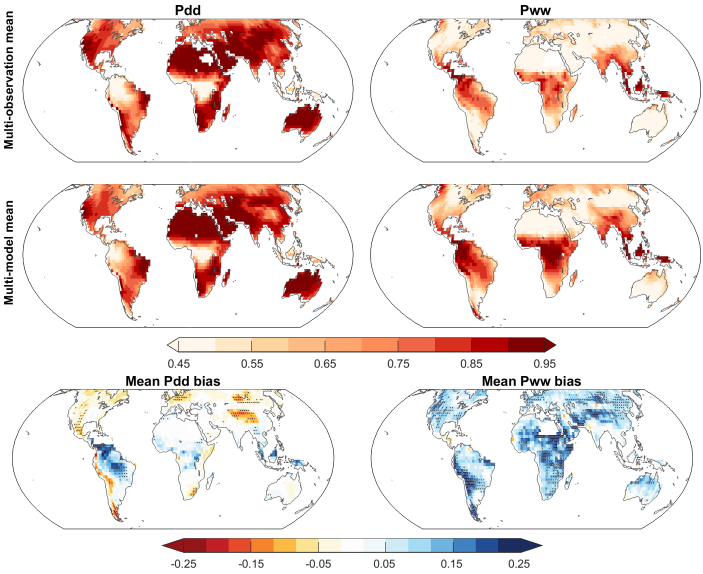

Figure B.4: *Multi-observation and multi-model mean Pdd and Pww and their model model error for September-November.*

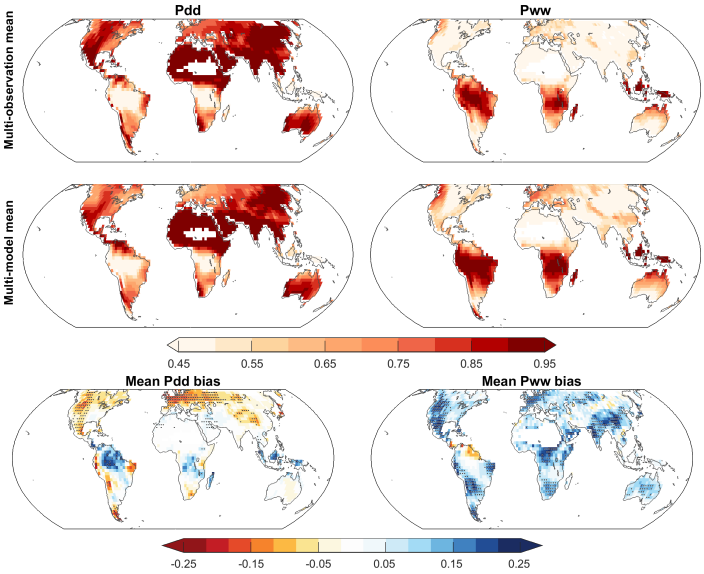

Figure B.5: *Multi-observation and multi-model mean Pdd and Pwv and their model model error for December-February.*

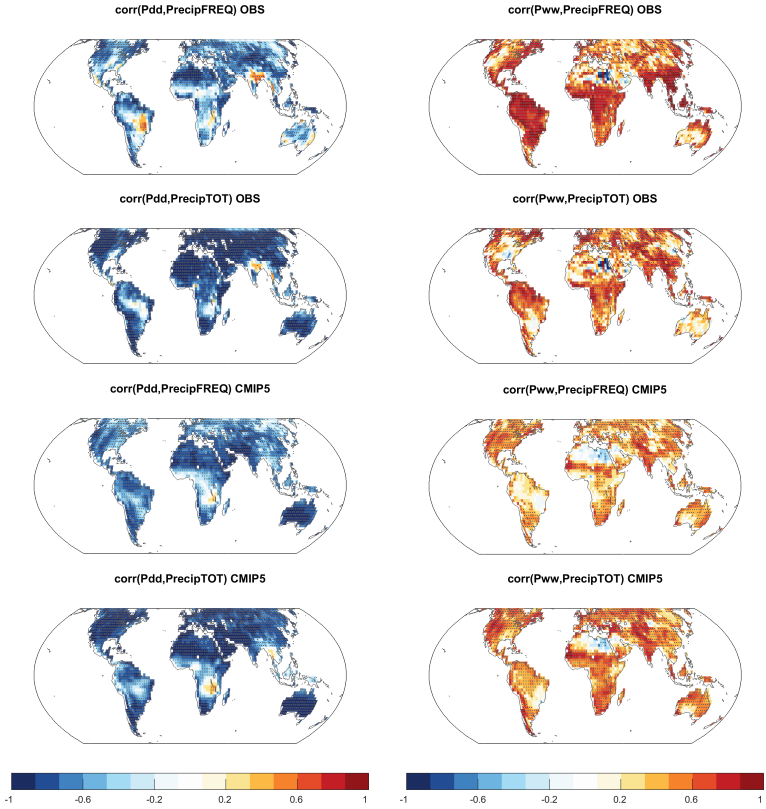

Figure B.6: *Correlation coefficient between dry (Pdd) and wet (Pww) persistence indices and total amount (precipTOT) and frequency (precipFREQ) of precipitation across different observational products (OBS) and CMIP5 models. The stippling indicates grid cells with 5 % level of significance.*

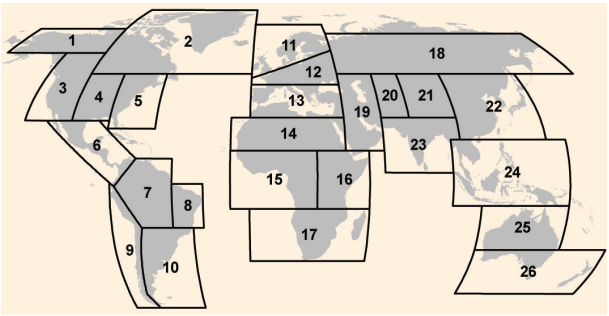

Figure B.7: *Definitions of regions used in Table B.2 and Figure B.8-B.12. Analyses only include land areas. Adapted from Seneviratne and Nicholls (2012)*

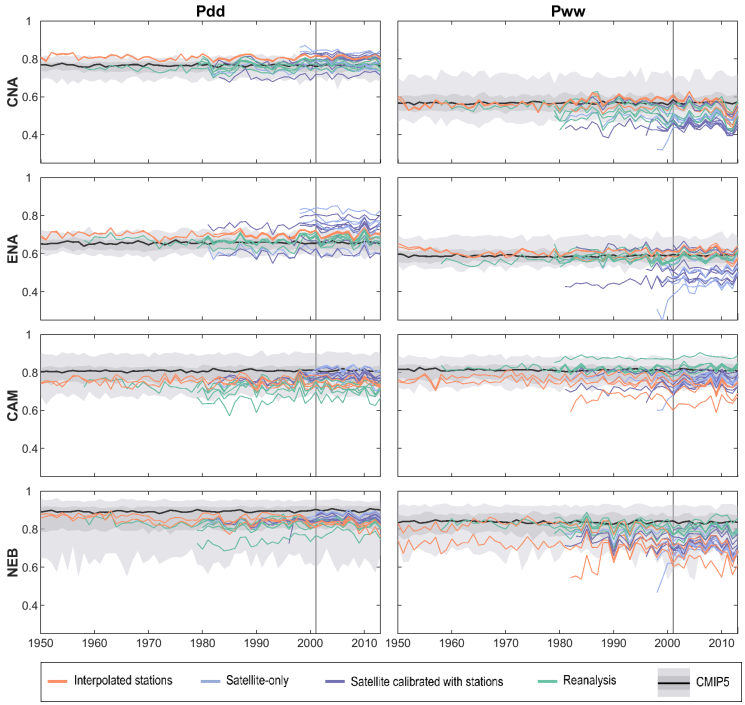

Figure B.8: *Same as Figure 3.5 in CNA, ENA, CAM, and NEB*

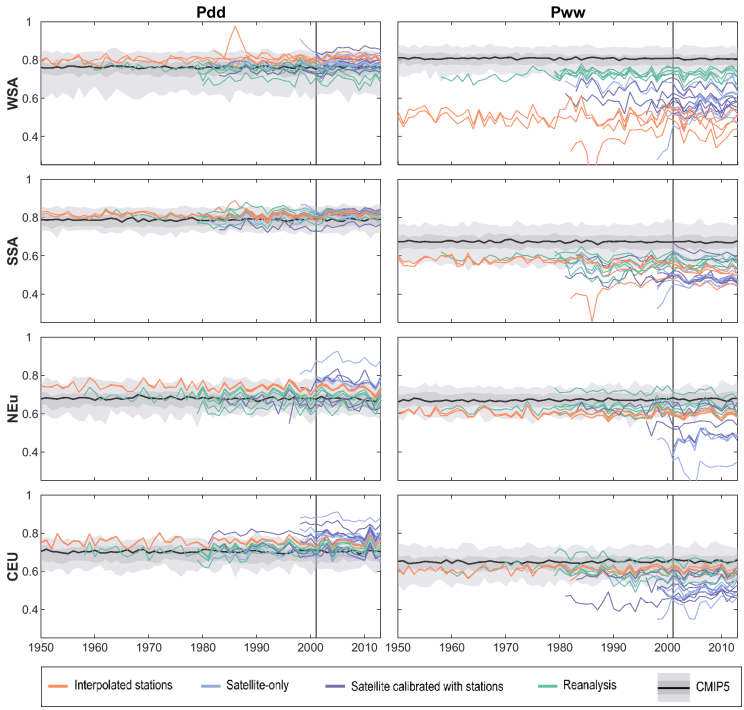

Figure B.9: *Same as Figure 3.5 in WSA, SSA, NEU, and CEU*

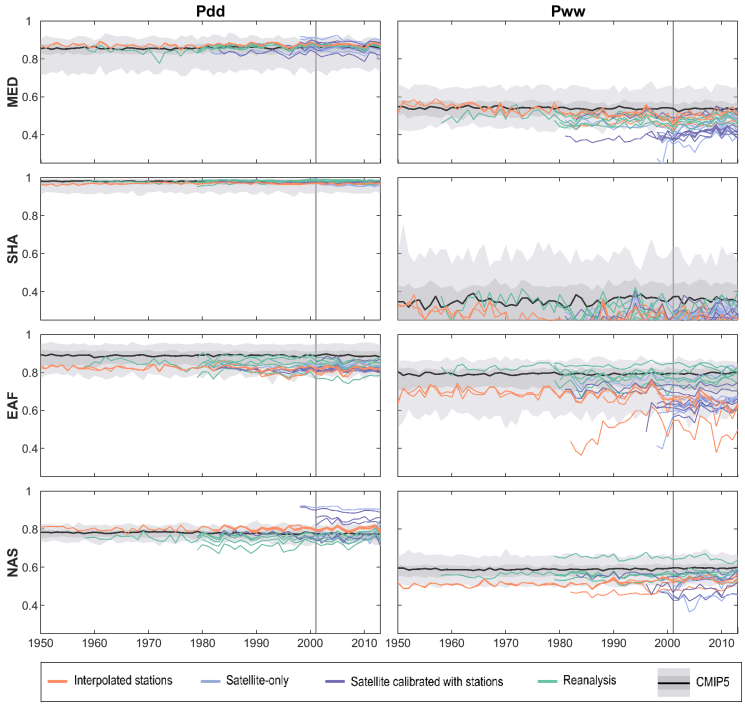

Figure B.10: *Same as Figure 3.5 in MED, SHA, EAF, and NAS*

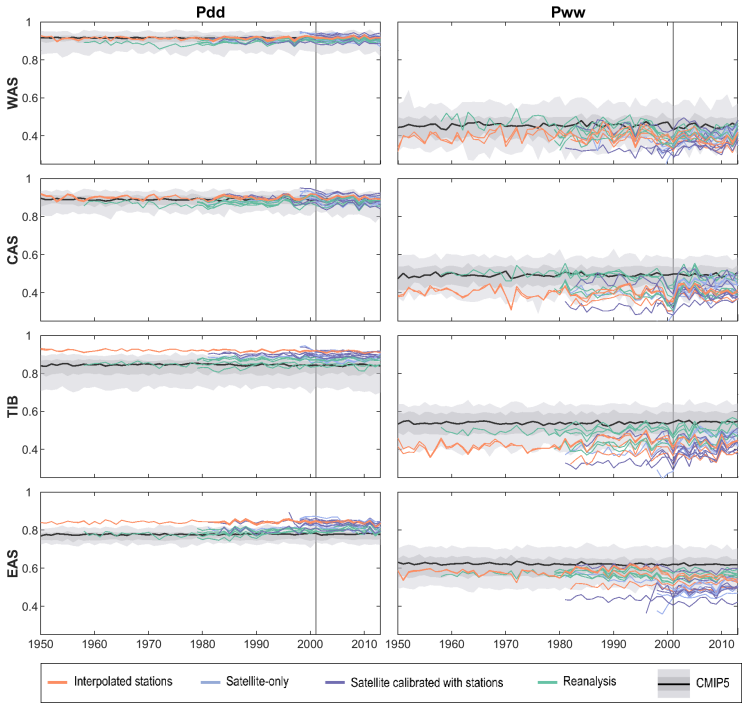

Figure B.11: *Same as Figure 3.5 in different regions*

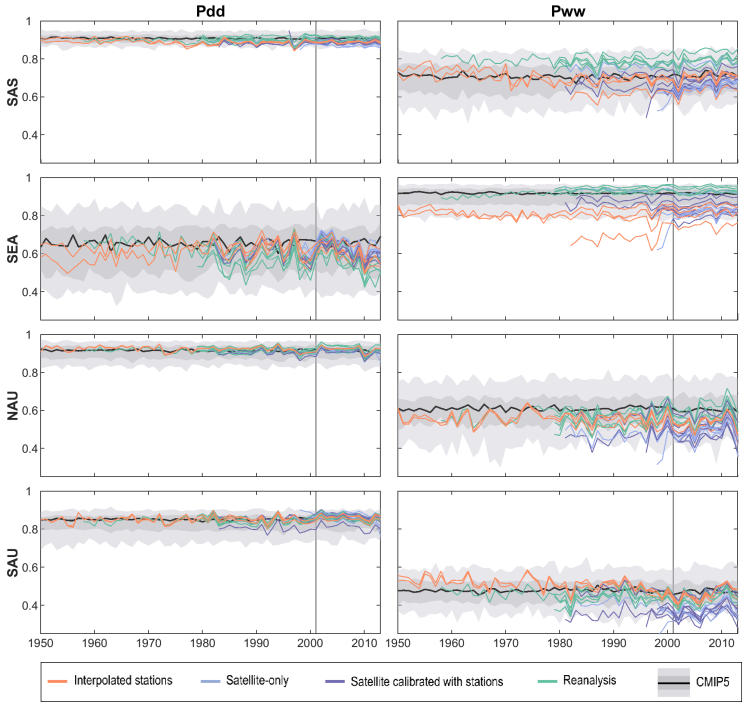

Figure B.12: *Same as Figure 3.5 in WAS, CAS, TIB, and EAS*

C | Appendix for Chapter 4

C.1 Supplementary figures

This supporting information provides the sensitivity of the soil moisture-precipitation (SMP) and number of events to spatial resolution is presented for a observational data set. Also, the SMP feedback metrics estimated by individual observational data sets and models, which are presented as mean in the main article. The ratio of land areas with different combinations of SMP feedback metrics with 0.1 and 0.02 significance levels are presented in Figures C.5 and C.6. Further discussion on individual model features is presented as well.

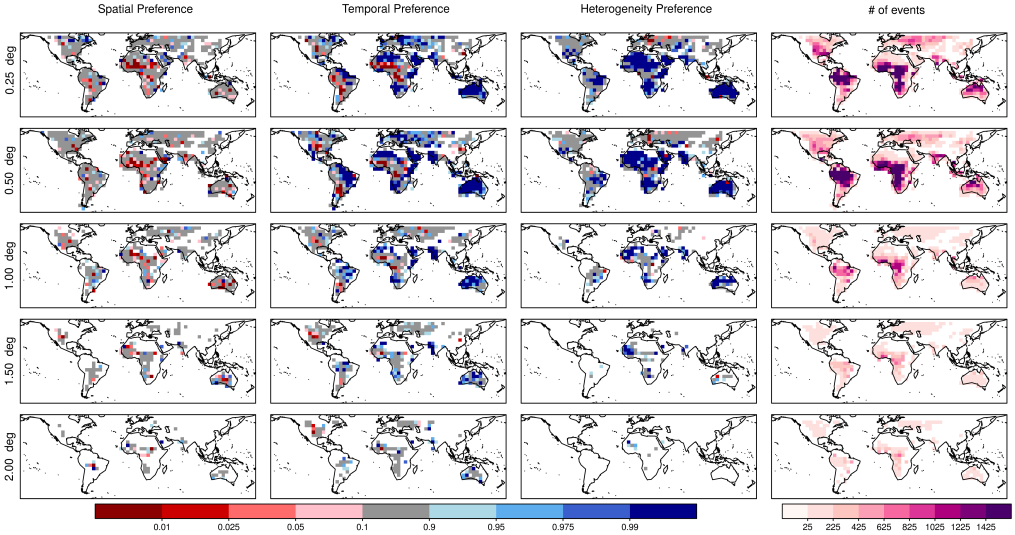

Figure C.1: *Soil moisture-precipitation feedback metrics (Ys, Yt and Yh) and number of afternoon rainfall events (2002-2011) from CMORPH precipitation and GLEAM soil moisture at different spatial resolutions.*

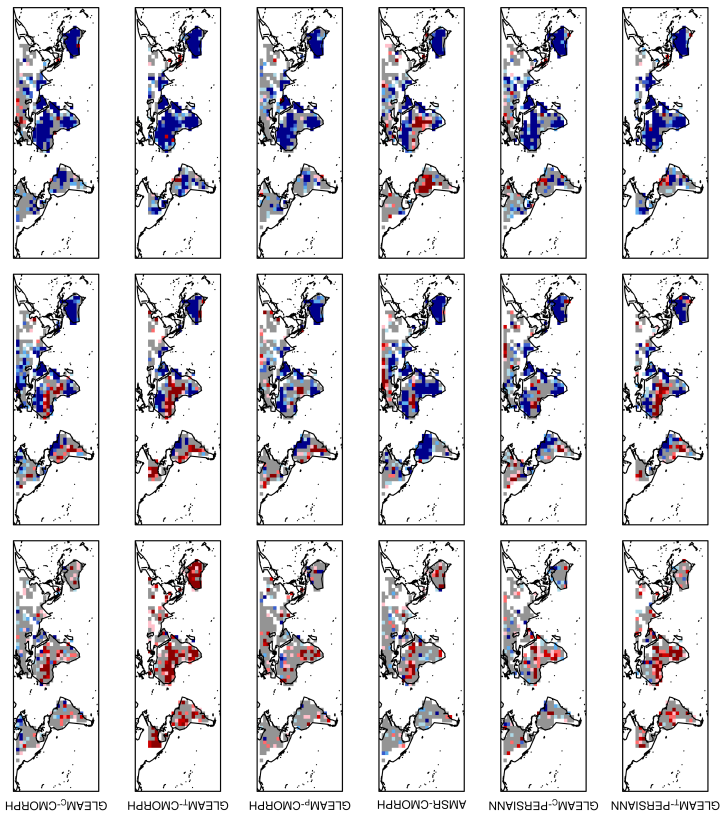

Figure C.2: *Soil moisture-precipitation feedback metrics (Ys, Yt and Yh) from observational data sets. $5° \times 5°$ boxes with less than 25 events are masked out (white) (continued in the next page)*

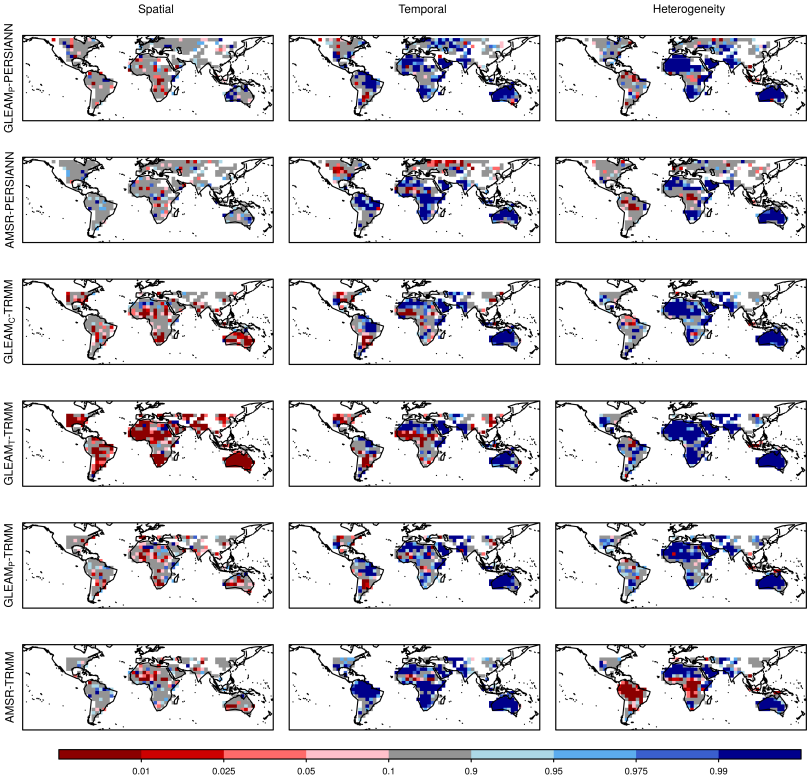

Figure C.3: *(continued) Soil moisture-precipitation feedback metrics (Ys, Yt and Yh) from observational data sets.* $5^\circ \times 5^\circ$ *boxes with less than 25 events are masked out (white)*

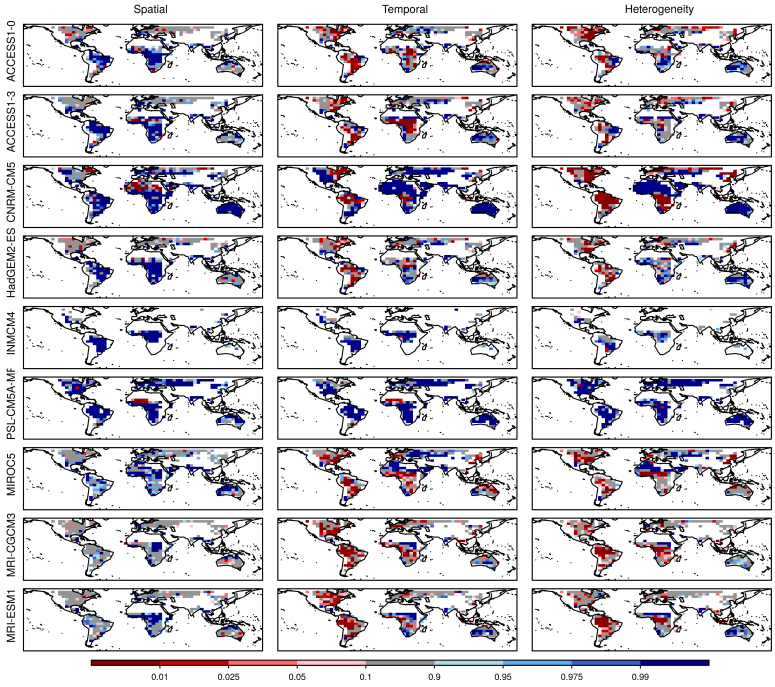

Figure C.4: *Soil moisture-precipitation feedback metrics (Ys, Yt and Yh) from CMIP5 models; Models are alphabetically ordered in rows.* $5^\circ \times 5^\circ$ *boxes with less than 25 events are masked out (white).*

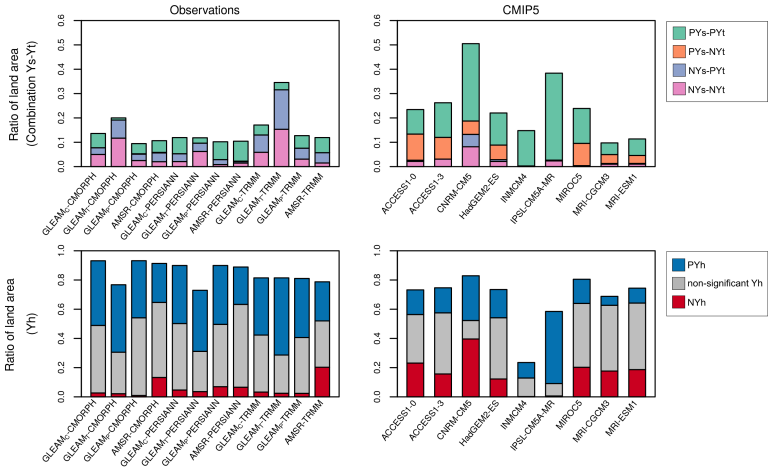

Figure C.5: *Same as Figure 4.2 but with significance level 0.1 (i.e., significantly negative for quantile values <0.05 and significantly positive for >0.95).*

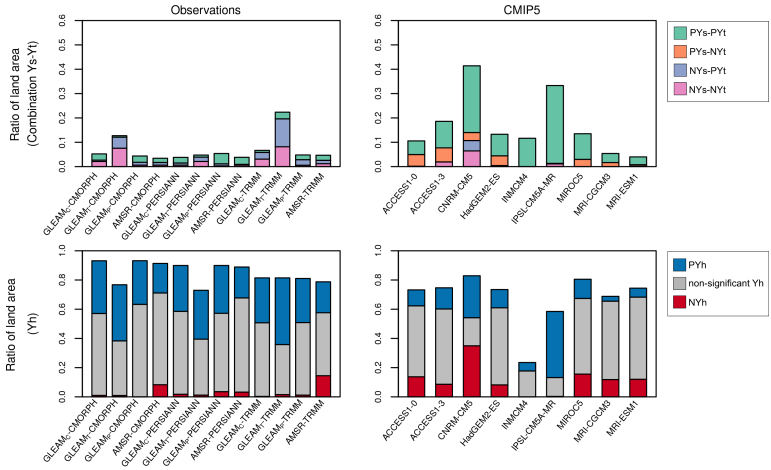

Figure C.6: *Same as Figure 4.2 but with significance level 0.02 (i.e., significantly negative for quantile values <0.01 and significantly positive for >0.99).*

C.2 Supplementary texts

Figure C.2 shows the three SMP feedback metrics in each GCM. Grid cells with insufficient observations are masked out. Models that share sub-schemes clearly show similarities in SMP feedback representation. ACCESS1-0 and HadGEM2-ES, which use the same atmospheric and land surface models (Table 4.1), and ACCESS1-3, which shares substantial parts of the model configuration with ACCESS1-0, show similar spatial pattern in all metrics. Ys in central and south Australia in ACCESS1-0 and HadGEM2-ES is moderately negative, but positive in ACCESS1-3. Some systematic negative Ys is also found in the central North America in ACCESS1-0. MRI-CGCM3 is a submodel of MRI-ESM1, without atmospheric chemistry and carbon cycle. Also these two models represent the feedbacks very similarly, though the signs of Yt and Yh in South Africa are contrasting. The strength of Ys in these two models is weaker than in the rest of the ensemble. CNRM-CM5 shows the strongest feedback signals also with largest spatial coverage. The strongly negative Ys in the Sahel and North Africa is noteworthy. IPSL-CM5A-MR shows consistent spatial pattern in all three metrics which are strongly positive in general, except for the strong negative Ys and Yt in western part of the Sahel. INMCM4 also shows the consistently positive signs in all metrics but covers small area. MIROC5 shows dominantly positive Ys with moderate strength. Yh and Yt in Australia are rarely positive in MIROC5 contrasting to other models. In all models, the spatial patterns of Yt and Yh are similar, unlike in observations, and such similarities are shared across different models. Overall, the mod-

els show dominantly negative signs in Americas and western sub-Sahara and non-significant or positive signs in the other regions with varying feedback strengths, except for INMCM4 and IPSL-CM5A-MR which show dominantly positive signs in all regions. Australia is one of few regions where the observed signs of the three SMP feedback metrics (negative Ys, positive Yt and Yh) are simultaneously captured in some models (ACCESS1-0, HadGEM2-ES, MRI-CGCM3). CNRM-CM5 also simulates such combination of feedback metrics in the Sahel.

Bibliography

Addor, N., O. Rössler, N. Köplin, M. Huss, R. Weingartner, and J. Seibert, 2014: Robust changes and sources of uncertainty in the projected hydrological regimes of Swiss catchments. *Water Resources Research*, **50 (10)**, 7541–7562, doi:10.1002/2014WR015549.

Ahn, M.-S., D. Kim, K. R. Sperber, I.-S. Kang, E. Maloney, D. Waliser, H. Hendon, and on behalf of WGNE MJO Task Force, 2017: MJO simulation in CMIP5 climate models: MJO skill metrics and process-oriented diagnosis. *Clim Dyn*, **49 (11)**, 4023–4045, doi:10.1007/s00382-017-3558-4.

Alexander, L. V. and J. M. Arblaster, 2017: Historical and projected trends in temperature and precipitation extremes in Australia in observations and CMIP5. *Weather and Climate Extremes*, **15**, 34–56, doi:10.1016/j.wace.2017.02.001.

Alexander, L. V., et al., 2006: Global observed changes in daily climate extremes of temperature and precipitation. *Journal of Geophysical Research: Atmospheres*, **111 (D5)**, doi:10.1029/2005JD006290.

Alfieri, L., P. Claps, P. D'Odorico, F. Laio, and T. M. Over, 2008: An Analysis of the Soil Moisture Feedback on Convective and Stratiform Precipitation. *Journal of Hydrometeorology*, **9 (2)**, 280–291, doi:10.1175/2007JHM863.1.

Annan, J. D. and J. C. Hargreaves, 2017: On the meaning of independence in climate science. *Earth System Dynamics*, **8 (1)**, 211–224, doi:https://doi.org/10.5194/esd-8-211-2017.

Ashouri, H., K.-L. Hsu, S. Sorooshian, D. K. Braithwaite, K. R. Knapp, L. D. Cecil, B. R. Nelson, and O. P. Prat, 2014: PERSIANN-CDR: Daily Precipitation Climate Data Record from Multisatellite Observations for Hydrological and Climate Studies. *Bull. Amer. Meteor. Soc.*, **96 (1)**, 69–83, doi:10.1175/BAMS-D-13-00068.1.

Ault, T. R., J. E. Cole, J. T. Overpeck, G. T. Pederson, and D. M. Meko, 2014: Assessing the Risk of Persistent Drought Using Climate Model Simulations

and Paleoclimate Data. *Journal of Climate*, **27 (20)**, 7529–7549, doi:10.1175/JCLI-D-12-00282.1.

Ault, T. R., J. E. Cole, and S. St. George, 2012: The amplitude of decadal to multidecadal variability in precipitation simulated by state-of-the-art climate models. *Geophysical Research Letters*, **39 (21)**, L21 705, doi:10.1029/2012GL053424.

Basawa, I., T. A. Green, W. McCormick, and R. Taylor, 1990: Asymptotic bootstrap validity for finite markov chains. *Communications in Statistics - Theory and Methods*, **19 (4)**, 1493–1510, doi:10.1080/03610929008830275.

Bêche, L. A., P. G. Connors, V. H. Resh, and A. M. Merenlender, 2009: Resilience of fishes and invertebrates to prolonged drought in two California streams. *Ecography*, **32 (5)**, 778–788, doi:10.1111/j.1600-0587.2009.05612.x.

Beck, H. E., et al., 2017: Global-scale evaluation of 22 precipitation datasets using gauge observations and hydrological modeling. *Hydrology and Earth System Sciences*, **21 (12)**, 6201–6217, doi:https://doi.org/10.5194/hess-21-6201-2017.

Becker, A., P. Finger, A. Meyer-Christoffer, B. Rudolf, K. Schamm, U. Schneider, and M. Ziese, 2013: A description of the global land-surface precipitation data products of the Global Precipitation Climatology Centre with sample applications including centennial (trend) analysis from 1901-present. *Earth System Science Data*, **5 (1)**, 71–99, doi:10.5194/essd-5-71-2013.

Bellenger, H., E. Guilyardi, J. Leloup, M. Lengaigne, and J. Vialard, 2014: ENSO representation in climate models: from CMIP3 to CMIP5. *Climate Dynamics*, **42 (7-8)**, 1999–2018, doi:10.1007/s00382-013-1783-z.

Betts, A. K., 1986: A new convective adjustment scheme. Part I: Observational and theoretical basis. *Quarterly Journal of the Royal Meteorological Society*, **112 (473)**, 677–691, doi:10.1002/qj.49711247307.

Bjerknes, J., 1969: Atmospheric teleconnections from the equatorial pacific. *Mon. Wea. Rev.*, **97 (3)**, 163–172, doi:10.1175/1520-0493(1969)097<0163:ATFTEP>2.3.CO;2.

Boberg, F., P. Berg, P. Thejll, W. J. Gutowski, and J. H. Christensen, 2010: Improved confidence in climate change projections of precipitation further evaluated using daily statistics from ENSEMBLES models. *Clim Dyn*, **35 (7-8)**, 1509–1520, doi:10.1007/s00382-009-0683-8.

Boé, J., 2018: Interdependency in Multimodel Climate Projections: Component Replication and Result Similarity. *Geophysical Research Letters*, **45 (6)**, 2771–2779, doi:10.1002/2017GL076829.

Bonan, G. B., 2008: Forests and Climate Change: Forcings, Feedbacks, and the Climate Benefits of Forests. *Science*, **320 (5882)**, 1444–1449, doi:10.1126/science.1155121.

Bougeault, P. and P. Bougeault, 1985: A Simple Parameterization of the Large-Scale Effects of Cumulus Convection.

Bunde, A., U. Büntgen, J. Ludescher, J. Luterbacher, and H. von Storch, 2013: Is there memory in precipitation? *Nature Climate Change*, **3 (3)**, 174–175, doi:10.1038/nclimate1830.

Chang, C.-P., Y. Zhang, and T. Li, 2000: Interannual and Interdecadal Variations of the East Asian Summer Monsoon and Tropical Pacific SSTs. Part I: Roles of the Subtropical Ridge. *J. Climate*, **13 (24)**, 4310–4325, doi:10.1175/1520-0442(2000)013<4310:IAIVOT>2.0.CO;2.

Chikira, M., 2010: A Cumulus Parameterization with State-Dependent Entrainment Rate. Part II: Impact on Climatology in a General Circulation Model. *Journal of the Atmospheric Sciences*, **67 (7)**, 2194–2211, doi:10.1175/2010JAS3317.1.

Collins, W. J., et al., 2011: Development and evaluation of an Earth-System model - HadGEM2. *Geosci. Model Dev.*, **4 (4)**, 1051–1075, doi:10.5194/gmd-4-1051-2011.

Compo, G. P., J. S. Whitaker, and P. D. Sardeshmukh, 2006: Feasibility of a 100-Year Reanalysis Using Only Surface Pressure Data. *Bulletin of the American Meteorological Society*, **87 (2)**, 175–190, doi:10.1175/BAMS-87-2-175.

Contractor, S., et al., 2019: Rainfall Estimates on a Gridded Network (REGEN) – A global land-based gridded dataset of daily precipitation from 1950–2013. *Hydrology and Earth System Sciences Discussions*, 1–30, doi:https://doi.org/10.5194/hess-2018-595.

Cook, B. I., T. R. Ault, and J. E. Smerdon, 2015: Unprecedented 21st century drought risk in the American Southwest and Central Plains. *Science Advances*, **1 (1)**, e1400 082–e1400 082, doi:10.1126/sciadv.1400082.

Cook, B. I., G. B. Bonan, and S. Levis, 2006: Soil Moisture Feedbacks to Precipitation in Southern Africa. *J. Climate*, **19 (17)**, 4198–4206, doi:10.1175/JCLI3856.1.

Cox, P. M., D. Pearson, B. B. Booth, P. Friedlingstein, C. Huntingford, C. D. Jones, and C. M. Luke, 2013: Sensitivity of tropical carbon to climate change constrained by carbon dioxide variability. *Nature*, **494 (7437)**, 341–344, doi:10.1038/nature11882.

Crawley, M. J., 2005: Analysis of Variance. *Statistics: An Introduction using R*, John Wiley & Sons, London, UK, 155–185.

Croci-Maspoli, M., C. Schwierz, and H. C. Davies, 2007: Atmospheric blocking: space-time links to the NAO and PNA. *Clim Dyn*, **29 (7)**, 713–725, doi:10.1007/s00382-007-0259-4.

Cui, W., X. Dong, B. Xi, and A. Kennedy, 2017: Evaluation of Reanalyzed Precipitation Variability and Trends Using the Gridded Gauge-Based Analysis over the CONUS. *J. Hydrometeor.*, **18 (8)**, 2227–2248, doi:10.1175/JHM-D-17-0029.1.

Dai, A., 2006: Precipitation characteristics in eighteen coupled climate models. *Journal of Climate*, **19 (18)**, 4605–4630.

Dai, A., 2011: Drought under global warming: a review. *Wiley Interdisciplinary Reviews: Climate Change*, **2 (1)**, 45–65, doi:10.1002/wcc.81.

Dash, S. K., M. A. Kulkarni, U. C. Mohanty, and K. Prasad, 2009: Changes in the characteristics of rain events in India. *Journal of Geophysical Research: Atmospheres*, **114 (D10)**, doi:10.1029/2008JD010572.

Dee, D. P., et al., 2011: The ERA-Interim reanalysis: configuration and performance of the data assimilation system. *Quarterly Journal of the Royal Meteorological Society*, **137 (656)**, 553–597, doi:10.1002/qj.828.

Dirmeyer, P. A., R. D. Koster, and Z. Guo, 2006: Do Global Models Properly Represent the Feedback between Land and Atmosphere? *J. Hydrometeor*, **7 (6)**, 1177–1198, doi:10.1175/JHM532.1.

Dix, M., et al., 2013: The ACCESS coupled model: documentation of core CMIP5 simulations and initial results. *Australian Meteorological and Oceanographic Journal*, **63 (1)**, 83–99, doi:10.22499/2.6301.006.

Douville, H., F. Chauvin, and H. Broqua, 2001: Influence of Soil Moisture on the Asian and African Monsoons. Part I: Mean Monsoon and Daily Precipitation. *J. Climate*, **14 (11)**, 2381–2403, doi:10.1175/1520-0442(2001)014<2381:IOSMOT>2.0.CO;2.

Duerinck, H. M., R. J. van der Ent, N. C. van de Giesen, G. Schoups, V. Babovic, and P. J.-F. Yeh, 2016: Observed Soil Moisture-Precipitation Feedback in Illinois: A Systematic Analysis over Different Scales. *Journal of Hydrometeorology*, **(2016)**.

Efron, B. and R. J. Tibshirani, 1994: *An introduction to the bootsrap*. CRC Press.

Eltahir, E. A. B. and R. L. Bras, 1996: Precipitation recycling. *Reviews of Geophysics*, **34 (3)**, 367–378, doi:10.1029/96RG01927.

Emanuel, K. A., 1991: A Scheme for Representing Cumulus Convection in Large-Scale Models. *J. Atmos. Sci.*, **48 (21)**, 2313–2329, doi:10.1175/1520-0469(1991)048<2313:ASFRCC>2.0.CO;2.

Ferraro, R. R., F. Weng, N. C. Grody, and A. Basist, 1996: An Eight-Year (1987-1994) Time Series of Rainfall, Clouds, Water Vapor, Snow Cover, and Sea Ice Derived from SSM/I Measurements. *Bull. Amer. Meteor. Soc.*, **77 (5)**, 891–906, doi:10.1175/1520-0477(1996)077<0891:AEYTSO>2.0.CO;2.

Findell, K. L. and E. A. B. Eltahir, 2003: Atmospheric Controls on Soil Moisture-Boundary Layer Interactions. Part I: Framework Development. *J. Hydrometeor.*, **4 (3)**, 552–569, doi:10.1175/1525-7541(2003)004<0552:ACOSML>2.0.CO;2.

Ford, T. W., S. M. Quiring, B. Thakur, R. Jogineedi, A. Houston, S. Yuan, A. Kalra, and N. Lock, 2018: Evaluating Soil Moisture-Precipitation Interactions Using Remote Sensing: A Sensitivity Analysis. *J. Hydrometeor.*, **19 (8)**, 1237–1253, doi:10.1175/JHM-D-17-0243.1.

Fosser, G., S. Khodayar, and P. Berg, 2015: Benefit of convection permitting climate model simulations in the representation of convective precipitation. *Clim Dyn*, **44 (1)**, 45–60, doi:10.1007/s00382-014-2242-1.

Funk, C., et al., 2015: The climate hazards infrared precipitation with stations-a new environmental record for monitoring extremes. *Scientific Data*, **2**, 150 066, doi:10.1038/sdata.2015.66.

Garcia-Carreras, L. and D. J. Parker, 2011: How does local tropical deforestation affect rainfall? *Geophysical Research Letters*, **38 (19)**, doi:10.1029/2011GL049099.

Gates, W. L., et al., 1999: An overview of the results of the Atmospheric Model Intercomparison Project (AMIP I). *Bulletin of the American Meteorological Society*, **80 (1)**, 29–55.

Gentine, P., A. A. M. Holtslag, F. D'Andrea, and M. Ek, 2013: Surface and Atmospheric Controls on the Onset of Moist Convection over Land. *J. Hydrometeor.*, **14 (5)**, 1443–1462, doi:10.1175/JHM-D-12-0137.1.

Gershunov, A. and T. P. Barnett, 1998: Interdecadal Modulation of ENSO Teleconnections. *Bull. Amer. Meteor. Soc.*, **79 (12)**, 2715–2726, doi:10.1175/1520-0477(1998)079<2715:IMOET>2.0.CO;2.

Gregory, D. and P. R. Rowntree, 1990: A Mass Flux Convection Scheme with Representation of Cloud Ensemble Characteristics and Stability-Dependent Closure. *Mon. Wea. Rev.*, **118 (7)**, 1483–1506, doi:10.1175/1520-0493(1990)118<1483:AMFCSW>2.0.CO;2.

Griffin, D. and K. J. Anchukaitis, 2014: How unusual is the 2012-2014 California drought?: GRIFFIN AND ANCHUKAITIS. *Geophysical Research Letters*, **41 (24)**, 9017–9023, doi:10.1002/2014GL062433.

Groisman, P. Y. and R. W. Knight, 2008: Prolonged Dry Episodes over the Conterminous United States: New Tendencies Emerging during the Last 40 Years. *J. Climate*, **21 (9)**, 1850–1862, doi:10.1175/2007JCLI2013.1.

Guilbert, J., A. K. Betts, D. M. Rizzo, B. Beckage, and A. Bomblies, 2015: Characterization of increased persistence and intensity of precipitation in the northeastern United States. *Geophysical Research Letters*, **42 (6)**, 1888–1893, doi:10.1002/2015GL063124.

Guillod, B. P., B. Orlowsky, D. G. Miralles, A. J. Teuling, and S. I. Seneviratne, 2015: Reconciling spatial and temporal soil moisture effects on afternoon rainfall. *Nature Communications*, **6**, 6443, doi:10.1038/ncomms7443.

Guillod, B. P., et al., 2014: Land-surface controls on afternoon precipitation diagnosed from observational data: uncertainties and confounding factors. *Atmospheric Chemistry and Physics*, **14 (16)**, 8343–8367, doi:10.5194/acp-14-8343-2014.

Hall, A. and X. Qu, 2006: Using the current seasonal cycle to constrain snow albedo feedback in future climate change. *Geophysical Research Letters*, **33 (3)**, doi:10.1029/2005GL025127.

Harding, K. J. and P. K. Snyder, 2015: The Relationship between the Pacific-North American Teleconnection Pattern, the Great Plains Low-Level Jet, and North Central U.S. Heavy Rainfall Events. *J. Climate*, **28 (17)**, 6729–6742, doi:10.1175/JCLI-D-14-00657.1.

Harou, J. J., J. Medellín-Azuara, T. Zhu, S. K. Tanaka, J. R. Lund, S. Stine, M. A. Olivares, and M. W. Jenkins, 2010: Economic consequences of optimized water management for a prolonged, severe drought in California. *Water Resources Research*, **46 (5)**, doi:10.1029/2008WR007681.

Harris, I., P. Jones, T. Osborn, and D. Lister, 2014: Updated high-resolution grids of monthly climatic observations - the CRU TS3.10 Dataset. *International Journal of Climatology*, **34 (3)**, 623–642, doi:10.1002/joc.3711.

Hawkins, E. and R. Sutton, 2009: The potential to narrow uncertainty in regional climate predictions. *Bulletin of the American Meteorological Society*, **90 (8)**, 1095–1107.

Hohenegger, C., P. Brockhaus, C. S. Bretherton, and C. Schär, 2009: The Soil Moisture-Precipitation Feedback in Simulations with Explicit and Parameterized Convection. *J. Climate*, **22 (19)**, 5003–5020, doi:10.1175/2009JCLI2604.1.

Hourdin, F., et al., 2013: Impact of the LMDZ atmospheric grid configuration on the climate and sensitivity of the IPSL-CM5a coupled model. *Clim Dyn*, **40 (9-10)**, 2167–2192, doi:10.1007/s00382-012-1411-3.

Houze, R. A., S. S. Chen, D. E. Kingsmill, Y. Serra, and S. E. Yuter, 2000: Convection over the Pacific Warm Pool in relation to the Atmospheric Kelvin-Rossby Wave. *J. Atmos. Sci.*, **57 (18)**, 3058–3089, doi:10.1175/1520-0469(2000)057<3058:COTPWP>2.0.CO;2.

Hoy, A., A. Schucknecht, M. Sepp, and J. Matschullat, 2014: Large-scale synoptic types and their impact on European precipitation. *Theor Appl Climatol*, **116 (1)**, 19–35, doi:10.1007/s00704-013-0897-x.

Hsu, H., M.-H. Lo, B. P. Guillod, D. G. Miralles, and S. Kumar, 2017: Relation between precipitation location and antecedent/subsequent soil moisture spatial patterns: Precipitation-Soil Moisture Coupling. *Journal of Geophysical Research: Atmospheres*, **122 (12)**, 6319–6328, doi:10.1002/2016JD026042.

Hsu, K.-l., X. Gao, S. Sorooshian, and H. V. Gupta, 1997: Precipitation Estimation from Remotely Sensed Information Using Artificial Neural Networks. *J. Appl. Meteor.*, **36 (9)**, 1176–1190, doi:10.1175/1520-0450(1997)036<1176:PEFRSI>2.0.CO;2.

Huffman, G. J., R. F. Adler, M. M. Morrissey, D. T. Bolvin, S. Curtis, R. Joyce, B. McGavock, and J. Susskind, 2001: Global Precipitation at One-Degree Daily Resolution from Multisatellite Observations. *J. Hydrometeor.*, **2 (1)**, 36–50, doi:10.1175/1525-7541(2001)002<0036:GPAODD>2.0.CO;2.

Huffman, G. J., et al., 2007: The TRMM Multisatellite Precipitation Analysis (TMPA): Quasi-Global, Multiyear, Combined-Sensor Precipitation Estimates at Fine Scales. *J. Hydrometeor.*, **8 (1)**, 38–55, doi:10.1175/JHM560.1.

HURRELL, J. W. and H. VAN LOON, 1997: DECADAL VARIATIONS IN CLIMATE ASSOCIATED WITH THE NORTH ATLANTIC OSCILLATION. *Climatic Change*, **36 (3)**, 301–326, doi:10.1023/A:1005314315270.

Jackson, B. B., 1975: Markov mixture models for drought lengths. *Water Resources Research*, **11 (1)**, 64–74.

Jha, B., Z.-Z. Hu, and A. Kumar, 2014: SST and ENSO variability and change simulated in historical experiments of CMIP5 models. *Clim Dyn*, **42 (7)**, 2113–2124, doi:10.1007/s00382-013-1803-z.

Joyce, R. J., J. E. Janowiak, P. A. Arkin, and P. Xie, 2004: CMORPH: A Method that Produces Global Precipitation Estimates from Passive Microwave and Infrared Data at High Spatial and Temporal Resolution. *J. Hydrometeor.*, **5 (3)**, 487–503, doi:10.1175/1525-7541(2004)005<0487:CAMTPG>2.0.CO;2.

Kalnay, E., et al., 1996: The NCEP/NCAR 40-Year Reanalysis Project. *Bull. Amer. Meteor. Soc.*, **77 (3)**, 437–472, doi:10.1175/1520-0477(1996)077<0437:TNYRP>2.0.CO;2.

Kelley, C. P., S. Mohtadi, M. A. Cane, R. Seager, and Y. Kushnir, 2015: Climate change in the Fertile Crescent and implications of the recent Syrian drought. *Proceedings of the National Academy of Sciences*, **112 (11)**, 3241–3246, doi:10.1073/pnas.1421533112.

Keyantash, J. and J. A. Dracup, 2002: The quantification of drought: an evaluation of drought indices. *Bulletin of the American Meteorological Society*, **83 (8)**, 1167–1180.

Kharin, V. V. and F. W. Zwiers, 2002: Climate Predictions with Multimodel Ensembles. *J. Climate*, **15 (7)**, 793–799, doi:10.1175/1520-0442(2002)015<0793:CPWME>2.0.CO;2.

Kidd, C. and V. Levizzani, 2011: Status of satellite precipitation retrievals. *Hydrology and Earth System Sciences*, **15 (4)**, 1109–1116, doi:https://doi.org/10.5194/hess-15-1109-2011.

Knutti, R., R. Furrer, C. Tebaldi, J. Cermak, and G. A. Meehl, 2009: Challenges in Combining Projections from Multiple Climate Models. *J. Climate*, **23 (10)**, 2739–2758, doi:10.1175/2009JCLI3361.1.

Kobayashi, S., et al., 2015: The JRA-55 Reanalysis: General Specifications and Basic Characteristics. *Journal of the Meteorological Society of Japan. Ser. II*, **93 (1)**, 5–48, doi:10.2151/jmsj.2015-001.

Koster, R. D. and M. J. Suarez, 2001: Soil Moisture Memory in Climate Models. *J. Hydrometeor.*, **2 (6)**, 558–570, doi:10.1175/1525-7541(2001)002<0558:SMMICM>2.0.CO;2.

Koster, R. D., et al., 2004: Regions of Strong Coupling Between Soil Moisture and Precipitation. *Science*, **305 (5687)**, 1138–1140, doi:10.1126/science.1100217.

Koster, R. D., et al., 2006: GLACE: The Global Land-Atmosphere Coupling Experiment. Part I: Overview. *J. Hydrometeor*, **7 (4)**, 590–610, doi:10.1175/JHM510.1.

Koster, R. D., et al., 2010: Contribution of land surface initialization to subseasonal forecast skill: First results from a multi-model experiment. *Geophysical Research Letters*, **37 (2)**, doi:10.1029/2009GL041677.

Krishnan, R. and M. Sugi, 2003: Pacific decadal oscillation and variability of the Indian summer monsoon rainfall. *Climate Dynamics*, **21 (3)**, 233–242, doi:10.1007/s00382-003-0330-8.

Krzywinski, M., N. Altman, and P. Blainey, 2014: Points of Significance: Nested designs. *Nat Meth*, **11 (10)**, 977–978, doi:10.1038/nmeth.3137.

Kubota, T., et al., 2007: Global Precipitation Map Using Satellite-Borne Microwave Radiometers by the GSMaP Project: Production and Validation. *IEEE Transactions on Geoscience and Remote Sensing*, **45 (7)**, 2259–2275, doi:10.1109/TGRS.2007.895337.

Kumar, S., V. Merwade, J. L. Kinter, and D. Niyogi, 2013: Evaluation of Temperature and Precipitation Trends and Long-Term Persistence in CMIP5 Twentieth-Century Climate Simulations. *J. Climate*, **26 (12)**, 4168–4185, doi:10.1175/JCLI-D-12-00259.1.

Kummerow, C. and L. Giglio, 1994: A Passive Microwave Technique for Estimating Rainfall and Vertical Structure Information from Space. Part I: Algorithm Description. *J. Appl. Meteor.*, **33 (1)**, 3–18, doi:10.1175/1520-0450(1994)033<0003:APMTFE>2.0.CO;2.

Kushnir, Y., R. Seager, M. Ting, N. Naik, and J. Nakamura, 2010: Mechanisms of Tropical Atlantic SST Influence on North American Precipitation Variability. *J. Climate*, **23 (21)**, 5610–5628, doi:10.1175/2010JCLI3172.1.

Lambert, F. H. and M. R. Allen, 2009: Are Changes in Global Precipitation Constrained by the Tropospheric Energy Budget? *Journal of Climate*, **22 (3)**, 499–517, doi:10.1175/2008JCLI2135.1.

Langford, S., S. Stevenson, and D. Noone, 2014: Analysis of Low-Frequency Precipitation Variability in CMIP5 Historical Simulations for Southwestern North America. *Journal of Climate*, **27 (7)**, 2735–2756, doi:10.1175/JCLI-D-13-00317.1.

Lau, K.-M., J. H. Kim, and Y. Sud, 1996: Intercomparison of Hydrologic Processes in AMIP GCMs. *Bull. Amer. Meteor. Soc.*, **77 (10)**, 2209–2228, doi:10.1175/1520-0477(1996)077<2209:IOHPIA>2.0.CO;2.

Lauer, A., et al., 2018: Process-level improvements in CMIP5 models and their impact on tropical variability, the Southern Ocean, and monsoons. *Earth System Dynamics*, **9 (1)**, 33–67, doi:https://doi.org/10.5194/esd-9-33-2018.

Laux, P., G. Jäckel, R. M. Tingem, and H. Kunstmann, 2010: Impact of climate change on agricultural productivity under rainfed conditions in Cameroon-A method to improve attainable crop yields by planting date adaptations. *Agricultural and Forest Meteorology*, **150 (9)**, 1258–1271, doi:10.1016/j.agrformet.2010.05.008.

Lee, K. S., J. Sadeghipour, and J. A. Dracup, 1986: An approach for frequency analysis of multiyear drought durations. *Water Resources Research*, **22 (5)**, doi:10.1029/WR022i005p00655.

Lenggenhager, S., M. Croci-Maspoli, S. BrÃűnnimann, and O. Martius, 2018: On the dynamical coupling between atmospheric blocks and heavy precipitation events: A discussion of the southern Alpine flood in October 2000. *Quarterly Journal of the Royal Meteorological Society*, **0 (ja)**, doi:10.1002/qj.3449.

Lorenz, R., et al., 2016: Influence of land-atmosphere feedbacks on temperature and precipitation extremes in the GLACE-CMIP5 ensemble. *Journal of Geophysical Research: Atmospheres*, **121 (2)**, 607–623, doi:10.1002/2015JD024053.

Mandelbrot, B. B. and J. R. Wallis, 1969: Some long-run properties of geophysical records. *Water Resources Research*, **5 (2)**, 321–340.

Mathier, L., L. Perreault, B. Bobée, and F. Ashkar, 1992: The use of geometric and gamma-related distributions for frequency analysis of water deficit. *Stochastic Hydrology and Hydraulics*, **6 (4)**, 239–254.

Matsui, T., V. Lakshmi, and E. Small, 2003: Links between Snow Cover, Surface Skin Temperature, and Rainfall Variability in the North American Monsoon System. *J. Climate*, **16 (11)**, 1821–1829, doi:10.1175/1520-0442(2003)016<1821:LBSCSS>2.0.CO;2.

Matsuura, K. and C. J. Willmott, 2012: Terrestrial Precipitation: 1900-2010 Gridded Monthly Time Series.

McKee, T. B., N. J. Doesken, and J. Kleist, 1993: The relationship of drought frequency and duration to time scales. *Proceedings of the 8th Conference on Applied Climatology*, American Meteorological Society Boston, MA, Vol. 17, 179–183.

McPhaden, M. J., X. Zhang, H. H. Hendon, and M. C. Wheeler, 2006: Large scale dynamics and MJO forcing of ENSO variability. *Geophysical Research Letters*, **33 (16)**, doi:10.1029/2006GL026786.

Meehl, G. A., 1994: Influence of the Land Surface in the Asian Summer Monsoon: External Conditions versus Internal Feedbacks. *J. Climate*, **7 (7)**, 1033–1049, doi:10.1175/1520-0442(1994)007<1033:IOTLSI>2.0.CO;2.

Meinke, H., P. DeVoil, G. L. Hammer, S. Power, R. Allan, R. C. Stone, C. Folland, and A. Potgieter, 2005: Rainfall variability at decadal and longer time scales: signal or noise? *Journal of Climate*, **18 (1)**, 89–96.

Miralles, D. G., T. R. H. Holmes, R. A. M. De Jeu, J. H. Gash, A. G. C. A. Meesters, and A. J. Dolman, 2011: Global land-surface evaporation estimated from satellite-based observations. *Hydrol. Earth Syst. Sci.*, **15 (2)**, 453–469, doi:10.5194/hess-15-453-2011.

Moon, H., L. Gudmundsson, and S. I. Seneviratne, 2018: Drought Persistence Errors in Global Climate Models. *Journal of Geophysical Research: Atmospheres*, **123 (7)**, 3483–3496, doi:10.1002/2017JD027577.

Morrison, H. and A. Gettelman, 2008: A New Two-Moment Bulk Stratiform Cloud Microphysics Scheme in the Community Atmosphere Model, Version 3 (CAM3). Part I: Description and Numerical Tests. *J. Climate*, **21 (15)**, 3642–3659, doi:10.1175/2008JCLI2105.1.

Nicolai-Shaw, N., J. Zscheischler, M. Hirschi, L. Gudmundsson, and S. I. Seneviratne, 2017: A drought event composite analysis using satellite remote-sensing based soil moisture. *Remote Sensing of Environment*, doi:10.1016/j.rse.2017.06.014.

Ning, L. and R. S. Bradley, 2016: NAO and PNA influences on winter temperature and precipitation over the eastern United States in CMIP5 GCMs. *Clim Dyn*, **46 (3)**, 1257–1276, doi:10.1007/s00382-015-2643-9.

Orlowsky, B. and S. I. Seneviratne, 2010: Statistical Analyses of Land-Atmosphere Feedbacks and Their Possible Pitfalls. *Journal of Climate*, **23 (14)**, 3918–3932, doi:10.1175/2010JCLI3366.1.

Orlowsky, B. and S. I. Seneviratne, 2013: Elusive drought: uncertainty in observed trends and short- and long-term CMIP5 projections. *Hydrology and Earth System Sciences*, **17 (5)**, 1765–1781, doi:10.5194/hess-17-1765-2013.

Orth, R. and S. I. Seneviratne, 2012: Analysis of soil moisture memory from observations in Europe. *Journal of Geophysical Research*, **117 (D15)**, doi:10.1029/2011JD017366.

Owe, M., R. d. Jeu, and T. Holmes, 2008: Multisensor historical climatology of satellite-derived global land surface moisture. *Journal of Geophysical Research: Earth Surface*, **113 (F1)**, doi:10.1029/2007JF000769.

Pelletier, J. D. and D. L. Turcotte, 1997: Long-range persistence in climatological and hydrological time series: analysis, modeling and application to drought hazard assessment. *Journal of Hydrology*, **203 (1-4)**, 198–208.

Pfleiderer, P. and D. Coumou, 2018: Quantification of temperature persistence over the Northern Hemisphere land-area. *Clim Dyn*, **51 (1)**, 627–637, doi:10.1007/s00382-017-3945-x.

Poli, P., et al., 2016: ERA-20c: An Atmospheric Reanalysis of the Twentieth Century. *J. Climate*, **29 (11)**, 4083–4097, doi:10.1175/JCLI-D-15-0556.1.

Power, S., F. Tseitkin, V. Mehta, B. Lavery, S. Torok, and N. Holbrook, 1999: Decadal climate variability in Australia during the twentieth century. *International Journal of Climatology*, **19 (2)**, 169–184, doi:10.1002/(SICI)1097-0088(199902)19:2<169::AID-JOC356>3.0.CO;2-Y.

Quiring, S. M. and T. N. Papakryiakou, 2003: An evaluation of agricultural drought indices for the Canadian prairies. *Agricultural and Forest Meteorology*, **118 (1)**, 49–62, doi:10.1016/S0168-1923(03)00072-8.

Rienecker, M. M., et al., 2011: MERRA: NASA's Modern-Era Retrospective Analysis for Research and Applications. *J. Climate*, **24 (14)**, 3624–3648, doi: 10.1175/JCLI-D-11-00015.1.

Rio, C. and F. Hourdin, 2008: A Thermal Plume Model for the Convective Boundary Layer: Representation of Cumulus Clouds. *J. Atmos. Sci.*, **65 (2)**, 407–425, doi:10.1175/2007JAS2256.1.

Roca, R., L. V. Alexander, G. Potter, M. Bador, R. Jucá, S. Contractor, M. G. Bosilovich, and S. Cloché, 2019: FROGs: a daily 1° × 1° gridded precipitation database ofrain gauge, satellite and reanalysis products. *Earth System Science Data Discussions*, 1–36, doi:https://doi.org/10.5194/essd-2019-51.

Rodrigues, R. R. and T. Woollings, 2016: Impact of Atmospheric Blocking on South America in Austral Summer. *Journal of Climate*, **30 (5)**, 1821–1837, doi: 10.1175/JCLI-D-16-0493.1.

Rosa, D. and W. D. Collins, 2013: A case study of subdaily simulated and observed continental convective precipitation: CMIP5 and multiscale global climate models comparison. *Geophys. Res. Lett.*, **40 (22)**, 5999–6003, doi:10. 1002/2013GL057987.

Rozas, V. and I. García-González, 2012: Too wet for oaks? Inter-tree competition and recent persistent wetness predispose oaks to rainfall-induced dieback in Atlantic rainy forest. *Global and Planetary Change*, **94-95**, 62–71, doi:10.1016/j.gloplacha.2012.07.004.

Saha, S., et al., 2010: The NCEP Climate Forecast System Reanalysis. *Bulletin of the American Meteorological Society*, **91 (8)**, 1015–1058, doi:10.1175/ 2010BAMS3001.1.

Salvucci, G. D., J. A. Saleem, and R. Kaufmann, 2002: Investigating soil moisture feedbacks on precipitation with tests of Granger causality. *Advances in water Resources*, **25 (8)**, 1305–1312.

Santanello, J. A., et al., 2017: Land-Atmosphere Interactions: The LoCo Perspective. *Bull. Amer. Meteor. Soc.*, **99 (6)**, 1253–1272, doi:10.1175/ BAMS-D-17-0001.1.

Schamm, K., M. Ziese, K. Raykova, A. Becker, P. Finger, A. Meyer-Christoffer, and U. Schneider, 2015: GPCC Full Data Daily Version 1.0 at 1.0Âř: Daily Land-Surface Precipitation from Rain-Gauges built on GTS-based and Historic Data. doi:https://doi.org/10.5676/dwd_gpcc/fd_d_v1_100, type: dataset.

Scherrer, S. C., M. Croci-Maspoli, C. Schwierz, and C. Appenzeller, 2006: Two-dimensional indices of atmospheric blocking and their statistical relationship with winter climate patterns in the Euro-Atlantic region. *International Journal of Climatology*, **26 (2)**, 233–249, doi:10.1002/joc.1250.

Schmidli, J. and C. Frei, 2005: Trends of heavy precipitation and wet and dry spells in Switzerland during the 20th century. *International Journal of Climatology*, **25 (6)**, 753–771, doi:10.1002/joc.1179.

Schneider, U., A. Becker, P. Finger, A. Meyer-Christoffer, M. Ziese, and B. Rudolf, 2014: GPCC's new land surface precipitation climatology based on quality-controlled in situ data and its role in quantifying the global water cycle. *Theor Appl Climatol*, **115 (1)**, 15–40, doi:10.1007/s00704-013-0860-x.

Schubert, S. D., et al., 2016: Global Meteorological Drought: A Synthesis of Current Understanding with a Focus on SST Drivers of Precipitation Deficits. *Journal of Climate*, **29 (11)**, 3989–4019, doi:10.1175/JCLI-D-15-0452.1.

Seleshi, Y. and U. Zanke, 2004: Recent changes in rainfall and rainy days in Ethiopia. *International Journal of Climatology*, **24 (8)**, 973–983, doi:10.1002/joc.1052.

Semenov, V. and L. Bengtsson, 2002: Secular trends in daily precipitation characteristics: greenhouse gas simulation with a coupled AOGCM. *Climate Dynamics*, **19 (2)**, 123–140, doi:10.1007/s00382-001-0218-4.

Seneviratne, S. I., T. Corti, E. L. Davin, M. Hirschi, E. B. Jaeger, I. Lehner, B. Orlowsky, and A. J. Teuling, 2010: Investigating soil moisture-climate interactions in a changing climate: A review. *Earth-Science Reviews*, **99 (3-4)**, 125–161, doi:10.1016/j.earscirev.2010.02.004.

Seneviratne, S. I. and N. Nicholls, 2012: Changes in climate extremes and their impacts on the natural physical environment. Tech. rep., 109–230 pp.

Seneviratne, S. I., et al., 2006: Soil moisture memory in AGCM simulations: Analysis of global land-atmosphere coupling experiment (GLACE) data. *Journal of Hydrometeorology*, **7 (5)**, 1090–1112.

Seneviratne, S. I., et al., 2013: Impact of soil moisture-climate feedbacks on CMIP5 projections: First results from the GLACE-CMIP5 experiment: GLACE-CMIP5 EXPERIMENT. *Geophysical Research Letters*, **40 (19)**, 5212–5217, doi:10.1002/grl.50956.

Sericola, B., 2013: Discrete-Time Markov Chains. *Markov Chains: Theory and Applications*, ISTE Ltd and John Wiley & Sons, Inc., London, Great Britain, 76–87, doi:10.1002/9781118731543.ch1.

Shanahan, T. M., et al., 2009: Atlantic forcing of persistent drought in West Africa. *science*, **324 (5925)**, 377–380.

Sharma, T. C. and U. S. Panu, 2014: Modeling of hydrological drought durations and magnitudes: Experiences on Canadian streamflows. *Journal of Hydrology: Regional Studies*, **1**, 92–106, doi:10.1016/j.ejrh.2014.06.006.

Sillmann, J., V. V. Kharin, X. Zhang, F. W. Zwiers, and D. Bronaugh, 2013: Climate extremes indices in the CMIP5 multimodel ensemble: Part 1. Model evaluation in the present climate: CLIMATE EXTREMES INDICES IN CMIP5. *Journal of Geophysical Research: Atmospheres*, **118 (4)**, 1716–1733, doi:10.1002/jgrd.50203.

Singh, D., M. Tsiang, B. Rajaratnam, and N. S. Diffenbaugh, 2014: Observed changes in extreme wet and dry spells during the South Asian summer monsoon season. *Nature Climate Change*, **4 (6)**, 456–461, doi:10.1038/nclimate2208.

Small, E. E., 2001: The influence of soil moisture anomalies on variability of the North American Monsoon System. *Geophysical Research Letters*, **28 (1)**, 139–142, doi:10.1029/2000GL011652.

Sousa, P. M., R. M. Trigo, D. Barriopedro, P. M. M. Soares, A. M. Ramos, and M. L. R. Liberato, 2017: Responses of European precipitation distributions and regimes to different blocking locations. *Clim Dyn*, **48 (3)**, 1141–1160, doi:10.1007/s00382-016-3132-5.

Spracklen, D. V., S. R. Arnold, and C. M. Taylor, 2012: Observations of increased tropical rainfall preceded by air passage over forests. *Nature*, **489 (7415)**, 282–285, doi:10.1038/nature11390.

Stagge, J. H., L. M. Tallaksen, L. Gudmundsson, A. F. Van Loon, and K. Stahl, 2015: Candidate Distributions for Climatological Drought Indices (SPI and SPEI). *Int. J. Climatol.*, **35 (13)**, 4027–4040, doi:10.1002/joc.4267.

Steinemann, A., 2014: Drought Information for Improving Preparedness in the Western States. *Bull. Amer. Meteor. Soc.*, **95 (6)**, 843–847, doi:10.1175/BAMS-D-13-00067.1.

Stensrud, D. J., J.-W. Bao, and T. T. Warner, 2000: Using Initial Condition and Model Physics Perturbations in Short-Range Ensemble Simulations of Mesoscale Convective Systems. *Mon. Wea. Rev.*, **128 (7)**, 2077–2107, doi:10.1175/1520-0493(2000)128<2077:UICAMP>2.0.CO;2.

Stine, S., 1994: Extreme and persistent drought in California and Patagonia during mediaeval time. doi:10.1038/369546a0.

Sun, Q., C. Miao, Q. Duan, H. Ashouri, S. Sorooshian, and K.-L. Hsu, 2018: A Review of Global Precipitation Data Sets: Data Sources, Estimation, and Intercomparisons. *Reviews of Geophysics*, **56 (1)**, 79–107, doi:10.1002/2017RG000574.

Tallaksen, L. M. and H. A. J. van Lanen, 2004: *Hydrological Drought: Processes and Estimation Methods for Streamflow and Groundwater*. Elsevier.

Tanarhte, M., P. Hadjinicolaou, and J. Lelieveld, 2012: Intercomparison of temperature and precipitation data sets based on observations in the Mediterranean and the Middle East: PRECIPITATION AND TEMPERATURE DATA SETS. *Journal of Geophysical Research: Atmospheres*, **117 (D12)**, doi:10.1029/2011JD017293.

Tatli, H., 2015: Detecting persistence of meteorological drought via the Hurst exponent. *Met. Apps*, **22 (4)**, 763–769, doi:10.1002/met.1519.

Taylor, C. M., C. E. Birch, D. J. Parker, N. Dixon, F. Guichard, G. Nikulin, and G. M. S. Lister, 2013: Modeling soil moisture-precipitation feedback in the Sahel: Importance of spatial scale versus convective parameterization. *Geophys. Res. Lett.*, **40 (23)**, 2013GL058 511, doi:10.1002/2013GL058511.

Taylor, C. M., R. A. M. de Jeu, F. Guichard, P. P. Harris, and W. A. Dorigo, 2012a: Afternoon rain more likely over drier soils. *Nature*, **489 (7416)**, 423–426, doi:10.1038/nature11377.

Taylor, C. M. and T. Lebel, 1998: Observational Evidence of Persistent Convective-Scale Rainfall Patterns. *Mon. Wea. Rev.*, **126 (6)**, 1597–1607, doi:10.1175/1520-0493(1998)126<1597:OEOPCS>2.0.CO;2.

Taylor, C. M., et al., 2011: New perspectives on land-atmosphere feedbacks from the African Monsoon Multidisciplinary Analysis. *Atmosph. Sci. Lett.*, **12 (1)**, 38–44, doi:10.1002/asl.336.

Taylor, I. H., E. Burke, L. McColl, P. Falloon, G. R. Harris, and D. McNeall, 2012b: Contributions to uncertainty in projections of future drought under climate change scenarios. *Hydrology and Earth System Sciences Discussions*, **9 (11)**, 12 613–12 653, doi:10.5194/hessd-9-12613-2012.

Taylor, K. E., R. J. Stouffer, and G. A. Meehl, 2012c: An Overview of CMIP5 and the Experiment Design. *Bulletin of the American Meteorological Society*, **93 (4)**, 485–498, doi:10.1175/BAMS-D-11-00094.1.

Tiedtke, M., 1989: A Comprehensive Mass Flux Scheme for Cumulus Parameterization in Large-Scale Models. *Mon. Wea. Rev.*, **117 (8)**, 1779–1800, doi:10.1175/1520-0493(1989)117<1779:ACMFSF>2.0.CO;2.

Trenberth, K. E., 1999: Atmospheric Moisture Recycling: Role of Advection and Local Evaporation. *J. Climate*, **12 (5)**, 1368–1381, doi:10.1175/1520-0442(1999)012<1368:AMRROA>2.0.CO;2.

Trenberth, K. E., L. Smith, T. Qian, A. Dai, and J. Fasullo, 2007: Estimates of the Global Water Budget and Its Annual Cycle Using Observational and Model Data. *J. Hydrometeor.*, **8 (4)**, 758–769, doi:10.1175/JHM600.1.

Trenberth, K. E., D. P. Stepaniak, and J. M. Caron, 2000: The Global Monsoon as Seen through the Divergent Atmospheric Circulation. *J. Climate*, **13 (22)**, 3969–3993, doi:10.1175/1520-0442(2000)013<3969:TGMAST>2.0.CO;2.

Trifiló, P., V. Casolo, F. Raimondo, E. Petrussa, F. Boscutti, M. A. Lo Gullo, and A. Nardini, 2017: Effects of prolonged drought on stem non-structural carbohydrates content and post-drought hydraulic recovery in Laurus nobilis L.: The possible link between carbon starvation and hydraulic failure. *Plant Physiology and Biochemistry*, **120**, 232–241, doi:10.1016/j.plaphy.2017.10.003.

Trigo, R. M., I. F. Trigo, C. C. DaCamara, and T. J. Osborn, 2004: Climate impact of the European winter blocking episodes from the NCEP/NCAR Reanalyses. *Climate Dynamics*, **23 (1)**, 17–28, doi:10.1007/s00382-004-0410-4.

Tuttle, J. D. and C. A. Davis, 2006: Corridors of Warm Season Precipitation in the Central United States. *Mon. Wea. Rev.*, **134 (9)**, 2297–2317, doi:10.1175/MWR3188.1.

Tuttle, S. and G. Salvucci, 2016: Empirical evidence of contrasting soil moisture-precipitation feedbacks across the United States. *Science*, **352 (6287)**, 825–828, doi:10.1126/science.aaa7185.

Valdes-Abellan, J., M. A. Pardo, and A. J. Tenza-Abril, 2017: Observed precipitation trend changes in the western Mediterranean region. *International Journal of Climatology*, **37 (S1)**, 1285–1296, doi:10.1002/joc.4984.

van der Ent, R. J., H. H. G. Savenije, B. Schaefli, and S. C. Steele-Dunne, 2010: Origin and fate of atmospheric moisture over continents: ORIGIN AND FATE OF ATMOSPHERIC MOISTURE. *Water Resources Research*, **46 (9)**, doi:10.1029/2010WR009127.

Van Loon, A. F., 2015: Hydrological drought explained: Hydrological drought explained. *Wiley Interdisciplinary Reviews: Water*, **2 (4)**, 359–392, doi:10.1002/wat2.1085.

Vicente-Serrano, S. M., S. Beguería, and J. I. LÃşpez-Moreno, 2009: A Multiscalar Drought Index Sensitive to Global Warming: The Standardized Precipitation Evapotranspiration Index. *J. Climate*, **23 (7)**, 1696–1718, doi:10.1175/2009JCLI2909.1.

Vinnarasi, R. and C. T. Dhanya, 2016: Changing characteristics of extreme wet and dry spells of Indian monsoon rainfall. *Journal of Geophysical Research: Atmospheres*, **121 (5)**, 2146–2160, doi:10.1002/2015JD024310.

Voldoire, A., et al., 2013: The CNRM-CM5.1 global climate model: description and basic evaluation. *Clim Dyn*, **40 (9-10)**, 2091–2121, doi:10.1007/s00382-011-1259-y.

Volodin, E. M., N. A. Dianskii, and A. V. Gusev, 2010: Simulating present-day climate with the INMCM4.0 coupled model of the atmospheric and oceanic general circulations. *Izv. Atmos. Ocean. Phys.*, **46 (4)**, 414–431, doi:10.1134/S000143381004002X.

Watanabe, M., et al., 2010: Improved Climate Simulation by MIROC5: Mean States, Variability, and Climate Sensitivity. *Journal of Climate*, **23 (23)**, 6312–6335, doi:10.1175/2010JCLI3679.1.

Weigel, A. P., M. A. Liniger, and C. Appenzeller, 2008: Can multi-model combination really enhance the prediction skill of probabilistic ensemble forecasts? *Quarterly Journal of the Royal Meteorological Society*, **134 (630)**, 241–260, doi:10.1002/qj.210.

Wetter, O., et al., 2014: The year-long unprecedented European heat and drought of 1540 - a worst case. *Climatic Change*, **125 (3-4)**, 349–363, doi:10.1007/s10584-014-1184-2.

Wheeler, M. C. and H. H. Hendon, 2004: An All-Season Real-Time Multivariate MJO Index: Development of an Index for Monitoring and Prediction. *Mon. Wea. Rev.*, **132 (8)**, 1917–1932, doi:10.1175/1520-0493(2004)132<1917:AARMMI>2.0.CO;2.

Wheeler, M. C., H. H. Hendon, S. Cleland, H. Meinke, and A. Donald, 2009: Impacts of the Madden-Julian Oscillation on Australian Rainfall and Circulation. *J. Climate*, **22 (6)**, 1482–1498, doi:10.1175/2008JCLI2595.1.

Wibig, J., 1999: Precipitation in Europe in relation to circulation patterns at the 500 hPa level. *International Journal of Climatology*, **19 (3)**, 253–269, doi:10.1002/(SICI)1097-0088(19990315)19:3<253::AID-JOC366>3.0.CO;2-0.

Wilby, R. L., C. Prudhomme, S. Parry, and K. G. L. Muchan, 2015: Persistence of Hydrometeorological Droughts in the United Kingdom: A Regional Analysis of Multi-Season Rainfall and River Flow Anomalies. *Journal of Extreme Events*, 1550006, doi:10.1142/S2345737615500062.

Xie, P., B. Rudolf, U. Schneider, and P. A. Arkin, 1996: Gauge-based monthly analysis of global land precipitation from 1971 to 1994. doi:10.1029/96JD01553.

Yao, Y. and D. Luo, 2015: Do European blocking events precede North Atlantic Oscillation events? *Adv. Atmos. Sci.*, **32 (8)**, 1106–1118, doi:10.1007/s00376-015-4209-5.

Yoshimura, H., R. Mizuta, and H. Murakami, 2015: A Spectral Cumulus Parameterization Scheme Interpolating between Two Convective Updrafts with Semi-Lagrangian Calculation of Transport by Compensatory Subsidence. *Monthly Weather Review*, **143 (2)**, 597–621, doi:10.1175/MWR-D-14-00068.1.

Yukimoto, S., et al., 2011: Meteorological Research Institute-Earth System Model Version 1 (MRI-ESM1) - Model Description -. Tech. Rep. 64, METEOROLOGICAL RESEARCH INSTITUTE, JAPAN, Technical reports of the meteorological research institute.

Zhang, C., 2013: Madden-Julian Oscillation: Bridging Weather and Climate. *Bull. Amer. Meteor. Soc.*, **94 (12)**, 1849–1870, doi:10.1175/BAMS-D-12-00026.1.

Zhang, C. and J. Gottschalck, 2002: SST Anomalies of ENSO and the Madden-Julian Oscillation in the Equatorial Pacific. *J. Climate*, **15 (17)**, 2429–2445, doi:10.1175/1520-0442(2002)015<2429:SAOEAT>2.0.CO;2.

Zhang, X., L. Alexander, G. C. Hegerl, P. Jones, A. K. Tank, T. C. Peterson, B. Trewin, and F. W. Zwiers, 2011: Indices for monitoring changes in extremes based on daily temperature and precipitation data. *Wiley Interdisciplinary Reviews: Climate Change*, **2 (6)**, 851–870, doi:10.1002/wcc.147.

Zolina, O., C. Simmer, S. K. Gulev, and S. Kollet, 2010: Changing structure of European precipitation: Longer wet periods leading to more abundant rainfalls. *Geophysical Research Letters*, **37 (6)**, doi:10.1029/2010GL042468.